U.S.N.A. --- Trident Scholar project report; no. 345 (2006)

DYNAMIC COMPUTER MODEL OF A STIRLING SPACE NUCLEAR POWER SYSTEM

by

Midshipman 1/c Justin L. R. Langlois, Class of 2006
United States Naval Academy
Annapolis, Maryland

_____
(signature)

Certification of Advisers Approval

CDR David D. Myre, USN
Aerospace Engineering Department

_____
(signature)

_____
(date)

Professor Martin E. Nelson
Mechanical Engineering Department

_____
(signature)

_____
(date)

Acceptance for the Trident Scholar Committee

Professor Joyce E. Shade
Deputy Director of Research & Scholarship

_____
(signature)

_____
(date)

USNA-1531-2

REPORT DOCUMENTATION PAGE

Form Approved
OMB No. 074-0188

1. AGENCY USE ONLY (Leave blank)	2. REPORT DATE	3. REPORT TYPE AND DATE COVERED
	4 May 2006	

4. TITLE AND SUBTITLE
Dynamic computer model of a Stirling space nuclear power system

5. FUNDING NUMBERS

6. AUTHOR(S)
Langlois, Justin L. R. (Justin Leander Russell), 1983-

7. PERFORMING ORGANIZATION NAME(S) AND ADDRESS(ES)		8. PERFORMING ORGANIZATION REPORT NUMBER

9. SPONSORING/MONITORING AGENCY NAME(S) AND ADDRESS(ES)		10. SPONSORING/MONITORING AGENCY REPORT NUMBER
US Naval Academy Annapolis, MD 21402		**Trident Scholar project report no. 345 (2006)**

11. SUPPLEMENTARY NOTES

12a. DISTRIBUTION/AVAILABILITY STATEMENT	12b. DISTRIBUTION CODE
This document has been approved for public release; its distribution is UNLIMITED.	

13. ABSTRACT In this project, the components of a Stirling space nuclear power system were modeled using MATLAB® and Simulink® under both steady state and transient conditions. Using information provided through NASA's Glenn Research Center, the Department of Energy's Naval Reactors, and literature from previous work in nuclear space power systems, the system architecture was developed. At steady state, the space power system was designed to produce 200 kW(e) and consisted of a NaK cooled fast reactor linked to four Stirling power converters via two NaK heat transfer loops connected by heat exchangers. A third NaK heat transfer loop was used to transport the waste heat of the Stirling converters to radiator panels, which radiate the heat into ambient space. Heat pipes were modeled which linked the secondary heat transfer loop to the Stirling converters and the third heat transfer loop to the radiator panels. An alternator was used to convert the thermal power input of the Stirling converters into electrical power. The model was based on combining the point reactor kinetic equations with transient energy, force, volume, and mass balances for system components outside the reactor. The model was tested with dynamic perturbations that included small reactivity changes in the reactor, Stirling converter failures, effects of planetary albedo, and electrical resistance load changes. At steady state, the model produced the expected temperatures, pressures, flow rates, and heat flows. The dynamic simulations indicated that the overall system would be load following and stable to external perturbations. However, in cases that varied the electrical load resistance, the thermal efficiency of the Stirling converters were significantly affected.

14. SUBJECT TERMS: Stirling space nuclear power system ; space power system ; nuclear power ; converters	15. NUMBER OF PAGES **134**
	16. PRICE CODE

17. SECURITY CLASSIFICATION OF REPORT	18. SECURITY CLASSIFICATION OF THIS PAGE	19. SECURITY CLASSIFICATION OF ABSTRACT	20. LIMITATION OF ABSTRACT

Abstract

In this project, the components of a Stirling space nuclear power system were modeled using MATLAB® and Simulink® under both steady state and transient conditions. Using information provided through NASA's Glenn Research Center, the Department of Energy's Naval Reactors, and literature from previous work in nuclear space power systems, the system architecture was developed. At steady state, the space power system was designed to produce 200 kW(e) and consisted of a NaK cooled fast reactor linked to four Stirling power converters via two NaK heat transfer loops connected by heat exchangers. A third NaK heat transfer loop was used to transport the waste heat of the Stirling converters to radiator panels, which radiate the heat into ambient space. Heat pipes were modeled which linked the secondary heat transfer loop to the Stirling converters and the third heat transfer loop to the radiator panels. An alternator was used to convert the thermal power input of the Stirling converters into electrical power. The model was based on combining the point reactor kinetic equations with transient energy, force, volume, and mass balances for system components outside the reactor. The model was tested with dynamic perturbations that included small reactivity changes in the reactor, Stirling converter failures, effects of planetary albedo, and electrical resistance load changes. At steady state, the model produced the expected temperatures, pressures, flow rates, and heat flows. The dynamic simulations indicated that the overall system would be load following and stable to external perturbations. However, in cases that varied the electrical load resistance, the thermal efficiency of the Stirling converters were significantly affected.

Acknowledgements

Any project of this magnitude is always the result of multiple individuals. Although one author is listed, to say that one person wrote this document is truly an injustice. First, I would like to thank my advisers, Commander David Myre and Professor Martin Nelson, whose constant input, ideas, and experience played a large role in the progress of this project. Second, the information and help received from NASA and Naval Reactors provided a solid foundation from which to start and some idea of what the final product should provide. Most notably, I would like to thank Ed Lewandowski from NASA Glenn Research Center, Barry Penswick, and Mark Natale from Naval Reactors. Without Ed Lewandowski, I would probably still be trying to figure out how a Stirling converter works. Barry Penswick's help with the high power Stirling engine and Mark Natale's help with the reactor both removed the monumental hurdle of determining parameters for devices that have never actually been implemented.

I would like to thank all Naval Academy faculty involved with the Trident Scholar program. The committee readers (Professors Cerza, Nakos, and Zak), whose input provided important insight from a perspective of someone not directly involved in the project or the subject area, was crucial to my succcess. I would also like to acknowledge Professor Cerza's support and confidence at times when things were not running so smoothly. Also worth mentioning is the constant drive of Professor Shade, who helps connect all the pieces. All of the support from the various Naval Academy resources, such as Bob Disque and Mike Spinks in CADIG, Cindi Gallagher in MSC, Kelly Delikat in the Nuclear Lab, Nimitz Library, USNA Photo Lab, and the Public Affairs Office, all contributed in some way to make this project a success.

Most importantly, I would like to thank my parents, Gerald and Rita Langlois, and my fiancée, Rachel Pray, whose motivation and support are largely responsible for what I have accomplished in my life and for who I am today.

Table of Contents

List of Figures

List of Tables

Nomenclature

A	flow area of the unit cell
A_d	displacer cross sectional area
A_{evap}	evaporator area
A_{hx}	cross sectional flow area of a heat exchanger
A_n	cross-sectional area of space n
A_p	heat transfer area for primary coolant
A_{pist}	power piston cross sectional area
A_r	regenerator cross sectional area
A_{rad}	radiator surface area
A_{rod}	displacer rod cross sectional area
A_s	heat transfer area for secondary coolant
A_{wchan}	channel wetted area
A_{wh}	wetted heater area
A_{wk}	wetted cooler area
A_{wr}	wetted regenerator area
C	circuit capacitance
C_f	fuel specific heat
C_p	coolant specific heat
C_{pm}	coolant specific heat
C_{pm1}	coolant specific heat at reactor inlet temperature
C_{pm2}	coolant specific heat at reactor outlet temperature
D	damping coefficient
D_p	piston damping coefficient
D_f	fuel pin diameter
E	alternator voltage
$\dot{E}$	time derivative of the voltage
F	frictional force in a heat exchanger
F_p	damping force on the piston
$F(t)$	forcing function
I	circuit current
$\dot{I}$	first time derivative of the current
$\ddot{I}$	second time derivative of the current
L	alternator inductance
L_c	length of the condenser
L_e	length of the evaporator
L_f	length of a fuel rod
L_{hx}	heat exchanger length
L_{ind}	alternator inductance
L_r	regenerator length
L_t	tube length
K	local loss coefficient
N	number of fuel rod
N_{hp}	number of heat pipes
Nu	Nusselt number

Nu_1	Nusselt number for first heat exchanger primary fluid
Nu_2	Nusselt number for first heat exchanger secondary fluid
Nu_{chan}	channel flow Nusselt number
Nu_{rhpe}	Nusselt number of radiator heat pipe evaporator
N_t	number of tubes in heat exchanger
NTU_r	number of transfer units for the regenerator
P	reactor power
P_b	bounce space pressure
P_c	compression space pressure
P_e	expansion space pressure
Pe	Peclet number
Pe_{cr}	critical Peclet number
Pe_{rhpe}	flow Peclet number at the heat pipe
PE	reactor precursor power equivalence
Pr	Prandtl number
P_w	wetted perimeter
$\dot{Q}$	heat transfer rate between primary and secondary fluids
R	total resistive load
R_{alt}	alternator resistance
Re	Reynolds number
R_{gas}	gas constant
R_{hptot}	radiator heat pipe total thermal resistance
R_{load}	load resistance
R_{pc}	thermal resistance of the pipe at the condenser
R_{pe}	thermal resistance of the pipe at the evaporator
R_{wc}	thermal resistance of the wick at the condenser
R_{we}	thermal resistance of the wick at the evaporator
T_{ab}	section average coolant temperature
T_{abp}	section radiator panel temperature
T_{amb}	ambient space temperature
T_{arl}	channel exit coolant temperature
T_{brl}	section outlet temperature
T_{b1}	coolant temperature at heat exchanger entrance
$T_{c,i}$	colder fluid inlet temperature
$T_{c,o}$	colder fluid outlet temperature
T_{chan}	channel coolant temperature
T_d	average liquid metal temperature at the evaporator
T_f	average fuel core temperature
T_{fo}	equilibrium fuel temperature
T_h	heater gas temperature
$T_{h,i}$	hotter fluid inlet temperature
$T_{h,o}$	hotter fluid outlet temperature
T_i	temperature of the designated space, i
T_k	cooler gas temperature
T_m	average coolant temperature in reactor
T_{m1}	coolant temperature of reactor inlet

T_{m2}	coolant temperature at reactor outlet
T_{mo}	equilibrium coolant temperature
T_r	effective regenerator temperature
$T_r(x)$	temperature profile of the regenerator
T_{xrl}	channel entrance coolant temperature
T_{wh}	temperature of the heater wall
T_{wk}	temperature of the cooler wall
UA	overall heat transfer coefficient times the equivalent surface area of the heat exchanger
V	volume
V_{chan}	channel volume
V_{cs}	section coolant volume
V_f	fuel volume in reactor
V_m	coolant volume in reactor
V_{rad}	radiator volume
$\dot{W}_e$	electrical power produced by engine
X_p	maximum piston displacement
Z_{alt}	total impedance of the alternator circuit
Z_{ind}	alternator inductor impedance
Δp	pressure difference across a heat exchanger
Δp_h	heater pressure loss
Δp_k	cooler pressure loss
Δp_r	regenerator pressure loss
ΔT_{lm}	log mean temperature difference
Λ	neutron generation time
c_p	average specific heat, constant pressure
c_{pr}	radiator specific heat
c_v	average specific heat, constant volume
d_e	equivalent diameter of the flow passage
d_h	hydraulic diameter
d_i	heat exchanger tube inner diameter
d_{iw}	inner diameter of the wick
dm_{ck}	compression-cooler boundary mass flow rate
dm_{he}	heater-expansion boundary mass flow rate
dm_i	mass flow rate in
dm_{kr}	cooler-regenerator boundary mass flow rate
dm_o	mass flow rate out
dm_{rh}	regenerator-heater boundary mass flow rate
d_o	heat exchanger tube outer diameter
d_{op}	heat pipe outer diameter
d_{ow}	outer diameter of the wick
dQ	heat transfer rate
dQ_{hi}	ideal heater heat transfer
dQ_{hp}	heat transfer through the heat pipes
dQ_{ki}	ideal cooler heat transfer
dV_c	time derivative of compression space volume

dV_e	time derivative of expansion space volume
dW	rate of work, power
d_w	wire diameter
f	frequency
fr	friction factor
h	convection coefficient
h_{chan}	channel heat transfer coefficient
h_h	heater heat transfer coefficient
h_k	cooler heat transfer coefficient
h_{lp}	heat transfer coefficient from the liquid metal to the pipe
h_p	convection coefficient for heat exchanger primary coolant
h_r	regenerator heat transfer coefficient
h_s	convection coefficient for exchanger secondary coolant
k	fluid thermal conductivity
k_{alt}	alternator constant
k_{eff}	effective conductivity of the wick
k_f	fuel thermal conductivity
k_l	thermal conductivity of the working fluid
k_{NaK}	NaK thermal conductivity
k_p	conductivity of the pipe
k_s	spring constant
k_t	tube conductivity
k_m	conductivity of the coolant
m	mass of displacer or piston
m_c	compression space mass
$\dot{m}_{chan}$	coolant mass flow rate
m_e	expansion space mass
m_h	heater space mass
m_k	cooler space mass
$\dot{m}_m$	coolant mass flow rate
m_r	regenerator space mass
$\dot{m}_{rl}$	heat rejection loop mass flow rate
m_w	total mass of working gas
n	subscript designating space
p	working space pressure
p_f	fuel pin pitch
p_t	heat exchanger tube pitch
r_f	radius of fuel pin
t	time
u	fluid velocity
u_n	flow velocity in space n
x	mass position
$\dot{x}$	mass velocity
$\ddot{x}$	mass acceleration
x_p	piston displacement

$\dot{x}_p$	piston velocity
α_f	fuel temperature coefficient
α_m	coolant temperature coefficient
β	delayed neutron fraction
β	regenerator porosity
β_w	wick porosity
ε	radiator emissivity
ε_r	regenerator effectiveness
η	heat exchanger efficiency
η_{alt}	alternator efficiency
η_{conv}	instantaneous converter efficiency
λ	precursor decay constant
μ	fluid viscosity
μ_m	coolant viscosity
ρ	reactivity
ρ	fluid density
ρ_f	fuel density
ρ_{gr}	graphite density
ρ_m	coolant density
ρ_n	flow density in space n
ρ_{NaK}	NaK coolant density
ρ_o	initial reactivity
σ	Stephan-Boltzman constant
τ	time delay for the coolant to travel from the reactor to the heat exchanger
ω	angular frequency
ζ	damping ratio

"In conclusion then, the navigation of interplanetary space depends for its solution on the problem of atomic disintegration... Thus, something impossible will probably be accomplished through something else which has always been held equally impossible, but which remains so no longer."
- Robert H. Goddard, October 3, 1907

1. Background

While many components come together to make a spacecraft, the component that has the most significant impact on the spacecraft is its power system. If a spacecraft was compared to a human, its power system would be described as its cardiovascular system. All other functions of the spacecraft rely on it and the spacecraft would be inoperable without it. This is best shown by the recent Japanese spacecraft ADEOS-2, Advanced Earth Observing Satellite, which has been deemed "all but lost" after its power system suffered a catastrophic failure.[1] Therefore, space power systems must not only be designed to facilitate the operations of the spacecraft, but they must also be designed to withstand the variety of stimulus that the space environment has to offer. Large changes in current or voltage within the power system components can lead to decreased performance or failure of the subsystems. The failure or degradation of these components can render the spacecraft incapable of performing its mission.

In the recent past, the space community has consistently used photovoltaic and chemical means of providing power. These power systems have performed very well for their low power missions near Earth. However, their application to missions farther from the Earth or missions requiring higher power levels is very limited. Current state of the art solar cells, such as Spectrolab's Ultra Triple Junction solar cells, can reach efficiencies of almost thirty percent.[2,3] With a solar flux at the Earth of approximately 1360 W/m², a solar panel that is directly facing the sun at all times could theoretically produce power densities of around 400 W/m². To have a solar array capable of

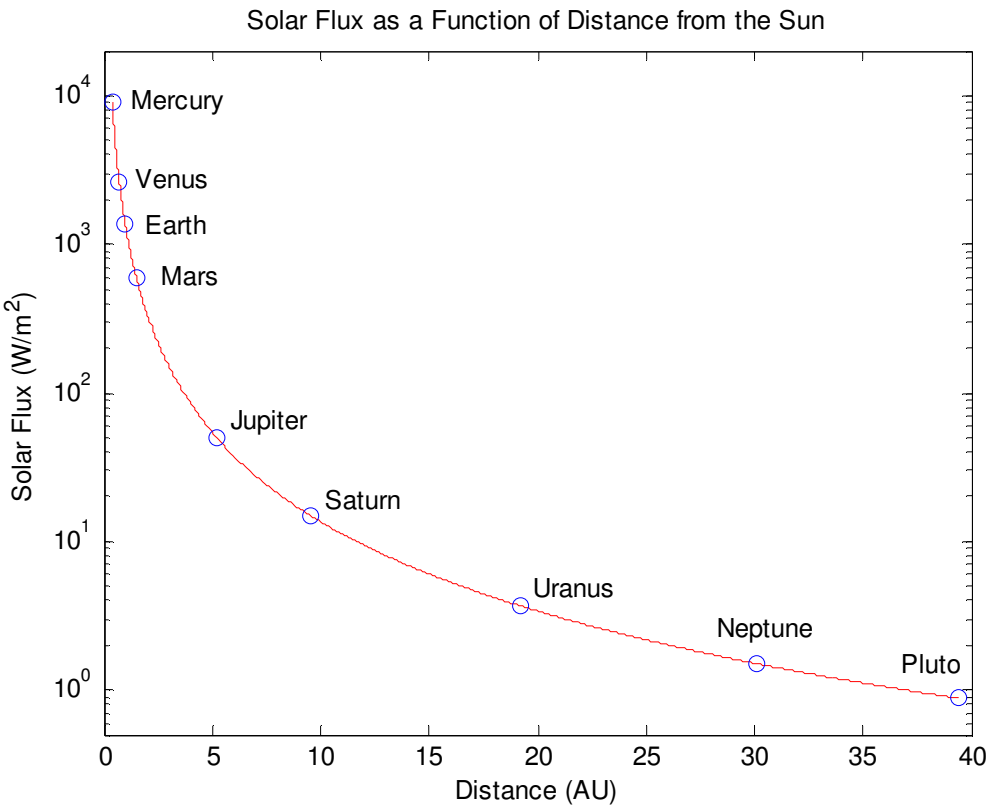

Figure 1-1. Solar energy flux relative to the Earth. (AU=astronautical unit, the distance between the centers of the Earth and Sun, 1.495x10^8 km)

producing 200 kW(e) of power, which is the approximate power level of the Prometheus spacecraft,[4] a solar array of 500 square meters would be needed. An array of this size would be the equivalent size of a tenth of a football field. This calculation neglects the degradation of the panels over time, the fraction of light reflected off the panels, the possibility of the Earth or other objects blocking the sunlight, and the extra panels needed for a power margin. The energy flux from the sun is also inversely proportional to the square of the distance from the Sun. So for a spacecraft orbiting Jupiter, which is five times farther from the Sun than the Earth, twenty-five times more solar panel area is needed to produce the same amount of power (Figure 1-1).[5] This means that a solar panel area equal to that of about three footballs fields would be required. Improvements in efficiency and mass alone will not solve these problems since the huge array areas

required for high power will create obstacles in structural integrity, stowing for launch, deployment in orbit, and sun pointing that are far from being solved with current technology.[6] The effects of the Sun also prevent the use of solar power for missions closer to the sun. The increase in energy and radiation from the Sun destroy solar panel materials when spacecraft get too close.

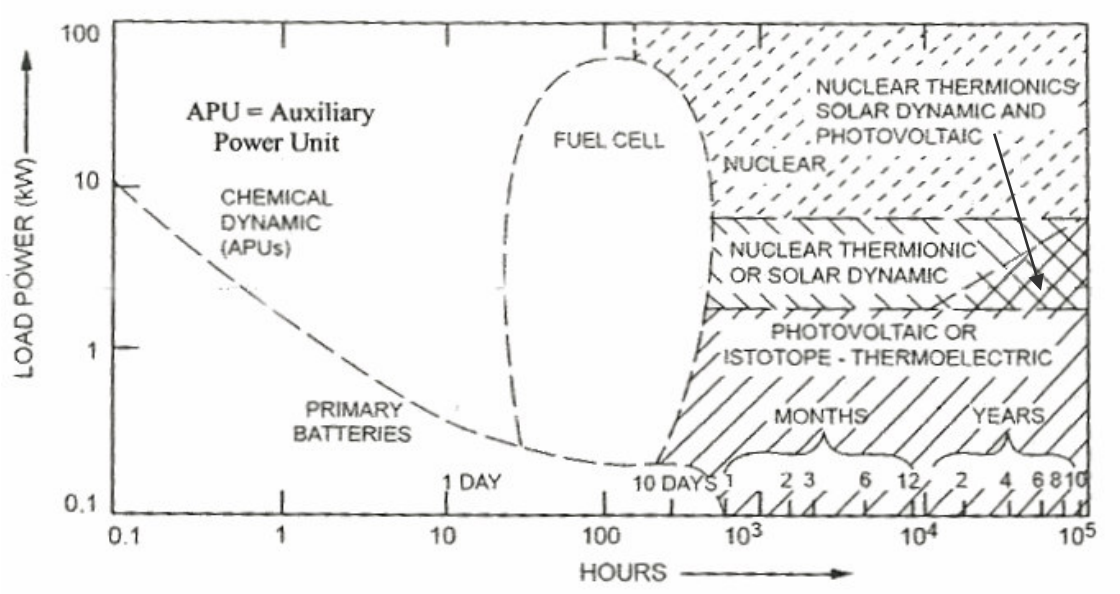

Figure 1-2. Space power sources as a function of mission power level and duration. [8]

In an effort to increase the capabilities of space exploration, the space community has turned to nuclear power as a source of continuous power for deep space missions. For lower power missions, radioisotope thermal generators (RTG's) have been extremely successful. RTG's use the thermal energy released by radioactive decay to produce electricity. Missions that have used RTG's include Pioneer, Voyager, Viking, and the more recent Cassini spacecraft. The Pioneer 10 spacecraft was still running on its RTG after 30 years in space.[7] The load produced by various space power sources versus mission duration is given in Figure 1-2.[8] As can be seen, RTG's are limited to around 2 kW(e) if they are to be cost efficient.

In order to accomplish deep space missions that require higher power levels, the space community has turned to fission reactors for the solution. This is because fission of one kilogram of uranium-235 produces 500,000 times the amount of energy released by the decay of one kilogram Plutonium-238 (used in RTG's) over ten years.[9] Starting as early as the mid-1950's, the United States explored fission reactors as a space power source with the Systems for Nuclear Auxiliary Power (SNAP) program. This program resulted in the only reactor flown in space by the United States. Also, Russia has been using small fission reactors as space power sources since the early 1960's.[10] In the late 1970's, the United Nations Working Group on the Use of Nuclear Power Sources in Outer Space recognized the advantages of nuclear power in space and recommended its use for

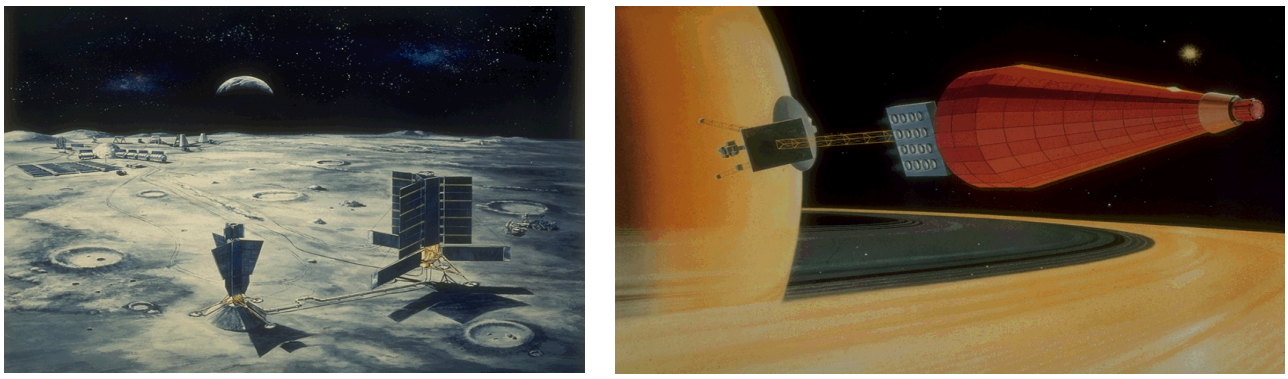

Figure 1-3. SP-100 surface power concept (left) and nuclear electric propulsion spacecraft concept (right). [12]

technical pursuits.[11] Shortly thereafter, the United States reinitiated its pursuit of nuclear fission power in space with the SP-100 program (Figure 1-3). The SP-100 program lasted until the early 1990's and consisted of studies for various nuclear fission power spacecraft configurations and missions.[12] The studies provided positive insight into the use of nuclear fission power in space and recommended several concepts. Since there was never a mission requirement for the SP-100 program, the program was canceled without ever completing a space mission.[13]

Today, even with the advances in solar panel materials and efficiency over the past decade, NASA has come to the conclusion that nuclear fission power is necessary for high power, deep space missions. NASA recently initiated the Prometheus Project to

Figure 1-4. The conceptual design of the JIMO nuclear electric propulsion spacecraft. [14]

make the vision of space nuclear power and propulsion into a reality by developing missions along with the technology. The first proposed mission for the project was the Jupiter Icy Moons Orbiter (JIMO, Figure 1-4), which would use a nuclear powered, electric propulsion spacecraft to investigate three of Jupiter's moons in great detail.[14] NASA has recently reconsidered JIMO and postponed the mission due to the high risks involved.[15] Instead, the Prometheus Program will develop a lower risk mission for the initial Prometheus undertaking. NASA is pursuing this lower risk and lower cost program to increase the likelihood of success. One of the proposals for this initial mission includes a surface power system for the Moon or Mars, similar to the SP-100 program.

With the technology provided by NASA, a mission to Mars can be achieved three times faster than with current chemical propellants.[16] For propulsion, chemical

propellants are the standard fuel for launch into Earth orbits. While this will most likely continue to be the case for future missions, propulsion from Earth orbits to distant locations of the solar system become costly or time consuming using chemical propellants. For example, the mass of the current Atlas V 500 series rocket with Centaur upper stage is 91.5% propellant.[17] This leaves little room for improvement in terms of launching a spacecraft farther into the solar system. Either the mass of the spacecraft has to be reduced by removing components or more fuel has to be added. If the spacecraft's time of flight is to be reduced, even more fuel must be added. This is due to the fact that specific impulse, which measures how efficiently a rocket can achieve a velocity change for a given mass of propellant, is four to twelve times less for chemical propellants than for the electrostatic ion engines proposed for the JIMO mission.[18] As a result, spacecraft using chemical propulsion are limited to having only 10-20% of its mass as the payload, while nuclear power and propulsion are able to raise this number to forty percent.[19] With nuclear power, ion engines (Figure 1-5) would have the capability of continuous operation without prohibiting the use of other instruments or systems on the spacecraft.[20]

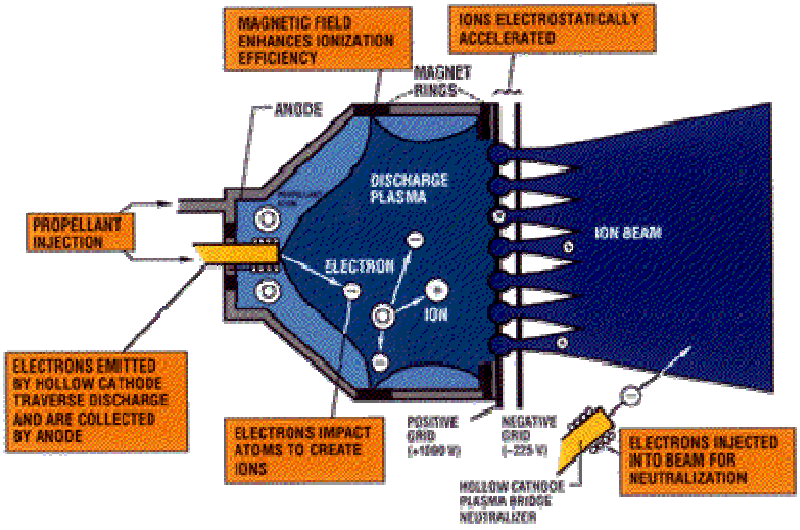

Figure 1-5. Conceptual diagram of electric propulsion. [20]

However, the nuclear reactor is just one of several system components that will make up the space power system. Another major system component is the energy converter, the object which will convert the thermal energy of the nuclear reactor into electrical power. Most highly developed space nuclear power system studies have involved thermoelectric converters, which use the electrical potential created by the temperature gradient across a material to produce electricity. However, these converters have very low efficiency (≈ 5%)[21] and NASA is currently considering the mechanical alternatives using power converters based on Brayton and Stirling cycles.

In a NASA contractor report, the performance of Stirling and Brayton converters in the SP-100 power system is compared.[22] The results of the report assert that when an SP-100 reactor is coupled with Brayton or Stirling cycle engines with the same power requirement, the Stirling cycle option has a greater net cycle thermal efficiency and lasts longer (Table 1-1).[22] This means that Stirling cycle engines have the potential for longer

Parameter	Brayton	Stirling
Net Power (kW)	550	550
Gross Power (kW)	582	596
Reactor Thermal Power (kW)	2,309	1,850
Net Cycle Thermal Efficiency (%)	**23.8**	**29.7**
Possible Carnot Efficiency (%)*	68.77	52.41
Full Power Lifetime (yrs)	7.6	9.6
Operating/Redundant Converters	3/1	3/1
Temperatures (K)		
Reactor Outlet	1,355	1,355
Average Maximum	1,300	1,265
Average Minimum	406	602
Radiator Area (m^2)	590	210
System Mass (kg), 1000 Vdc	15,768	14,932
System Mass (kg), 1000 Vrms, 1 kHz	14,903	15,217

Table 1-1. SP-100 Brayton vs. Stirling comparison. [22]
***Field added by the author.**

mission life or lower launch weight. Additionally, the Brayton cycle option has received significant attention in terms of analysis and modeling. Thus a study of the Stirling option could produce some meaningful results in an area that has received less attention. This is especially true for a model of large Stirling engines such as those used for the SP-100 design. Creating a model using this size of a Stirling engine and coupling the engine to a nuclear reactor are both very unique undertakings. For this project, a computer model of a Stirling nuclear power system was created using MATLAB® and Simulink® software. The model development completed the following objectives:

(1) Developed time-variant computer models for the thermodynamic, mechanical, and electrical processes of the reactor, Stirling engines, radiators, alternators, and heat transfer components.

(2) Used empirical data from Naval Reactors and NASA to determine system parameters (sizes, ratios, etc.).

(3) Validated the model mathematically and physically (engineering).

(4) Tested the system's stability by modeling the response to possible perturbations (i.e. engine failure, reactivity changes).

(5) Increased system performance characteristics such as efficiency or specific power.

The most significant objectives were (1) and (2). All other objectives were secondary and were based on the thorough completion of the first two objectives.

The system studied consists of several components which have been previously investigated in-depth. While the behavior of the individual components of this system is well studied and understood, the resulting behavior of the combination of the non-linear systems has never been undertaken before now. Since Stirling converters are being considered as one of the main options for future space power system development, this study provides knowledge for the possible development of these future systems.

2. System Overview

The process of nuclear electric power (NEP) can be simply stated as the conversion of thermal energy released by nuclear reactions to electrical energy. For this research, the

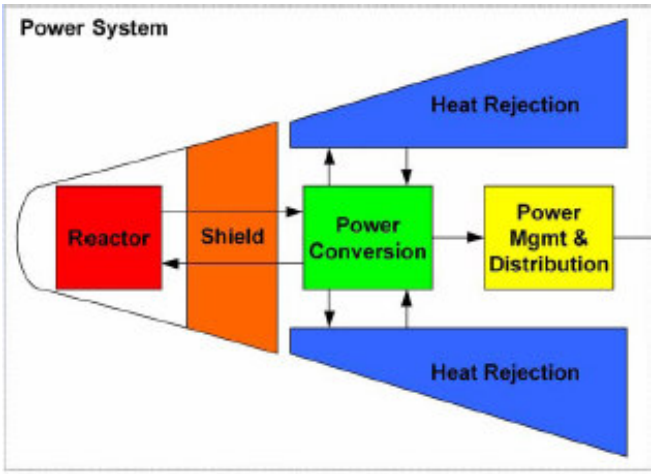

Figure 2-1. General NEP structure. [20]

three sections of the NEP system that were modeled and evaluated are the reactor, power conversion, and heat rejection components.[23] This section gives an overview of the components that are included within these sections for a Stirling nuclear space power system.

The reactor chosen for this research is a liquid metal fast reactor (LMFR). A LMFR consists of an original fuel source of enriched uranium, which is uranium that has a higher than naturally occurring percentage of uranium-235. This enriched uranium also contains uranium-238, which can absorb fast neutrons to produce plutonium-239. In unconstrained fission, a neutron is absorbed by a fissile nucleus. The nucleus becomes unstable and splits, releasing energy, neutrons, and fission products (Figure2-2).[24] For uranium-235 and plutonium-239, 2.6 and 2.98 neutrons are released, respectively, on average in a fast reactor.[25]

A fast reactor is a system in which neutrons maintain an energy near the magnitude they are produced. To accomplish this, materials which contain low atomic mass

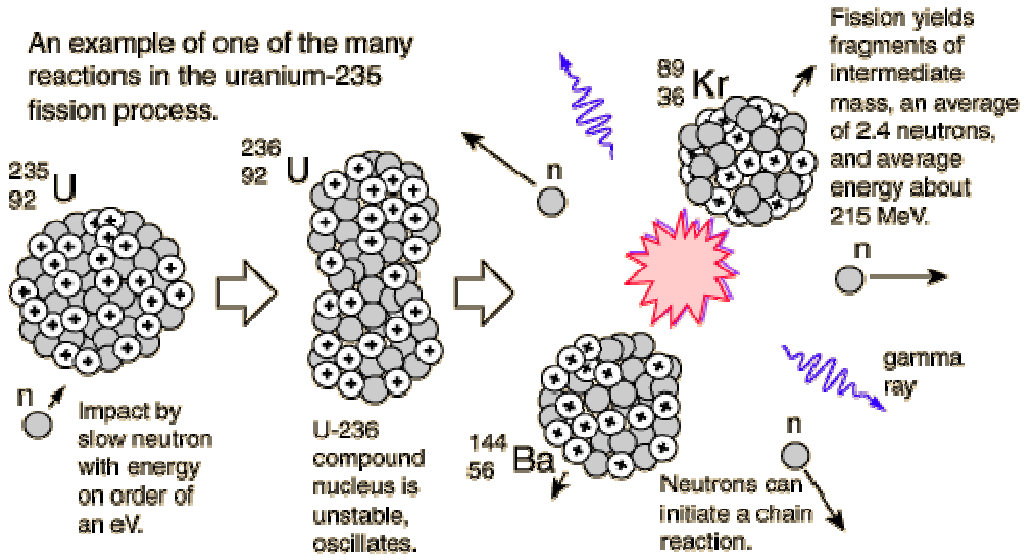

Figure 2-2. Fission of uranium-235. In a fast reactor, the average number of neutrons released increases to 2.6. [24]

elements, such as water, must not be present. Liquid metals work well since they have relatively high atomic masses. For this research, sodium-potassium metal (NaK) is used as the liquid metal coolant. Sodium-potassium allows the reactor to achieve high power densities, defined as power produced per unit volume, due to its high conductivity combined with its relatively high boiling point.[25]

The heat transfer from the reactor to the Stirling engines is facilitated by two sodium-potassium heat transfer loops as shown in Figure 2-3. Two fluid loops are used to avoid material degradation issues that may result from the radioactive isotopes created in the primary loop when coolant passes through the reactor. For example, sodium will absorb neutrons to form the beta-gamma emitter ^{24}Na. By using two loops linked with a heat exchanger, the radioactive isotopes can be contained within the primary loop and the

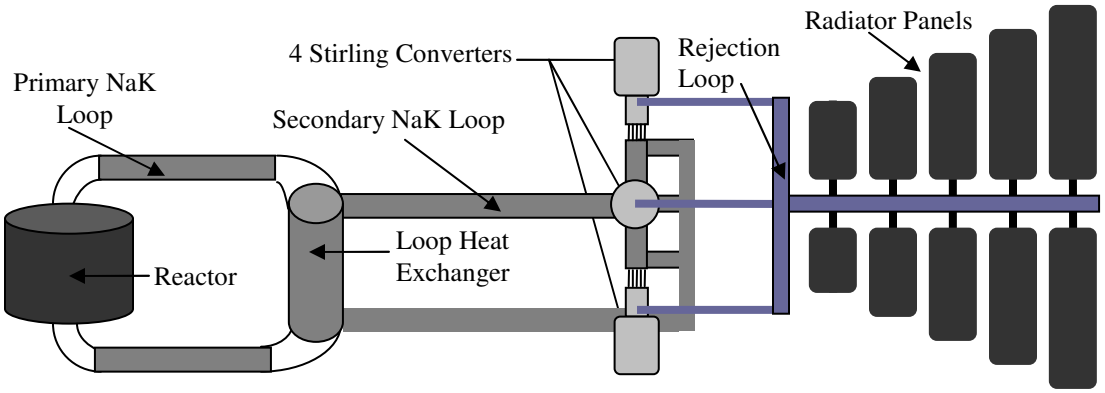

Figure 2-3. Schematic of the Stirling space nuclear power system (not to scale).

reactor while a non-radioactive secondary loop can transfer heat directly to the Stirling converters. This two loop configuration is commonly used with a LMFR.

The problem of moving the heat from the second heat transfer loop to the Stirling engine was investigated during the design process for the SP-100 power system. A method chosen by the SP-100 program is shown in Figure 2-4 and has been adopted for this project.[26] This method involves using heat pipes with evaporator ends exposed to the secondary loop coolant flow and condenser ends integrated into the geometry of the Stirling hot end heat exchanger. A heat pipe is a device that uses a working fluid saturated between liquid and gas phases to transfer heat. A saturated fluid is a fluid that

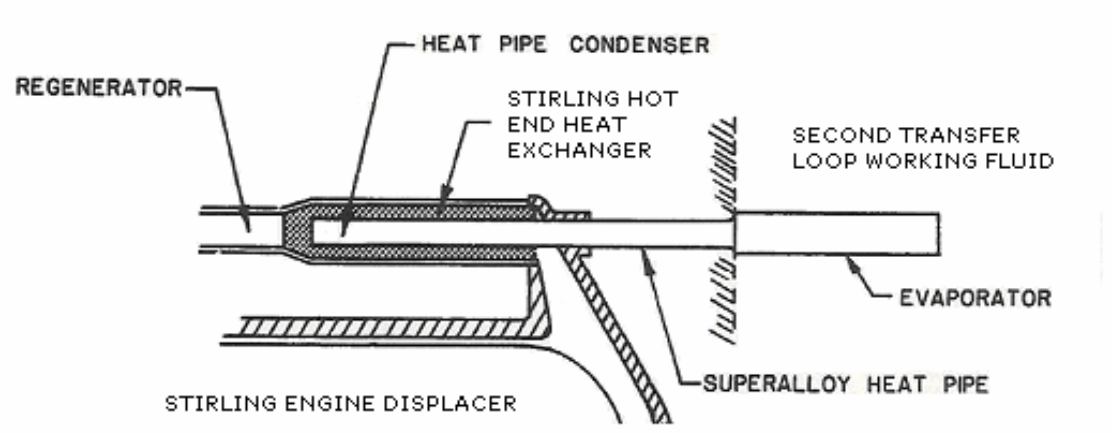

Figure 2-4. Design to transfer heat from the liquid metal of the second heat transfer loop to the heater of the Stirling engine.[26]

is in the process of changing phases, such as liquid to gas. While changing phases, the working fluid maintains an almost constant temperature as the energy it receives is used to overcome the latent heat of vaporization and complete the phase change. The working fluid absorbs energy at one end of the heat pipe and releases energy at the other, which keeps the working fluid temperature within the saturated region (Figure 2-5).[27] The constant temperature of the saturated fluid results in a small temperature drop across the

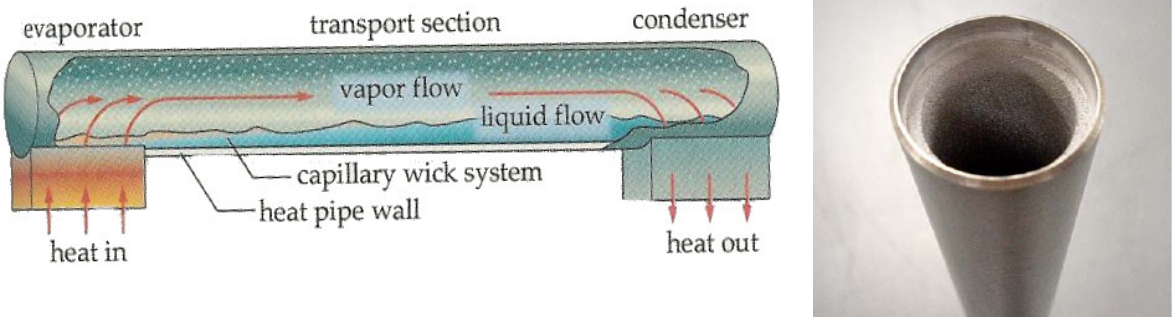

Figure 2-5. Basic process of a heat pipe, left, and a cross-section of an actual heat pipe, right. [27, 46]

heat pipe.

A Stirling converter is a device capable of using the temperature difference provided by a heat source and a heat sink to produce work via a gaseous working fluid. The ideal Stirling cycle consists of four processes: isothermal compression, isometric heat addition,

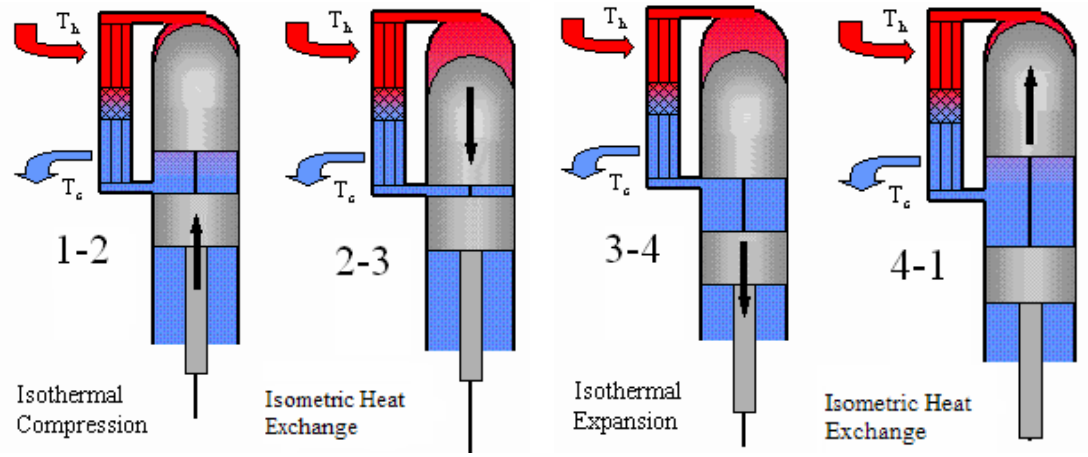

Figure 2-6. Ideal Stirling cycle with single piston and displacer. (www.grc.nasa.gov/WWW/tmsb/stirling/Slidepage_4.html)

isothermal expansion, and isometric heat rejection (Figure 2-6). This ideal cycle has the capability of producing Carnot efficiency, which is the maximum theoretical efficiency a thermodynamic cycle can have for a given hot to cold fluid temperature ratio (T_h/T_c). However, for the practical application of Stirling power converters, this ideal cycle is not beneficial and can never be completely achieved. In order to model such an ideal cycle where net work is maximized, the ideal Stirling P-V relationship shown in Figure 2-7 requires the frequency of the cycle to approach zero.[28] Yet, the purpose of the Stirling converter is to produce power, which is the product of the net work created per cycle and the frequency. If the frequency of the converter approaches zero, the power of the converter approaches zero and converter power is sacrificed for efficiency. So, in reality, the Stirling converter is operated at some frequency and the pressure volume diagram becomes less ideal in shape (Figure 2-7).[29,30]

The main components of the Stirling converter are the heater, regenerator, cooler, displacer, power piston, and alternator. The heater and cooler provide a continuous heat source and sink, respectively, for the Stirling converter. The regenerator adds efficiency to the cycle by cooling the hot gas as it moves from the expansion space to the

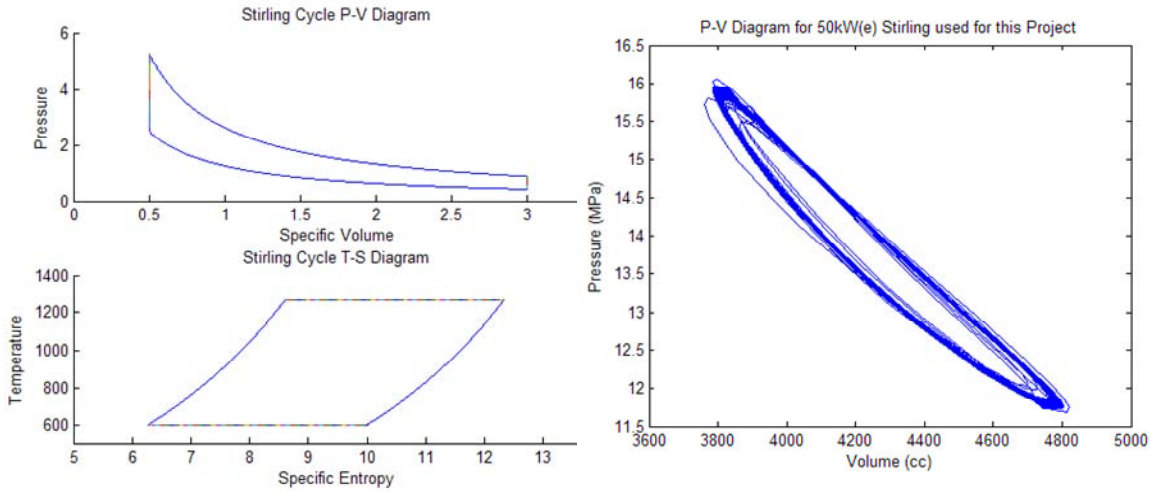

Figure 2-7. Comparison of an ideal (left) and a practical (right) pressure-volume diagram for a Stirling converter. The net work of the cycle is the area within the curve.

compression space and by heating the cold gas as it moves from the compression space to the expansion space. The displacer is a moving component that separates the cold compression space from the hot expansion space. It is the pressure and temperature

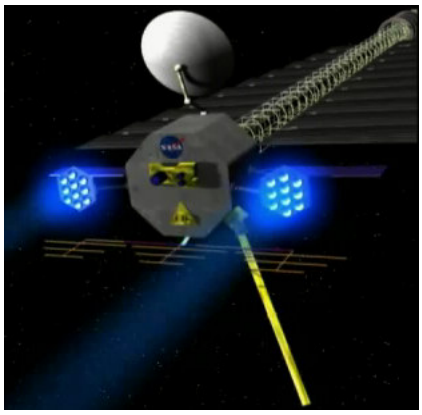

Figure 2-8. Conceptual drawing of JIMO propulsion, radar, and communication systems [31].

gradients across the displacer that create force imbalances on the moving components of the Stirling converters, the piston and displacer. These forces convert the thermal energy of the working fluid into the motion of the piston or displacer. The mechanical energy, or motion, of the piston is then converted into electrical energy using a linear alternator. The linear alternator consists of magnets that are linked to the piston and coiled wires that are linked to the Stirling casing. The motion of the magnets produces a voltage within the coils based on the velocity of the piston. This voltage then creates current and electric power based on the impedance of the associated electrical circuit. The resulting electrical power can be used for scientific instruments, energy storage, or any other device that requires electricity. For the JIMO mission, this would include the Prometheus spacecraft's radar and electric propulsion units, and other spacecraft subsystems (Figure 2-8).[31]

In order for Stirling power converters to convert thermal energy into electrical power, there must be a heat source and a heat sink. The heat source for the Stirling converters is

the heat generated by the nuclear reactor. The heat sink for the Stirling converters is deep space, and the heat rejection is accomplished using heat pipes in combination with radiator panels. The excess heat of the Stirling cycle is transferred to a liquid water loop by forced convection. Heat pipes transfer the heat from the fluid loop to the radiators. Due to the small temperature drop across heat pipes, they provide an equalized energy distribution to the radiators that helps maximize the radiation of heat into space for a given radiator geometry, which in turn minimizes the amount of radiator surface area needed.[32] Since radiators are the second largest source of system mass, minimizing their mass is an important factor in the overall system design, but was beyond the scope of this project.

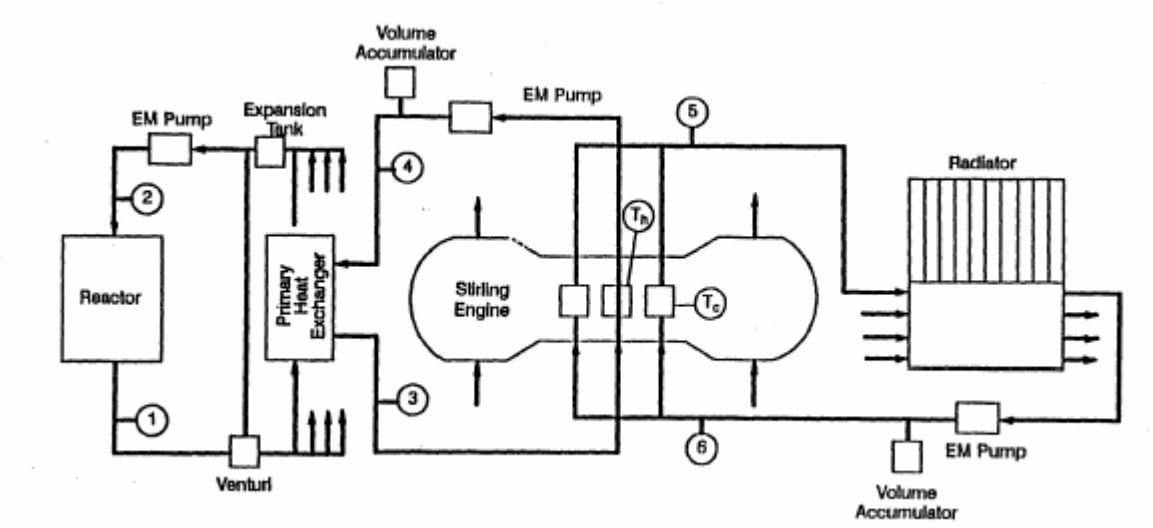

Figure 2-9. Diagram of the SP-100 general system design. The system modeled by this research is of the same general design. [22]

The following sections (3-5) provide a detailed description of the model chosen and the applicable assumptions and parameters for each component of the Stirling space nuclear power system. The mathematics and science behind each model are elaborated upon and justified. Section 3 discusses the reactor and the connected heat transfer loops.

Section 4 describes the Stirling converters and Section 5 details the heat rejection system. Then, the component and integrated component simulation results are presented and discussed in Section 6. The final section, Section 7, concludes with a brief summary of the work accomplished, conclusions made, and a recommendation for future work.

3. Reactor, Heat Exchanger, and Heat Pipe Models

3.1 Nuclear Reactor

The reactor that is modeled for this project is a 600 kW(t) fast fission reactor consisting of uranium nitride fuel and sodium potassium coolant. Its dynamic behavior is modeled using the one group point kinetics equations, which treats the reactor as a point source of power and ignores the loss of fuel mass over time. The latter assumption does not produce significant error since tests are run over relatively short time periods with respect to fuel consumption. The equations used also simplify the many possible combinations of fission products into one average group. The point kinetics equations use the properties of the reactor's fuel, coolant, and geometry to model the reactor's power, component temperatures, and other factors over time.[33]

$$\frac{dP}{dt} = \frac{\rho - \beta}{\Lambda} P + \lambda PE \qquad 3\text{-}1$$

$$\frac{dPE}{dt} = \frac{\beta}{\Lambda} P - \lambda PE \qquad 3\text{-}2$$

$$\rho = \rho_o + \alpha_f (T_f - T_{fo}) + \alpha_m (T_m - T_{mo}) \qquad 3\text{-}3$$

where:
P = reactor power
PE = reactor precursor power equivalence
ρ = reactivity (ρ_o = initial reactivity)
β = delayed neutron fraction
Λ = neutron generation time
λ = precursor decay constant
α_f = fuel temperature coefficient
α_m = coolant temperature coefficient
T_m = coolant temperature
T_f = average fuel core temperature
T_{mo} = equilibrium coolant temperature
T_{fo} = equilibrium fuel temperature

Equations 3-1 and 3-2 of the point kinetics equations relate the rate of change of the reactor's power and precursor power equivalence to the time dependent variables of reactivity (ρ), power (P), and precursor power equivalence (PE) and the reactor constants of delayed neutron fraction, neutron generation time, and precursor decay constant. The power of the reactor is a result of fission and the precursor power equivalence is a function of fission product decay. The reactivity of a reactor is a function of the neutron multiplication factor, k, where k is the ratio of the number of neutrons in the present generation and the number of neutrons in the preceding generation (Equations 3-4 and 3-5). For a reactor producing a steady power level, the number of neutrons in one generation produces an equal amount of neutrons in the next generation. This state corresponds to a multiplication factor value of one and a reactivity value of zero.

$$\rho = \frac{k-1}{k} \qquad 3\text{-}4$$

$$k = \frac{\#\text{ of neutrons in present generation}}{\#\text{ of neutrons in the preceding generation}} \qquad 3\text{-}5$$

Equation 3-3 determines the reactor's reactivity at a given time according to the initial values of the reactivity, fuel temperature, coolant temperature and the values of fuel and coolant temperature and temperature coefficient. The temperature coefficients of the fuel and coolant use a linear approximation to characterize the change in the reactor's reactivity due to temperature change. Values for the temperature coefficients are a function of the materials that make up the fuel and coolant. The temperature coefficient plays a large role in the stability of the reactor since it defines the response of the reactor due to temperature change. The temperatures of the fuel and the coolant affect their density and nuclear cross sections, which in turn affect the overall reactivity of the

reactor. To have a self-stabilizing reactor, a negative fuel temperature coefficient is required. A negative fuel temperature coefficient decreases the reactivity as temperature rises and increases the reactivity as temperature decreases. Therefore, a negative fuel temperature coefficient results in the reactor naturally trying to maintain its current power level. On the other hand, a positive fuel temperature coefficient will cause the reactor to diverge from its current power level.

The neutron generation time is typically about the same value for all fast reactors. The delayed neutron fraction and decay constant are properties of Uranium-235. Using these values and the initial condition of zero reactivity, the steady state reactor precursor power equivalence can be determined for a 600 kW(t) reactor power (Equations 3-1 and 3-2). This power level was calculated using the 200 kW(e) power requirement and the assumption that the Stirling converters have about thirty-three percent efficiency. The power level of the reactor changes the temperatures of the fuel and coolant according to relationships that are dependent on the reactors geometry, materials, and coolant flow rate. For a square lattice circular fuel pin geometry (Figure 3-1), these relationships can

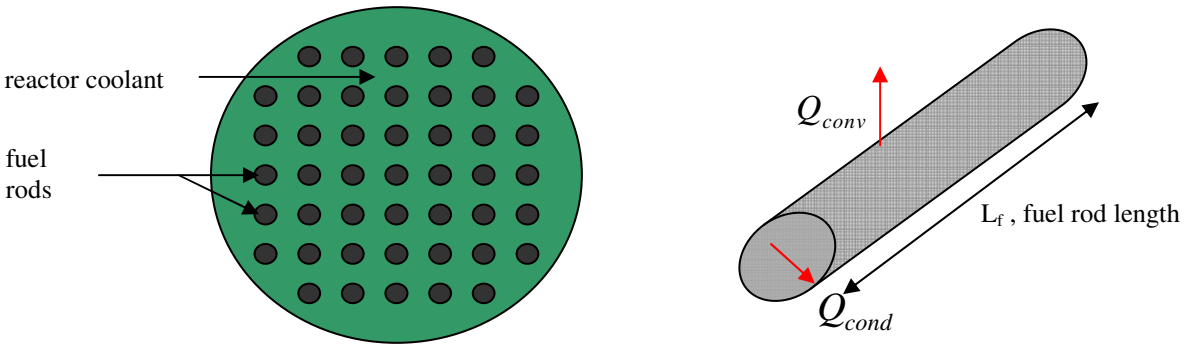

Figure 3-1. Circular fuel pin geometry with square lattice.

be expressed by Equations 3-6 through 3-9.[34] The state of the different system components is monitored by calculating temperature as a function of time. This method makes it easier to discover model errors and predict component interaction.

$$\rho_f V_f C_f \frac{dT_f}{dt} = P - \frac{4\pi N L_f k_f}{1 + 2k_f /(r_f h)}(T_f - T_m) \qquad 3\text{-}6$$

$$\rho_m V_m C_{pm} \frac{dT_m}{dt} = \frac{4\pi N L_f k_f}{1 + 2k_f /(r_f h)}(T_f - T_m) + 2\dot{m}_m (C_{pm1} T_{m1} - C_{pm} T_m) \qquad 3\text{-}7$$

where:
ρ_f = fuel density
ρ_m = coolant density
C_f = fuel specific heat
C_{pm} = coolant specific heat
C_{pm1} = coolant specific heat at reactor inlet temperature
C_{pm2} = coolant specific heat at reactor outlet temperature
N = number of fuel rod
L_f = length of a fuel rod
k_f = fuel thermal conductivity
r_f = radius of fuel pin
h = convection coefficient
$\dot{m}_m$ = coolant mass flow rate
T_f = average fuel core temperature
$T_m = (T_{m1} + T_{m2})/2$ = average coolant temperature in reactor
T_{m1} = coolant temperature of reactor inlet
T_{m2} = coolant temperature at reactor outlet
V_f = fuel volume in reactor
V_m = coolant volume in reactor

Originally, a lumped capacitance model was considered, which neglects the thermal temperature gradients within the fuel pin and assumes that the fuel is one uniform temperature. However, for the lumped capacitance method to be valid, the Biot number has to be much less than one (Bi<0.1).[35] The Biot number is calculated using Equations 3-8 and 3-9.

$$Bi = \frac{hL_f}{k_f} \qquad 3\text{-}8$$

$$h = \frac{k_m}{d_e} Nu \qquad 3\text{-}9$$

where: k_m = conductivity of the coolant

$d_e = \frac{4A}{P_w}$ equivalent diameter of the flow passage
A = flow area of the unit cell (Figure 3-2)
P_w = wetted perimeter ($2\pi r_f$ for this geometry)
Nu = Nusselt number

Since the Biot number was close to one hundred, the thermal resistance of the fuel rod was included by using the geometry shown in Figure 3-1. The temperature of the fuel pin surface can be eliminated by mathematical manipulation of the conduction and convection equations, resulting in the form of Equations 3-6 and 3-7. The Nusselt number in Equation 3-10 is valid when the condition in Equation 3-11 is met. The high conductivity of liquid metals results in their ability to assume a constant Nusselt number based on the pitch to diameter ratio of the fuel lattice if the Peclet number is below the critical Peclet number. The critical Peclet number for this problem was 460, which is significantly greater than NaK's Peclet number of 17 in this case.

$$Nu = 7.0 + 4.24(p_f / D_f)^{1.52} \qquad 3\text{-}10\ [36]$$

if $$Pe \le Pe_{cr} \qquad 3\text{-}11$$

where: p_f = fuel pin pitch (Figure 3-2)
$D_f = 2r_f$ = fuel pin diameter (Figure 3-2)
Pe = RePr = Peclet number
Re = Reynolds number, $\mathrm{Re} = \rho_m u d_e / \mu_m$
Pr = Prandtl number, $\mathrm{Pr} = C_{pm}\mu_m / k_m$
Pe_{cr} = critical Peclet number
C_{pm} = coolant specific heat
μ_m = coolant viscosity

Coolant enters the reactor at a temperature lower than the fuel's temperature. Energy is then transferred from the fuel to the coolant as the coolant flows along the length of the fuel rod. The coolant mass flow rate and temperature difference across the fuel

determines the thermal energy that the fuel adds to the coolant. This interaction can be modeled using the conservation of energy in the reactor coolant (Equation 3-7).

The geometry of the reactor consists of cylindrical fuel rods arranged in a square lattice (Figure3-2 and 3-3). The reactor can be modeled as a series of unit cells, shown in Figure 3-2. The number of fuel pins, fuel mass, coolant mass, and steady state

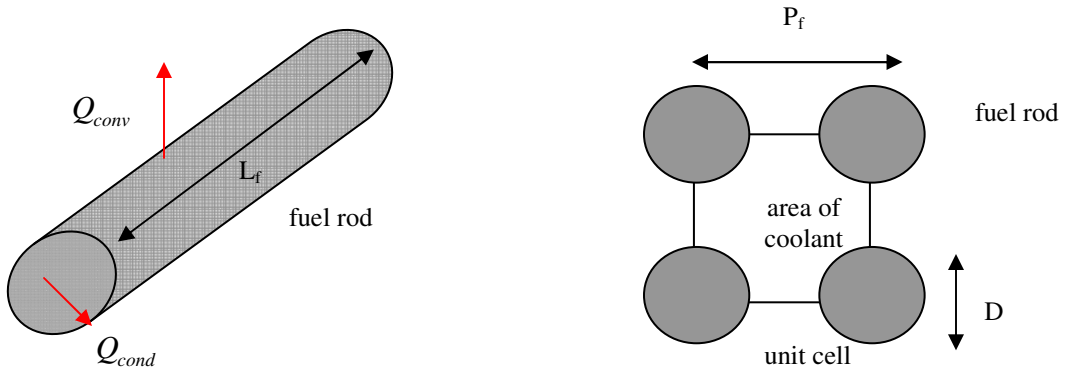

Figure 3-2. (left) A fuel rod conducts the heat from the nuclear reactions to its surface by the relationship $Q_{cond}=4\pi L_f k_f(T_f-T_s)$, where T_s is the fuel surface temperature. The heat is then convected to the coolant according to $Q_{conv}=2h\pi r_f L_f(T_s-T_m)$. (right) Unit cell showing fuel pitch, P_f, and diameter, D.

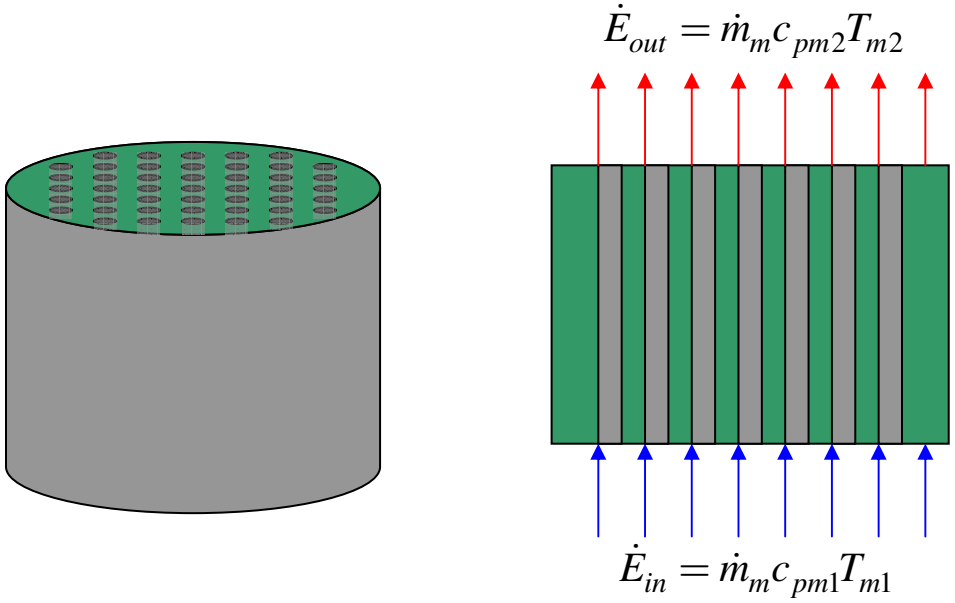

Figure 3-3. The reactor's geometry consists of cylindrical fuel pins arranged in a square lattice. The coolant enters from one end, is heated by the fuel pins, and exits the other end of the reactor.

temperature differences across the reactor were based on estimates provided by Naval Reactors.[4] Using the 100 degrees Kelvin coolant temperature drop across the reactor provided by Naval Reactors, the mass flow rate through the reactor was calculated with Equation 3-12.

$$\dot{m} = \frac{P}{c_{pm}(T_{m2} - T_{m1})} \qquad 3\text{-}12$$

Where: P = reactor power
$c_{pm} = (c_{pm1}+c_{pm2})/2$ = average coolant specific heat in reactor
$T_{m2} - T_{m1}$ = coolant temperature drop across the reactor

The size of the fuel pins was then calculated by breaking the reactor down into unit cells (Figure3-2). The wetted area for heat transfer per unit cell was found to be the sum of four quarters of a cylinder, or the equivalent of one cylinder. Based upon the range of 50-70 centimeters for the fuel pin length provided by Naval Reactors,[4] Equation 3-13 was then used to determine the radius of the fuel pin for given pitch to diameter ratio. This equation describes the relationship between the power per fuel rod and the fuel pins geometry and material properties.

$$\frac{P}{N} = \frac{4\pi L_f k_f}{1 + 2k_f/(r_f h)}(T_f - T_m) \qquad 3\text{-}13$$

The coolant convection heat transfer coefficient, h, was calculated using Equations 3-9 and 3-10. The value for the pitch to diameter ratio was iterated until a fuel temperature was found that was well below the melting point of the uranium nitride fuel. The equilibrium reactor parameters for the model found by this process are listed in the table below.

Sub-System Parameter	Steady State Value
Reactor Power, kW(t)	600
Reactor Precursor Power Equivalence, GW	50.6
Reactor Reactivity	0
Fuel Temperature, K	1097.6
Average Reactor Coolant Temperature, K	950
Reactor Coolant Inlet Temperature, K	900
Reactor Coolant Outlet Temperature, K	1000

Table 3-1. Reactor Model Parameters

3.2 Heat Transfer Loops

After the heat from the reactor is transferred to the coolant, the coolant must travel to a heat exchanger via a transfer loop. Within the primary transfer loop, the higher temperature coolant passes through piping from the reactor to the heat exchanger. Upon exiting the heat exchanger, the cooler fluid passes through a pipe from the heat exchanger back to the reactor. Due to the rate at which the coolant is being pumped in the loop, the axial conduction and heat losses along the length of the pipe were ignored.

The two main losses in the transfer loops is the radiation of heat from the pipe into space and the loss in pressure due to the friction between the fluid and the walls of the pipe. The loss due to radiation has been previously calculated by Naval Reactors and found to be three to four orders of magnitude lower than the power of the reactor.[4] Consequently, radiation losses were neglected in this study. The pressure loss of the fluid in the pipes is overcome by pumps. The power required to run these pumps is a parasitic loss that decreases the total available power produced by the Stirling converters. In any future system design, it will have to be decided whether to overcome this loss by increasing the power level of the reactor or to decrease the power available to run the

desired scientific equipment or other electrical loads, but this decision is beyond the scope of this project.

The NaK heat transfer loops were modeled with a time delay. The temperature of the coolant coming out of the reactor becomes the temperature of the coolant entering the heat exchanger after the length of time required for the coolant to transverse the piping between the reactor and the heat exchanger. This effect was modeled using the following equation.

$$\frac{dT_{b1}}{dt} = \frac{T_{m2} - T_{b1}}{\tau} \qquad 3\text{-}14$$

where: T_{b1} = coolant temperature at heat exchanger entrance
T_{m2} = coolant temperature leaving the reactor
τ = time delay for the coolant to travel from the reactor to the heat exchanger

Additionally, Simulink® provided a time delay tool which modeled the time lag exactly by holding values constant and outputting them at a specified length of time later. All the other sections of transfer loops were modeled in this same manner.

3.3 Heat Exchanger Linking Primary and Secondary Transfer Loops

In order to transfer the heat from the primary transfer loop to the secondary transfer loop, a shell and tube heat exchanger as shown in Figure 3-4 was assumed as this type of

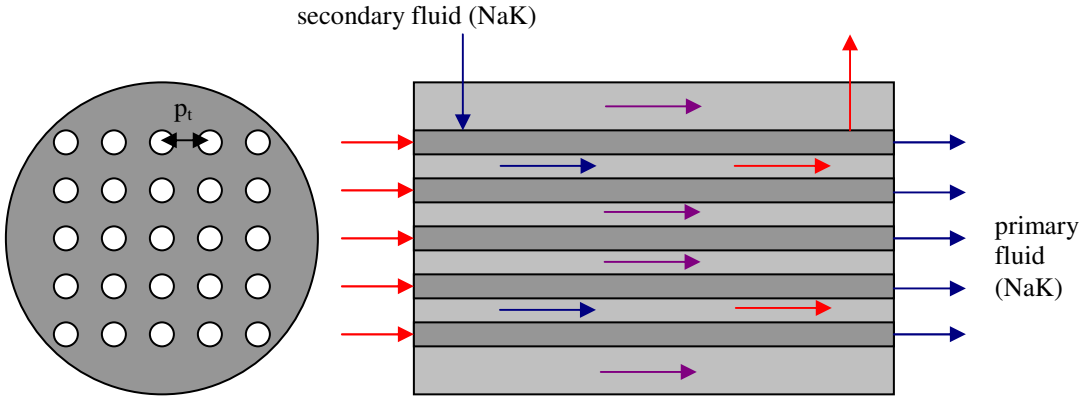

Figure 3-4. Shell and tube heat exchanger, with tube pitch, p_t.

heat exchanger is commonly employed in reactor systems. Due to the high conductivity of the primary coolant (NaK), a one pass heat exchanger was assumed to be sufficient. The primary loop coolant enters the tubes of the heat exchanger at the temperature it left the reactor. While in the heat exchanger, the primary coolant transfers heat to the secondary coolant (also NaK) that is flowing around the outside of the tubes via conduction through the heat exchanger tubes. The Biot number was calculated for a single tube and found to be on the order of one hundred, which means that the heat exchanger tubes cannot be treated with a lumped capacitance model. Therefore, the heat transfer rate between the primary and secondary fluid was calculated using the relationships given in Equations 3-15 and 3-16.[35]

$$\dot{Q} = UA\Delta T_{lm} \qquad 3\text{-}15$$

$$UA = \frac{1}{\frac{1}{h_p A_p} + \frac{\ln(d_o / d_i)}{2\pi k_t L_t N_t} + \frac{1}{h_s A_s}} \qquad 3\text{-}16$$

where: $\dot{Q}$ = heat transfer rate between primary and secondary fluids
UA = overall heat transfer coefficient times the equivalent surface area of the heat exchanger
ΔT_{lm} = log mean temperature difference
h_p = convection coefficient for heat exchanger primary coolant
h_s = convection coefficient for exchanger secondary coolant
$A_p = \pi d_i L_t N_t$ = heat transfer area for primary coolant
$A_s = \pi d_o L_t N_t$ = heat transfer area for secondary coolant
d_i = heat exchanger tube inner diameter
d_o = heat exchanger tube outer diameter
k_t = tube conductivity
L_t = tube length
N_t = number of tubes in heat exchanger

Since the temperature of the primary and secondary coolant vary along the length of the heat exchanger, the log mean temperature difference was used to determine the heat transfer rate. The log mean temperature difference is defined in Equation 3-17.[35]

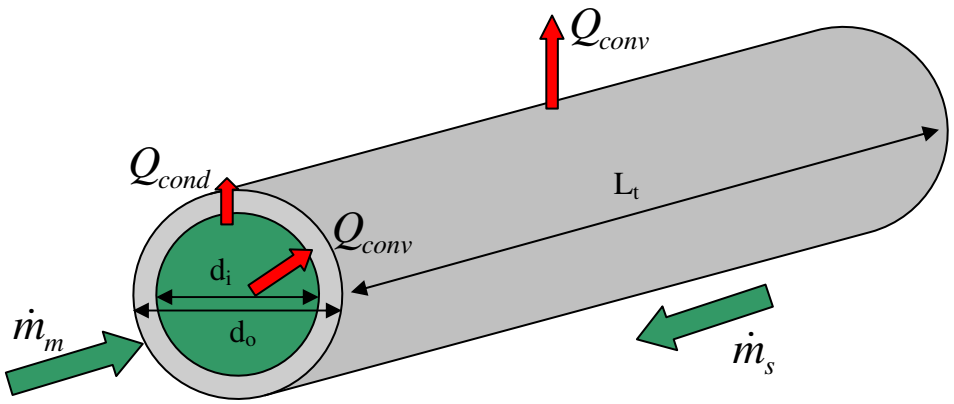

Figure 3-5. Individual tube of the heat exchanger. The hotter primary coolant passes through the inside of the tube while the colder secondary coolant flows around the tube. ($\dot{m}_m$ = primary mass flow rate, $\dot{m}_s$ = secondary mass flow rate)

$$\Delta T_{lm} = \frac{(T_{h,i} - T_{c,o}) - (T_{h,o} - T_{c,i})}{\ln\left(\frac{T_{h,i} - T_{c,o}}{T_{h,o} - T_{c,i}}\right)} \qquad 3\text{-}17$$

where: $T_{h,i}$ = hotter fluid inlet temperature
$T_{h,o}$ = hotter fluid outlet temperature
$T_{c,i}$ = colder fluid inlet temperature
$T_{c,o}$ = colder fluid outlet temperature

The heat transfer coefficients for the primary and secondary fluid were assumed constant due to the high thermal conductivity of the liquid metal coolant. However, the flow geometry is different than that of the reactor, so Equations 3-18 and 3-19 were used to determine the heat transfer coefficients.[36]

$$\mathrm{Nu}_1 = 4.82 + 0.697\frac{d_o}{d_i} \qquad 3\text{-}18$$

$$Nu_2 = 7 + 4.24\left(\frac{p_t}{d_o}\right)^{1.52} \qquad 3\text{-}19$$

where: Nu_1 = Nusselt number for first heat exchanger primary fluid
Nu_2 = Nusselt number for first heat exchanger secondary fluid
p_t = heat exchanger tube pitch

Using a process similar to that described above for the reactor, the dimensions of the heat exchanger were determined. However, the only available value for the heat exchanger was the inner diameter of the tubes, which was provided by a NASA contractor report on the SP-100 system and used as a guideline for heat exchanger size.[22] At a steady state condition, the temperature drop of the primary fluid in the heat exchanger is equal to its temperature rise in the reactor. Since the secondary loop also uses sodium-potassium, the secondary fluid also has the same temperature drop. This left the thickness of the tubes, pitch of the tubes, and length of the tubes as variables. By using the detailed sketches of the SP-100 design provided by the NASA contractor report, the length of the heat exchanger was chosen to be a half meter. The pitch and thickness of the heat exchanger tubes were then adjusted to provide a high heat exchanger efficiency, which was calculated using Equation 3-20.

$$\eta = \frac{T_{\mathrm{c,o}} - T_{h,o}}{T_{h,i} - T_{h,o}} \qquad \text{3-20}$$

where: η = exchanger efficiency
$T_{c,o}$ = cold side exit temperature
$T_{h,o}$ = hot side exit temperature
$T_{h,i}$ = hot side inlet temperature

In other words, the temperature difference between the hot temperature of the primary and secondary loops was minimized. Using this process, the efficiency of the exchanger was increased to 71 percent, but further increases in efficiency were determined to be a secondary goal compared to the primary effort of completing the system model.

3.4 Heat Pipes Linking Secondary Transfer Loop to the Stirling Engines

The method employed to link the secondary heat transfer loops to the Stirling converters consisted of placing the evaporator end of heat pipes into the liquid metal flow of the secondary loop and the condenser ends into the metal structure. This configuration was the most documented method found by the author.[26] The heat pipe exterior and wick are composed of titanium and the working fluid is potassium. These material choices were based on the recent work done by the Jet Propulsion Laboratory in the area of high temperature heat pipe applications.[37]

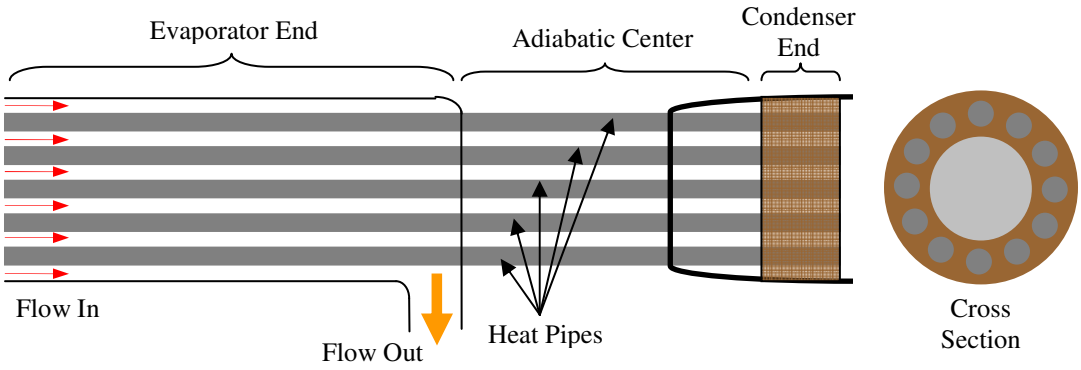

Figure 3-6. Conceptual sketch of the transfer loop-Stirling heat pipe interface (not to scale).

The heat pipe heat transfer of the heat pipes was calculated by determining the thermal resistances of the various portions of the heat pipe.[38] The thermal resistance of the working fluid, potassium, was assumed to be negligible compared to the resistances of the pipe and the wick at the condenser and evaporator. The thermal resistance of the pipe and wick of the evaporator and condenser are given by Equations 3-21 through 3-24.[38]

$$R_{pe} = \frac{\ln(d_{op} / d_{ow})}{2\pi L_e k_p} \qquad 3\text{-}21$$

where: R_{pe} = thermal resistance of the pipe at the evaporator
d_{op} = heat pipe outer diameter
d_{ow} = outer diameter of the wick

L_e = length of the evaporator
k_p = conductivity of the pipe

$$R_{we} = \frac{\ln(d_{ow} / d_{iw})}{2\pi L_e k_{eff}} \qquad 3\text{-}22$$

where: R_{we} = thermal resistance of the wick at the evaporator
d_{iw} = inner diameter of the wick
k_{eff} = effective conductivity of the wick

$$R_{pc} = \frac{\ln(d_{op} / d_{ow})}{2\pi L_c k_p} \qquad 3\text{-}23$$

where: R_{pc} = thermal resistance of the pipe at the condenser
L_c = length of the condenser

$$R_{wc} = \frac{\ln(d_{ow} / d_{iw})}{2\pi L_c k_{eff}} \qquad 3\text{-}24$$

where: R_{wc} = thermal resistance of the wick at the condenser

The value for the effective thermal conductivity of the wick is a combination of both the wick material and that of the working fluid. The wicks of the heat pipes chosen for this project consist of a woven screen mesh of the same material as the pipe and their effective thermal conductivity is found using the following relationship.[38]

$$k_{eff} = \frac{k_l((k_l+k_p)-(1-\beta_w)(k_l-k_p))}{(k_l+k_p)+(1-\beta_w)(k_l-k_p)} \qquad 3\text{-}25$$

where: k_l = thermal conductivity of the working fluid
β_w = wick porosity = 0.65

The heat transfer from the liquid metal of the secondary loop to the heater of the Stirling converter was calculated by including the thermal resistance of the heat transfer from the liquid metal to the pipes.

$$dQ_{hp} = \frac{\Delta T}{\sum R} = \frac{T_d - T_{wh}}{\frac{1}{N_{hp} h_{lp} A_{evap}} + R_{pe} + R_{we} + R_{pc} + R_{wc}} \qquad 3\text{-}26$$

where: dQ_{hp} = heat transfer through the heat pipes
T_d = average liquid metal temperature at the evaporator
T_{wh} = heater wall temperature
N_{hp} = number of heat pipes
h_{lp} = heat transfer coefficient from the liquid metal to the pipe
A_{evap} = evaporator area = $\pi d_{op} L_e$

The heat transfer to the Stirling heater is used by the Stirling converter to produce electricity. The model of the Stirling converter is described in detail in the next section.

4. Stirling Converter Model

4.1 Stirling Converter Analysis

Two simulation traits that are involved in a constant tradeoff are simulation speed and sophistication. While a main goal of a simulation is to recreate the real process as accurately as possible, accounting for all the variables will often lead to simulations that require an inordinate amount of computer resources or time to run. The Stirling engine has many variables and simultaneous processes that can become very complex. Therefore, in order to develop simulations that run at high enough speed for practical study of the engine's performance under varying conditions, simplifying assumptions were made to reduce the level of complexity of the model. An isothermal analysis is one of the simplest methods for developing a Stirling engine model that still accounts for all of the system's dynamics.

In this type of isothermal analysis it is assumed that temperatures in each space of the engine remain constant. By making this assumption, one is assuming the ideal performance of heat exchangers where the temperature of the gas is assumed equal to the heat exchanger wall. The efficacy of these simplifications is evaluated later in this section, but first the isothermal method is explained in detail.

The isothermal model is initially derived from the conservation of mass in the working spaces by breaking these spaces into five control volumes: the compression, cooler, regenerator, heater, and expansion spaces (Figure 4-1).[39,40]

$$m_w = m_c + m_k + m_r + m_h + m_e \qquad 4\text{-}1$$

where: m_w = total mass of working gas
m_c = compression space mass

m_k = cooler space mass
m_r = regenerator space mass
m_h = heater space mass
m_e = expansion space mass

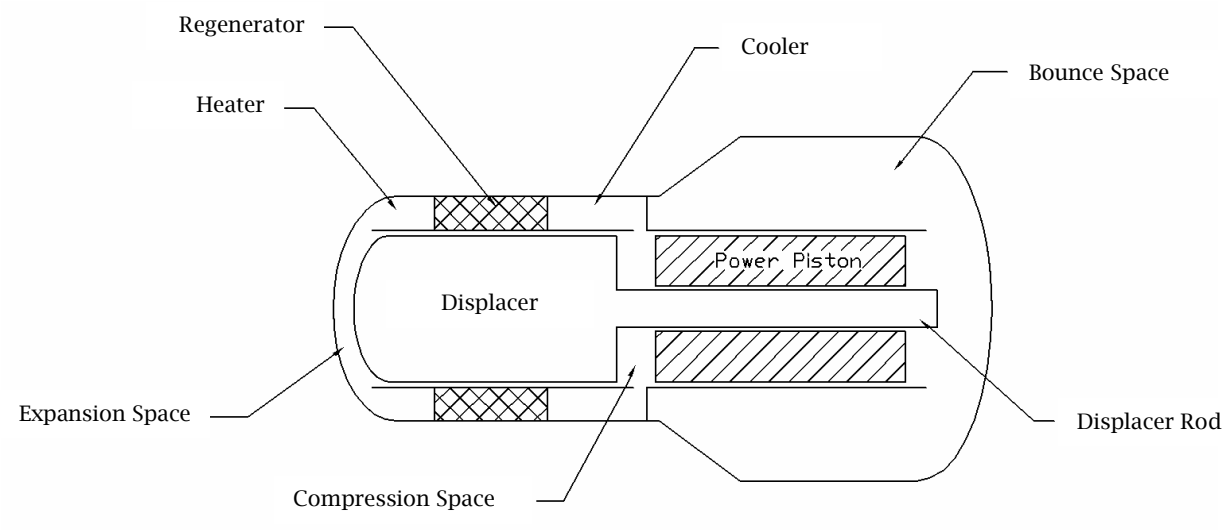

Figure 4-1. Geometry of a Stirling converter with a free power piston [].

Next, the assumption is made that the pressure, p, is nearly the same value throughout the working spaces. This assumption reflects the fact that the difference in pressures between the working spaces is small and can be accounted for later. Using the isobaric assumption and the ideal gas law, the following equation is produced.[39, 40] (Note that the same subscripts are used as in Equation 4-1)

$$m_w = \frac{pV_c}{R_{gas}T_c} + \frac{pV_k}{R_{gas}T_k} + \frac{pV_r}{R_{gas}T_r} + \frac{pV_h}{R_{gas}T_h} + \frac{pV_e}{R_{gas}T_e} \qquad 4\text{-}2$$

Since T_c=T_k, Equation 4-2 can be rewritten.

$$m_w = \frac{pV_c}{R_{gas}T_k} + \frac{pV_k}{R_{gas}T_k} + \frac{pV_r}{R_{gas}T_r} + \frac{pV_h}{R_{gas}T_h} + \frac{pV_e}{R_{gas}T_h} \qquad 4\text{-}3$$

where: p = working space pressure
V = volume of the designated space
R_{gas} = gas constant (helium)
T_i = temperature of the designated space, i

Solving for the working space pressure, one obtains Equation 4-4.

$$p = \frac{m_w R_{gas}}{\left(\frac{V_c}{T_k} + \frac{V_k}{T_k} + \frac{V_r}{T_r} + \frac{V_h}{T_h} + \frac{V_e}{T_h}\right)} = \frac{m_w R_{gas}}{S} \qquad 4\text{-}4$$

where: $S = \left(\frac{V_c}{T_k} + \frac{V_k}{T_k} + \frac{V_r}{T_r} + \frac{V_h}{T_h} + \frac{V_e}{T_h}\right)$

Note that the assumptions made allow pressure to be expressed as a function of two time variant parameters, the compression and expansion space volumes (V_c and V_e).[39] The temperature of the regenerator is assumed to be the effective temperature of the regenerator space obtained by integrating the temperature across the length of the regenerator. Since the regenerator wall temperature profile is produced by conduction from the heater to the cooler, the temperature of the wall is assumed to vary linearly across the regenerator length.[40]

$$m_r = \frac{V_r p}{R_{gas}} \int_0^{L_r} \frac{dx}{[(T_h - T_k)x + T_k L_r]} = \frac{V_r p}{R_{gas}} \frac{\ln(T_h / T_k)}{(T_h - T_k)} = \frac{V_r p}{R_{gas} T_r} \qquad 4\text{-}5$$

$$T_r = \frac{\ln(T_h / T_k)}{(T_h - T_k)} \qquad 4\text{-}6$$

where: L_r = regenerator length
$T_r(\mathrm{x}) = (T_h - T_k)x + T_k L_r$
= temperature profile of the regenerator
T_r = effective regenerator temperature

Next, the change in pressure with respect to time is calculated by taking the derivative of Equation 4-5.

$$dp = \frac{-m_w R_{gas}\left(\frac{dV_c}{T_k} + \frac{dV_e}{T_h}\right)}{S^2} * \qquad 4\text{-}7$$

The rates of change for the compression and expansion space volumes found in these equations were then determined using second order differential equations that represent the motion of the piston and displacer. These differential equations can be put into the general format of a one dimension translational mechanical system.[41]

$$m\ddot{x} + D\dot{x} + kx = F(t) \qquad 4\text{-}8$$

where: m = mass of displacer or piston
D = damping coefficient
k_s = spring constant
x = mass position
$\dot{x}$ = mass velocity
$\ddot{x}$ = mass acceleration
$F(t)$ = forcing function

For the engine configuration used in this research, the displacer damping force is negligible and the forcing function was defined by the pressures in the bounce, compression, and expansion spaces according to the geometry shown in Figure 4-1.[42] The displacement value, x, of zero is defined for the equilibrium position and the positive direction is toward the expansion space.

Thus, for the displacer in Figure 4-1, the damping is insignificant and the equation of motion becomes,

$$m_d \ddot{x}_d + k_d x_d = P_b A_{rod} + P_c A_{pist} - P_e A_d \qquad 4\text{-}9$$

where: P_b = bounce space pressure
P_c = compression space pressure

* In order to keep the same convention as previous literature, the prefix "d" will be used as a method of labeling the derivative with respect to time.

P_e = expansion space pressure
A_{rod} = displacer rod cross sectional area
A_{pist} = power piston cross sectional area
A_d = displacer cross sectional area

The power piston configuration for this study has insignificant spring contributions and its damping coefficient, D_p, is mostly a function of the alternator and is defined in detail later in this section. The equation of motion for the power piston is,

$$m_p\ddot{x}_p + D_p\dot{x}_p = (P_b - P_c)A_p \qquad 4\text{-}10$$

Now that the pressure and volume variations of the engine are known, the power of the engine can be determined.

$$dW = p(dV_c + dV_e) = p(A_p(\dot{x}_d - \dot{x}_p) - A_d\dot{x}_d) \qquad 4\text{-}11$$

where: dW = mechanical power from the working gas
dV_c = time derivative of compression space volume
$= A_p(\dot{x}_d - \dot{x}_p)$
dV_e = time derivative of expansion space volume
$= -A_d\dot{x}_d$

Finally, the heat transfer and energy losses are all that need to be determined in order to complete the energy balance for the entire engine. Before this can be done, however, the mass flow rates must be determined for each of the spaces. For the variable volume compression and expansion spaces, this is done using the differential form of the ideal gas law with the differential temperature term defined as zero (isothermal assumption).

$$\frac{dp}{p} + \frac{dV}{V} = \frac{dm}{m} + \frac{dT}{T} \qquad 4\text{-}12$$

$$dm = m\left(\frac{dp}{p} + \frac{dV}{V}\right) \qquad 4\text{-}13$$

This last equation can be simplified by creating a common denominator and using the ideal gas law.

$$dm = m\left(\frac{Vdp + pdV}{pV}\right) \qquad 4\text{-}14$$

$$dm_c = \frac{V_c dp + pdV_c}{R_{gas}T_k} \qquad 4\text{-}15$$

$$dm_e = \frac{V_e dp + pdV_e}{R_{gas}T_h} \qquad 4\text{-}16$$

The heat exchanger mass flow rates are also determined using the differential ideal gas equation, but assuming constant volume.

$$\frac{dp}{p} = \frac{dm}{m} \qquad 4\text{-}17$$

$$dm = m\frac{dp}{p} = \frac{Vdp}{R_{gas}T} \qquad 4\text{-}18$$

$$dm_k = \frac{V_k dp}{R_{gas}T_k} \qquad 4\text{-}19$$

$$dm_h = \frac{V_h dp}{R_{gas}T_h} \qquad 4\text{-}20$$

In order to ensure the continuity of mass, the mass flow rates at the boundaries between the spaces must be defined. A positive flow is defined as flow towards the expansion space in all of the following relationships.

$$dm_{ck} = -dm_c \qquad 4\text{-}21$$

$$dm_{kr} = dm_{ck} - dm_k \qquad 4\text{-}22$$

$$dm_{he} = dm_e \qquad 4\text{-}23$$

$$dm_{rh} = dm_{he} + dm_h \qquad 4\text{-}24$$

where: dm_{ck} = compression-cooler boundary mass flow rate
dm_{kr} = cooler-regenerator boundary mass flow rate
dm_{he} = heater-expansion boundary mass flow rate

dm_{rh} = regenerator-heater boundary mass flow rate

The boundary mass flows for the regenerator are then used in the one-dimensional continuity equation to determine the regenerator mass flow rate.

$$dm_r = dm_{kr} - dm_{rh} \qquad 4\text{-}25$$

Now that the mass flow rates are known, they can be used in the energy equation to determine the heat transfer of the heat exchangers. Ignoring the change in kinetic energy and the energy lost to friction, the energy balance for a generic volume can be calculated as follows.[40]

$$dQ + c_p(dm_i T_i - dm_o T_o) = dW + c_v d(mT) \qquad 4\text{-}26$$

where: dQ = heat transfer rate
c_p = average specific heat, constant pressure
c_v = average specific heat, constant volume
dm_i = mass flow rate in
dm_o = mass flow rate out
dW = rate of work, power

For isothermal conditions, this equation can be simplified further. The constant volume and temperatures of the heat exchangers results in the appearance of no heat transfer from these spaces. However, the heat transfer from these elements is what provides the energy for the maintaining the temperature of the variable volume spaces and the energy needed to do work. Therefore, we can redefine our control volumes as the combination of the heater and expansion spaces and the cooler and compression spaces. Using this procedure, the following relationship is determined.[40]

$$\oint dQ + RT \oint dm = \oint dW \qquad 4\text{-}27$$

The $\oint$ symbol represents the integral over a cycle. For steady state, the net mass flow rate is zero and the compression and expansion work rate becomes equal to the compression and expansion heat rate.[40] The subscript i is used to denote ideal conditions.

$$dQ_{ki} = dW_c \qquad 4\text{-}28$$

$$dQ_{hi} = dW_e \qquad 4\text{-}29$$

From this relationship, it can be shown that the efficiency of the engine is the Carnot efficiency. However, to determine the instantaneous heat transfer and to determine the heat transfer in non-steady state, we can substitute the mass flow rate into Equation 4-25 and establish the following relationship.

$$dQ_{ki} = -V_c dp \qquad 4\text{-}30$$

$$dQ_{hi} = -V_e dp \qquad 4\text{-}31$$

In order to overcome the artificiality of the ideal heat exchangers, the hot and cold end temperatures were assumed to be the value necessary to provide the heat transfer calculated in Equations 4-32 and 4-33. This will decrease the temperature range that the

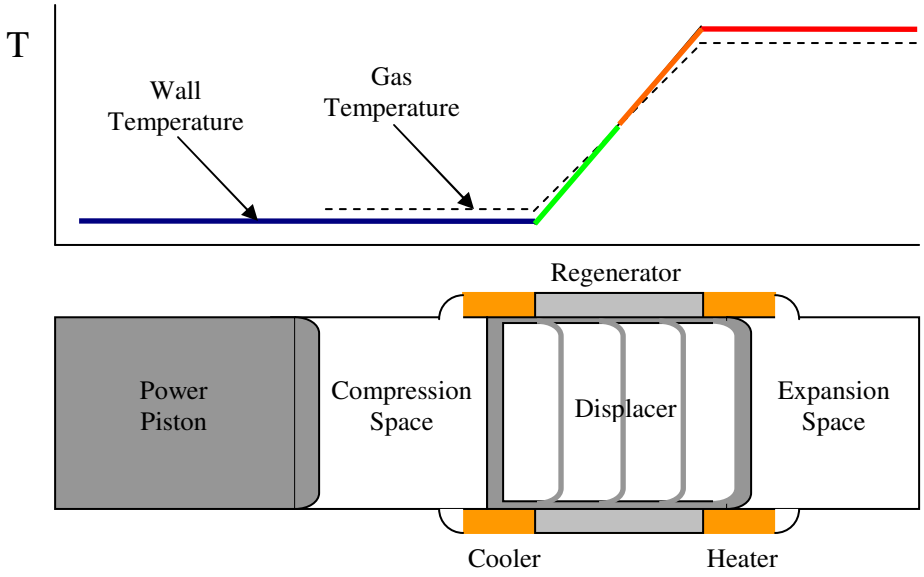

Figure 4-2. Assumed Wall and Gas Temperature Profiles of the Stirling converter.

engine gas experiences, which accounts for the fact that the heat exchangers are not ideal (Figure 4-2).[43]

$$T_h = T_{wh} - \frac{dQ_{hi}}{h_h A_{wh}} \qquad 4\text{-}32$$

$$T_k = T_{wk} - \frac{dQ_{ki}}{h_k A_{wk}} \qquad 4\text{-}33$$

where: T_h = heater gas temperature
T_k = cooler gas temperature
T_{wh} = temperature of the heater wall
T_{wk} = temperature of the cooler wall
dQ_{hi} = ideal heater heat transfer
dQ_{ki} = ideal cooler heat transfer
h_h = heater heat transfer coefficient
h_k = cooler heat transfer coefficient
A_{wh} = wetted heater area
A_{wk} = wetted cooler area

The regenerator's effectiveness was also considered. When the flow goes from the heater to the cooler, the flow will be at a higher temperature than the cooler. Also, when the flow is traveling from the cooler to the heater, the flow temperature will be lower than that of the heater. In both of these cases, the heat exchangers will have a higher magnitude of heat transfer than the original value calculated. This is accounted for by calculating the regenerator's effectiveness.[43]

$$dQ_k = dQ_{ki} - \left|dQ_{ri}\right|(1-\varepsilon) \qquad 4\text{-}34$$

$$dQ_h = dQ_{hi} + \left|dQ_{ri}\right|(1-\varepsilon) \qquad 4\text{-}35$$

$$\varepsilon_r = \frac{NTU_r}{1+NTU_r} \qquad 4\text{-}36$$

where: ε_r = regenerator effectiveness
NTU_r = number of transfer units for the regenerator

$$NTU_r = \frac{h_r A_{wr}}{2A_r} \qquad 4\text{-}37$$

where: h_r = regenerator heat transfer coefficient
A_{wr} = wetted regenerator area
A_r = regenerator cross sectional area

The two in the denominator of Equation 4-37 is due to the fact that the NTU value is accounting for both the heat transfer from the hot gas flow to the regenerator and from the regenerator to the subsequent cold gas flow. Using the values provided for the regenerator from NASA, the model never showed effectiveness values below 0.98. Therefore, disregarding this effect would not introduce significant error to the simulation.

Due to the isothermal assumption, the heat transfer values of the heat exchangers were taken to be cycle average values. To determine the heat transfer coefficients, the mass flow rates of the spaces were used to find the flow velocities. From the definition of mass flow rate, the velocity of the gas in each space is determined as follows.

$$u_n = \frac{dm_n}{\rho_n A_n} = \frac{dm_n V_n}{m_n A_n} \qquad 4\text{-}38$$

where: u_n = flow velocity in space n
ρ_n = flow density in space n
A_n = cross-sectional area of space n
n = subscript designating space

The mass of gas in each space is defined by the equation of state.

$$m_n = \frac{p_n V_n}{R_{gas} T_n} \qquad 4\text{-}39$$

The performance of this engine involves mostly laminar flow and some transitional flow. For the heater and cooler, which both consist of tubular channels, the following correlations were used for calculating the friction factor and Nusselt number.[44]

$$\text{for Re} \le 1502,\ fr = \frac{64}{\text{Re}} \qquad 4\text{-}40$$

$$\text{for Re}>1502,\ fr = \frac{0.184}{\text{Re}} \qquad 4\text{-}41$$

where: Re = Reynolds number
$= \rho u d_h / \mu$
ρ = fluid density
u = fluid velocity
$d_h = 4A/P_w$
= hydraulic diameter
P_w = wetted perimeter
μ = fluid viscosity
fr = friction factor

$$\text{for Pe} \le 1.5,\ Nu = 4.187(1 - 0.0439 Pe) \qquad 4\text{-}42$$

$$\text{for Pe} > 1.5,\ Nu = 3.6568(1 + 1.227 / Pe^2) \qquad 4\text{-}43$$

where: Pe = Peclet number
= RePr
Pr = Prandtl number
$= \mu c_p / k$
k = fluid thermal conductivity
Nu = Nusselt number

For the regenerator, which is a random fiber matrix (Figure 4-3),[45] the friction factor, wetted perimeter, and Nusselt number are calculated as follows.[46]

$$fr = \frac{192}{\text{Re}} + 4.53\,\text{Re}^{-0.67} \qquad 4\text{-}44$$

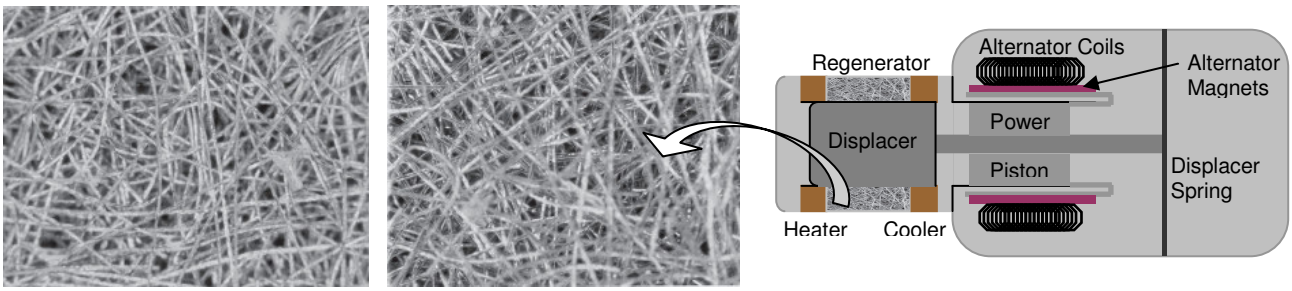

Fig 4-3. Random fiber regenerator matrices with 80%, left, and 88%, center, porosity and their location within a Stirling converter. (site)

$$P_w = \frac{4(1-\beta)A}{d_w} \qquad 4\text{-}45$$

$$Nu = 1 + 1.16 Pe^{0.66} \beta^{2.61} \qquad 4\text{-}46$$

where: β = regenerator porosity
= void volume/total volume
d_w = wire diameter

The heat transfer coefficients for the Stirling heat exchangers can then be calculated using the Nusselt numbers, fluid thermal conductivity, and the hydraulic diameter of the space.

$$h = \frac{Nu \cdot k}{d_h} \qquad 4\text{-}47$$

In order to determine the pressure in the expansion space, the flow losses in the Stirling heat exchangers are determined using the friction factors calculated in Equations 4-39, 4-40, and 4-43. These flow losses correlate to a change in pressure across each of the heat exchangers (cooler, heater, and regenerator) in the Stirling engine.

$$\Delta p = \frac{F}{A_{hx}} \qquad 4\text{-}48$$

where: Δp = pressure difference across a heat exchanger
F = frictional force in a heat exchanger
A_{hx} = cross sectional flow area of a heat exchanger

$$F = -V\left(\frac{fr}{d_h} + \frac{K}{L_{hx}}\right)\frac{\rho u|u|}{2} \qquad 4\text{-}49$$

where: V = heat exchanger fluid volume
K = local loss coefficient
L_{hx} = heat exchanger length

The local loss coefficient, K, accounts for bends in the flow and is usually assumed to be 1.5 for heater and cooler due to the ninety degree bends into the compression and expansion spaces (Figure 4-1).

$$P_c = p \qquad 4\text{-}50$$

$$P_e = P_c + \Delta p_k + \Delta p_r + \Delta p_h \qquad 4\text{-}51$$

where: P_c = compression space pressure
P_e = expansion space pressure
Δp_k = cooler pressure loss
Δp_r = regenerator pressure loss
Δp_h = heater pressure loss

4.2 Alternator Analysis

With the pressures known, the last parameter that must be calculated to determine the engine dynamics is the piston damping due to the alternator. The piston-alternator configuration consists of the piston, magnets that are attached to the piston, and wire coils that surround the piston magnets. The magnets are very close to the coils. This allows the alternator voltage to be calculated by a linear relationship to the piston velocity as follows:

$$E = k_{alt}\dot{x}_p \qquad 4\text{-}52$$

where: E = alternator voltage
k_{alt} = alternator constant (38.5 Vs/m)
$\dot{x}_p$ = piston velocity

This voltage induces a current in the coils that must be calculated using a second order equation describing the electrical circuit. The model currently does not have a capacitor, but capacitance is included in the following equation since tuning capacitors are often found in Stirling converters.

$$\dot{E} = k_{alt}\ddot{x}_p = L\ddot{I} + R\dot{I} + \frac{1}{C}I \qquad 4\text{-}53$$

where: $\dot{E}$ = time derivative of the voltage
L = alternator inductance
R = total resistive load
= alternator + load resistance
C = circuit capacitance (ignored)
$\ddot{I}$ = second time derivative of the current
$\dot{I}$ = first time derivative of the current
I = circuit current

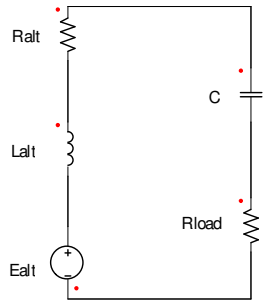

Figure 4-4. Schematic of the alternator circuit

Using the current calculated in Equation 4-53, the electrical power produced by an engine was calculated by multiplying the current, voltage, and efficiency.

$$\dot{W}_e = \eta_{alt} IE \qquad 4\text{-}54$$

where: $\dot{W}_e$ = electrical power produced by a single engine (50 kW(e))
η_{alt} = alternator efficiency

Since there are four engines in the system, the value calculated in Equation 4-54 must be multiplied by four to determine the total electrical energy produced. The net efficiency of the Stirling converter is then calculated by comparing the electrical energy produced to the thermal energy added.

$$\eta_{conv} = \frac{\dot{W}_e}{dQ_h} \qquad 4\text{-}55$$

where: η_{conv} = instantaneous converter efficiency

The average converter efficiency as a function of time can be determined by integrating the electrical power over time and dividing the result by the integral of the thermal power added to the converter.

The damping force on the piston was also calculated by multiplying the current value from Equation 4-53 by the alternator constant.

$$F_p = -k_{alt} I = \frac{-k_{alt}^2 \dot{x}_p}{Z_{alt}} = -D_p \dot{x}_p \qquad 4\text{-}56$$

$$D_p = \frac{k_{alt}^2}{Z_{alt}} \qquad 4\text{-}57$$

where: F_p = damping force on the piston
Z_{alt} = total impedance of the alternator circuit
D_p = damping coefficient

The total impedance includes the resistive load and the impedance of the inductor.

$$Z_{alt} = \left| R + Z_{ind} \right| = \sqrt{R^2 + (2\pi fL)^2} \qquad 4\text{-}58$$

where: Z_{ind} = inductor impedance
$= 2\pi fL\,\mathbf{j}$
f = frequency

The total electrical impedance was determined by assuming sinusoidal displacement and velocity of the piston (Equations 4-59 and 4-62).

$$x_p = X_p \sin(2\pi ft) \qquad 4\text{-}59$$

where x_p = piston displacement
X_p = maximum piston displacement (13 mm)
f = frequency (96.1 Hz)
t = time

The frequency of the piston was determined by using the second order system Laplace transfer function.[42]

$$\frac{X(s)}{F(s)} = \frac{\omega^2}{s^2 + 2\zeta\omega s + \omega^2} \qquad 4\text{-}60$$

where: ω = angular frequency
$= 2\pi f$
ζ = damping ratio

Using Equation 4-8, it can be shown the following relationships exist.

$$f = \frac{1}{2\pi}\sqrt{\frac{k}{m}} \qquad 4\text{-}61$$

To determine the frequency, the values for the displacer spring constant (k_d=3.1x10^6) and mass (m=8.5 kg) were used in Equation 4-59

$$f = \frac{1}{2\pi}\sqrt{\frac{3.1e6}{8.5}}$$
$$= 96.1 \text{ Hz}$$

By taking the derivative of Equation 4-59, the piston's velocity was approximated as follows.

$$\dot{x}_p = X_p(2\pi f)\cos(2\pi f t) \qquad 4\text{-}62$$

where: $\dot{x}_p$ = piston velocity

Then, Equations 4-52 and 4-62 were substituted into the electrical power relationship (Equation 4-63) and this equation was solved for the total electrical impedance of the alternator circuit.

$$\dot{W}_e = \frac{E_p^2}{2Z_{alt}} \qquad 4\text{-}63$$
$$= \frac{(k_{alt}\dot{x}_p)_p^2}{2Z_{alt}} = \frac{(2\pi f)^2 k_{alt}^2 X_p^2}{2Z_{alt}}$$

E_p = peak voltage

Equation 4-63 was then solved for the total impedance, resulting in Equation 4-64.

$$Z_{alt} = \frac{(2\pi f)^2 k_{alt}^2 X_p^2}{2\dot{W}_e} \qquad 4\text{-}64$$

$$= \frac{(2\pi \cdot 96.1)^2 (38.5)^2 (0.013)^2}{2(50000)}$$

$$Z_{alt} = 0.914\ \Omega$$

The load resistance was determined by using a steady-state relationship to represent the impedance of the inductor.

$$Z_{alt} = \sqrt{(R_{load} + R_{alt})^2 + Z_{ind}^2} \qquad 4\text{-}65$$

where: R_{load} = load resistance
R_{alt} = alternator resistance (0.028 Ω)
Z_{ind} = alternator inductor impedance

$$R_{load} = \sqrt{Z_{alt}^2 - Z_{ind}^2} - R_{alt}$$

$$= \sqrt{Z_{alt}^2 - (2\pi f L_{ind})^2} - R_{alt}$$

where: L_{ind} = alternator inductance (0.2 mH)

$$R_{load} = \sqrt{(0.914)^2 - (2\pi 96.1(2e-4))^2} - 0.028$$

$$= 0.878\ \Omega$$

Initial tests of the system produced errors. These errors were corrected by modeling the motion of the piston and displacer as perfect sinusoids with the phase angle given by NASA. This method was used instead of integrating the acceleration determined from Newton's Second Law. This sinusoidal simulation produced negative volumes, so the volume of the compression space was then increased until all volumes remained positive and the minimum volumes were no less than five percent of their respective mean values. This was achieved when the compression space value was increased thirty percent above the initial value provided by NASA.

Next, the sinusoidal restraint was removed from the piston and the simulation was run again using Newton's Second Law. During this simulation, the motion of the piston showed an overdamped response. This issue was resolved by evaluating the differential equations of motion (force balances) related to the power piston.

$$m_p \ddot{x}_p + k_{alt} I = (P_b - P_c) A_p = F_p(t) \qquad 4\text{-}66$$

$$\dot{E} = k_{alt} \ddot{x}_p = L\ddot{I} + R\dot{I} \qquad 4\text{-}67$$

$$F_p(t) = \frac{m_p L}{k_{alt}} \ddot{I} + \frac{m_p R}{k_{alt}} \dot{I} + k_{alt} I \qquad 4\text{-}68$$

Similarly to Equation 4-59, the mass of the power piston (m_p) can be related to its frequency (f or ω) by determining the transfer function of equation 4-65.

$$m_p = \frac{k_{alt}^2}{\omega^2 L_{ind}} \qquad 4\text{-}69$$

$$= \frac{38.5^2}{(2\pi 96.1)^2 (2e-4)}$$

$$= 20.3 \text{ kg}$$

When this value of the power piston mass was substituted for the value provided by NASA, 25 kilograms, the Stirling model reached steady state and closely matched the expected values for piston motion, displacer motion, and electrical power. The results of this simulation are shown in section 6 with the other simulation results.

Using all of these correlations, a simulation in MATLAB/Simulink was created to determine the performance of the Stirling engine. The analysis of these simulations is found in the Section 6. The listing of the engine parameters provided is attached in Appendix E.[42]

5. Heat Rejection System

The liquid metal heat rejection loop feeds through the coolers of the Stirling converters to absorb the waste heat and transport it to the radiators via heat pipes using NaK as a working fluid. NaK has large liquid temperature range (260-1060K under standard pressure), which allows it to be used for each of the three pumped loops of this system. The arrangement of the heat rejection system is displayed in Figure 5-1.

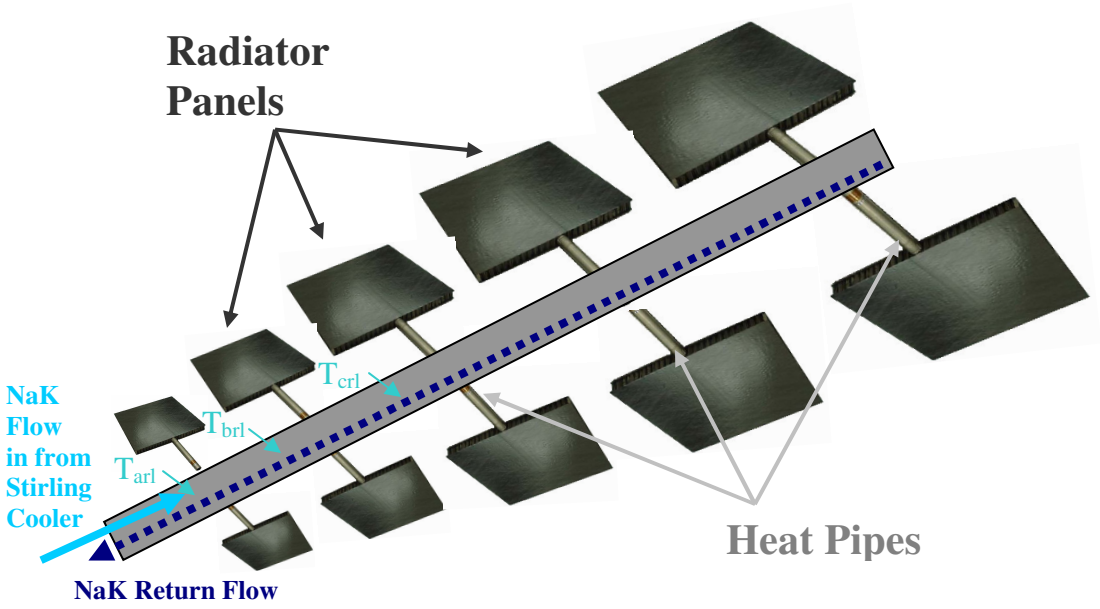

Figure 5-1. Heat Rejection System Configuration (Not to scale – system has 36 panels vice 10).

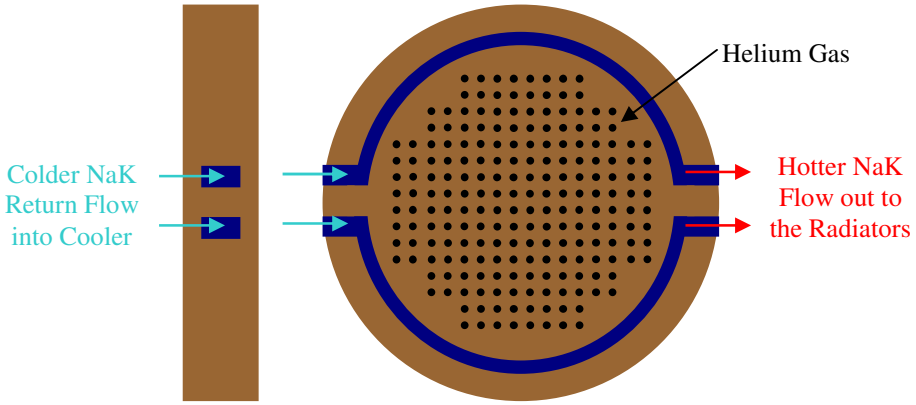

Figure 5-2. The side and top view of the interface of the cooler and the heat rejection loop.

The geometry of the interface of this pumped loop with a cooler is shown in Figure 5-2. The liquid metal flows through channels that run concentrically around the rows of holes that the gas (helium) in the cooler flows through. A figure of the Stirling converter cooler is given in Figure 4-1. The heat transfer to the liquid metal was treated as flow between two parallel plates, since this correlation was the most similar to the geometry of the channels.

$$h_{chan} = \frac{k_{NaK}}{d_h} Nu_{chan} \qquad 5\text{-}1\ ^{35}$$
$$= \frac{25}{0.00197} 9.49$$
$$= 1.203 \times 10^5 \ \frac{\mathrm{W}}{\mathrm{m}^2 K}$$

where: h_{chan} = channel heat transfer coefficient
k_{NaK} = NaK thermal conductivity
d_h = channel hydraulic diameter
Nu_{chan} = channel flow Nusselt number (9.49)

The change in temperature of the liquid metal in the Stirling engine cooler channels was calculated using the energy equation.

$$\frac{dT_{chan}}{dt} = \frac{1}{c_p \rho_{NaK} V_{chan}} \left(h_{chan} A_{wchan} (T_{wk} - T_{chan}) - c_p \dot{m}_{chan} (T_{arl} - T_{xrl}) \right) \quad 5\text{-}2$$

where: T_{chan} = channel coolant temperature
c_p = coolant specific heat (NaK)
ρ_{NaK} = coolant density (NaK)
V_{chan} = channel volume
A_{wchan} = channel wetted area
T_{wk} = cooler wall temperature
$\dot{m}_{chan}$ = coolant mass flow rate
T_{arl} = channel exit coolant temperature
T_{xrl} = channel entrance coolant temperature

From the cooler, the liquid metal flows toward the radiators through a circular pipe. Heat pipes are used to transfer heat from the pumped loop flow to the radiator panels.

The evaporator end of the heat pipe (see Figure 2-5) is embedded into the transfer loop pipe so that it is perpendicular to the oncoming flow. As shown in Figure 5-1, two heat pipes were placed at each location in order to create symmetry for the radiator panels on both sides of the coolant pipe. The Nusselt number for this liquid metal flow geometry was calculated using Equation 5-2.[32]

$$Nu_{rhpe} = 5 + 0.025 Pe_{rhpe}^{0.8} \qquad 5\text{-}3$$

where: Nu_{rhpe} = Nusselt number of radiator heat pipe evaporator
Pe_{rhpe} = flow Peclet number at the heat pipe

The condenser end of the heat pipe is embedded into the radiator panel. The heat pipes used for this portion of the system consist of titanium walls and wicks with water as the working fluid. The heat transfer through the heat pipes was modeled with thermal resistances as described in Section 3.4. The temperature of the NaK coolant at each section of two heat pipes is calculated similarly to Equation 5-2.

$$\frac{dT_{ab}}{dt} = \frac{1}{c_p \rho_{NaK} V_{cs}} \left(c_p \dot{m}_{rl} (T_{arl} - T_{brl}) - \frac{T_{ab} - T_{abp}}{R_{hptot}} \right) \qquad 5\text{-}4$$

where: T_{ab} = section average coolant temperature
V_{cs} = section coolant volume
$\dot{m}_{rl}$ = heat rejection loop mass flow rate
T_{arl} = section inlet temperature
T_{brl} = section outlet temperature
T_{abp} = section radiator panel temperature
R_{hptot} = radiator heat pipe total thermal resistance

Note that the section mass flow rate of the NaK in the rejection loop is four times larger than the channel mass flow rate since there are four Stirling converters in the model. Also, the section inlet temperature is assumed equal to the outlet temperature of the previous section, except after the last radiator where a time delay is added to account for

the time necessary for the flow to return to the Stirling converters. Each interval between sections is labeled alphabetically from a to s (Figure 5-1), except for the inlet temperature at the Stirling cooler.

Since titanium is a poor conductor, a graphite foam interface was used to connect the heat pipe condenser to the radiating fins of the radiator panels (Figure 5-3). This

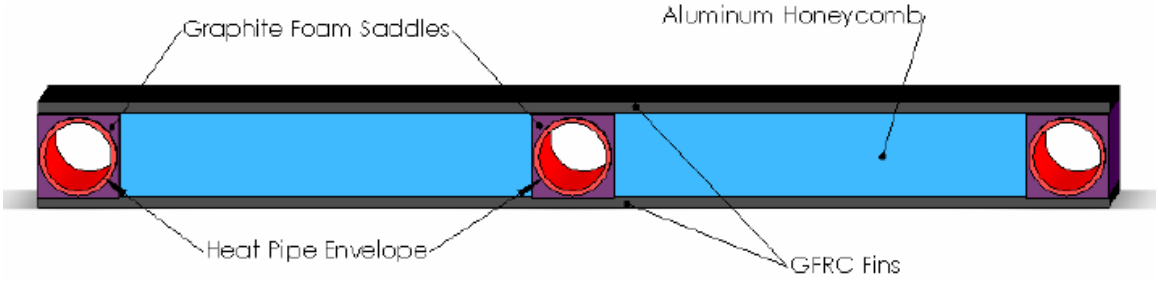

Figure 5-3. Diagram of radiator panel geometry [47].

configuration comes from recent research completed at Glenn Research Center.[47] The radiating fins were made of graphite fiber reinforced composite (GFRC), and were assumed to have an emissivity of 0.9.[47] Since the foam interface and radiator fins both primarily consist of graphite and have high conductivity perpendicular to the heat pipes, they were treated as a single thermal mass of the same temperature. The effect of heat transfer through the aluminum honeycomb is neglected (Figure 5-3). Due to symmetry, the fin temperature for each radiator pair was assumed to be the same. An energy balance was used to calculate the temperature of each pair of panels as given in Equation 5-5.

$$\frac{dT_{abp}}{dt} = \frac{1}{c_{pr}\rho_{gr}V_{rad}}\left(\frac{T_{ab}-T_{abp}}{R_{hptot}} - \varepsilon\sigma A_{rad}(T_{abp}^4 - T_{amb}^4)\right) \qquad 5\text{-}5$$

where: c_{pr} = radiator specific heat
ρ_{gr} = graphite density
V_{rad} = radiator volume
ε = radiator emissivity

σ = Stephan-Boltzman constant =5.67E-8 W/(m^2K^4)
A_{rad} = radiator surface area = 4 x radiator fin area
T_{amb} = ambient space temperature (usually 4 K)

The area of each set of radiator panels was based the width provided by a study of an identical system and a length perpendicular to the pumped loop such that the panels remained inside a 10 degree cone that is protected by shielding.[48] The final radiator model had the characteristics given in Table 5-1.

Variable	Value
Number of radiator panels	36
Total radiator area (m^2)	404.9
Total radiator mass (kg)	1,313
Radiator heat pipe diameter (cm)	2.54
Heat pipe wick outer diameter (cm)	2.29
Heat pipe wick inner diameter (cm)	2.04
Heat rejection loop mass flow rate (kg/s)	13.7
Rejection loop return time delay (s)	2.5
Steady state heat radiated (kW)	415

Table 5-1. Radiator model parameters.

The simulation results of the radiator model can be found in Section 6.

6. Simulation Results

This section describes the simulation results obtained from Simulink. Initially, each of the three main system components was modeled individually and tested (Sections 6.1 through 6.3). After each sub-model was verified, a model of the entire system was created by integrating each of the sub-models. Simulations of the entire system's response to various perturbations were then run (Section 6.4).

6.1 Partial Model Simulation Results for the Reactor, Heat Exchanger, and Transfer Loops

After the completion of the individual Simulink models of the reactor, heat transfer loops, and the heat exchanger that links the transfer loops, the individual models were linked and tested with a constant heat sink temperature. At steady state, this model produced the parameters given in Table 6-1.

Sub-System Parameter	Steady State Value
Reactor Power, kW(t)	600
Reactor Precursor Power Equivalence, GW (Gigawatt)	50.6
Reactor Reactivity	0
Fuel Temperature, K	1097.6
Average Reactor Coolant Temperature, K	950
Reactor Coolant Inlet Temperature, K	900
Reactor Coolant Outlet Temperature, K	1000
Heat Exchanger Primary Coolant Inlet Temperature, K	1000
Heat Exchanger Primary Coolant Outlet Temperature, K	900
Heat Exchanger Primary Coolant Average Temperature, K	950
Heat Exchanger Primary Wall Temperature, K	943.7
Heat Exchanger Secondary Wall Temperature, K	932.7
Heat Exchanger Secondary Coolant Inlet Temperature, K	870.7
Heat Exchanger Secondary Coolant Outlet Temperature, K	970.7
Heat Exchanger Secondary Coolant Average Temperature, K	920.7
Average Secondary Coolant Temperature at Sink, K	920.7
Secondary Heat Transfer Loop Sink Temperature, K	908.8

Table 6-1. Steady State Values for the Reactor-Heat Exchanger-Transfer Loops Partial Model.

The results supported the validity of this portion of the model by demonstrating the 100 K temperature difference across the reactor that was previously produced in similar

simulations by Naval Reactors. The temperature drop across the heat exchanger and secondary loop heat sink were also 100 K during the simulation. This shows that the heat transfer values across the system were all the same, as expected for steady state conditions.

For the first dynamic simulation (Table 6-2), the heat sink (Stirling heater) for the secondary transfer loop was given a constant heat rejection of 600 kW(t) while the reactivity of the reactor was given a step input of 0.001 at 5 seconds. This simulation is meant to model the effects of pulling a control rod partially out of the reactor. The reactor response for this transient is shown in Figures 6-1 and 6-2 (page 68). The responses of the heat exchanger and secondary loop are shown in Figures 6-3 and 6-4 (page 69), respectively. Further model results for this case are provided in Appendix A.

Reactor Test	Simulation	Variable Changed
1	0.001 Reactivity Increase	Reactivity
2	-0.001 Reactivity Decrease	Reactivity
3	10 K Increase in Stirling Heater Temperature	Heater Temperature
4	10 K Decrease in Stirling Heater Temperature	Heater Temperature

Table 6-2. Dynamic Simulations for Partial Model of Reactor, Heat Exchanger, and Transfer Loops.

These initial simulation results support that the model is working properly. As expected, the positive reactivity insertion increased the reactor power level. This increase in power level caused an immediate, sharp increase in the fuel temperature (≈ 40 K in one minute). The NaK coolant temperatures increase shortly thereafter. The outlet temperature rose the fastest, while the inlet temperature had a delayed response due to the transfer loop. The temperature increase propagated throughout the rest of the transfer loops as expected.

Due to the negative temperature coefficient of the reactor, the increasing temperature in the reactor after the positive reactivity insertion caused natural feedback effects, which returned the reactivity back to zero and the reactor to its original power level. Also

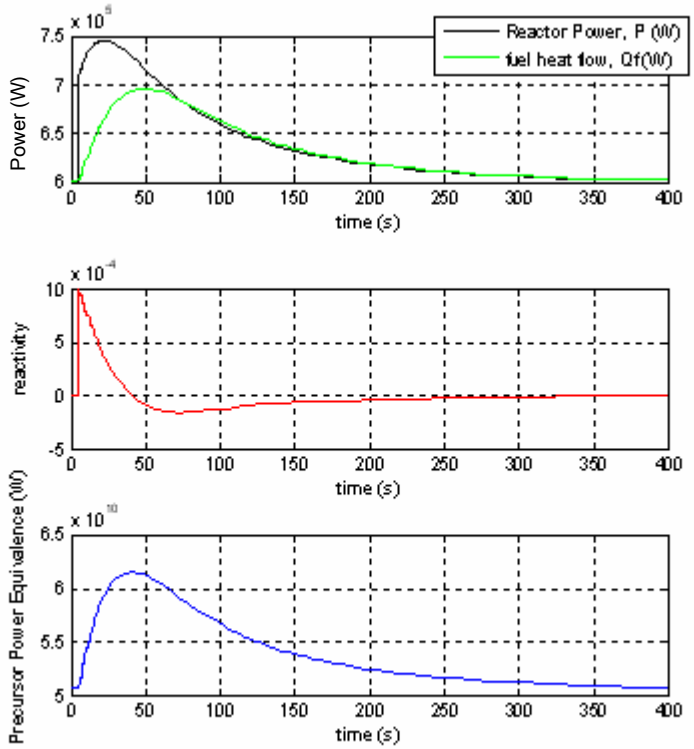

Figure 6-1. Partial model reactor response to 0.001 reactivity step input at 5 seconds. The reactor power increased with the reactivity increase and returned to the original value after 395 seconds.

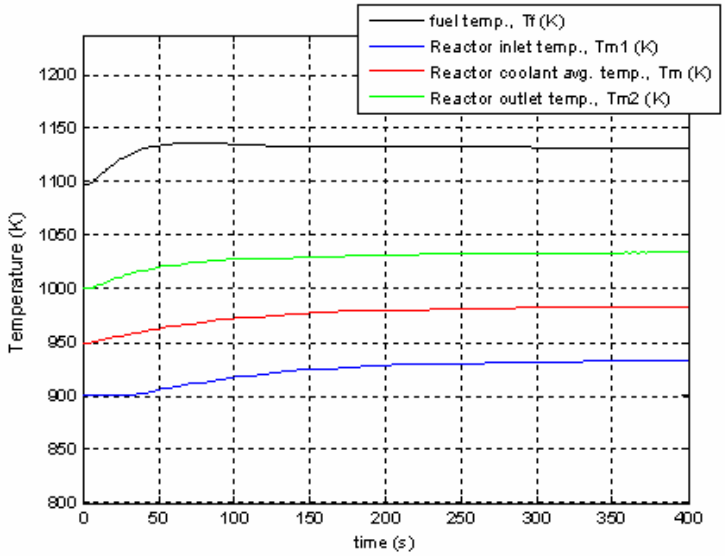

Figure 6-2. Partial model reactor response to 0.001 reactivity step input at 5 seconds. The reactor temperatures increase as a result, with fuel reacting the fastest and the inlet temperature reacting the slowest.

shown in Figure 6-1 is the heat flow from the fuel to the coolant and the precursor power equivalence, which takes into account the affects of the fission products.

When analyzed as a whole, the sub-system in the partial model had a constant heat rejection rate, but the heat addition increased with the reactivity insertion and returned

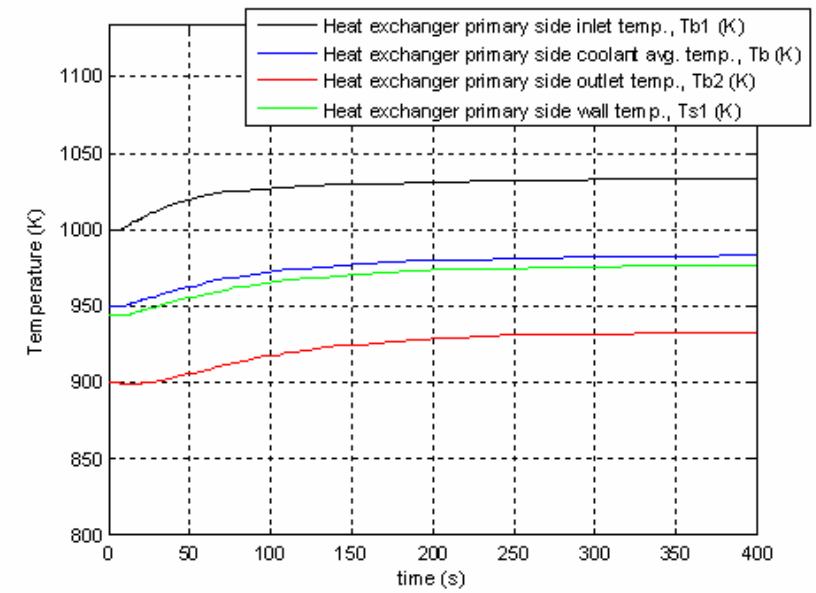

Figure 6-3. Partial model heat exchanger response to 0.001 reactivity step input at 5 seconds. The temperatures of the heat exchanger increase with a delay.

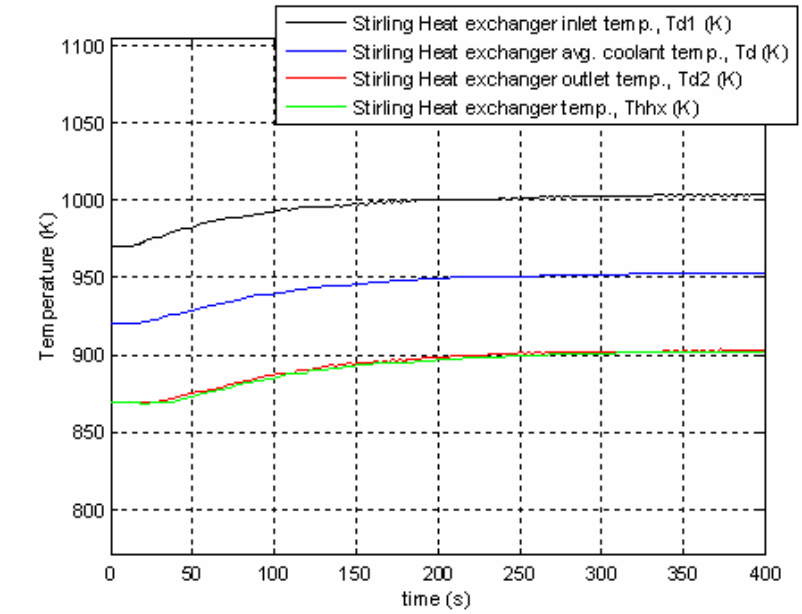

Figure 6-4. Partial model secondary loop response to 0.001 reactivity step input at 5 seconds. The temperatures of the secondary loop at the Stirling Heater increase with an

back to the original value after about 395 seconds. Therefore, the system had a net heat addition throughout the simulation, which explains why the final temperatures were higher than the initial temperatures. This test showed that this partial model functions correctly and that these components would tend to be stable and load following.

A similar simulation was run with a negative step input of -0.001 reactivity (Appendix B). This test simulates the partial insertion of a control rod. The system responded with the same magnitudes as the 0.001 reactivity insertion, but in the opposite direction. This test also showed that this partial model functions correctly and that these components would tend to be stable and load following.

The third dynamic simulation involved decreasing the secondary heat transfer loop sink temperature with a negative one degree Kelvin per second ramp input for ten seconds and observing the system response (Appendix C). This simulation replicates a increased power draw from the Stirling converters. The response for this case is shown in Figures 6-5 through 6-8 (pages 71-72). Figure 6-5 shows that the reactor power increased to meet the increased heat removal that occurred as the heat sink temperature decreased and that this response was delayed due to the transit time of the NaK in the transfer loops. However, this increase in power was small (only 1% of the original value) due to the small magnitude of the perturbation and the relatively fast response of the system (the reactor begins its response 5 seconds after the perturbation). The sub-system overcompensates slightly since the heat rejected by the second loop equalizes (after ≈ 195 seconds) with the heat addition from the reactor at a value slightly higher than the original value. This is verified by the final reactor power, reactivity, and heat sink temperature values. The results of test three provide further support that the sub-system in this partial model is stable and tends to be load following. The extra heat drawn from the Stirling converters was met with an increase in power in the reactor.

Test four conducted the same test but with a positive temperature increase (Appendix D). The simulation had the same response times and magnitudes, but in the opposite direction. Test four provides further evidence that the system is stable and load following.

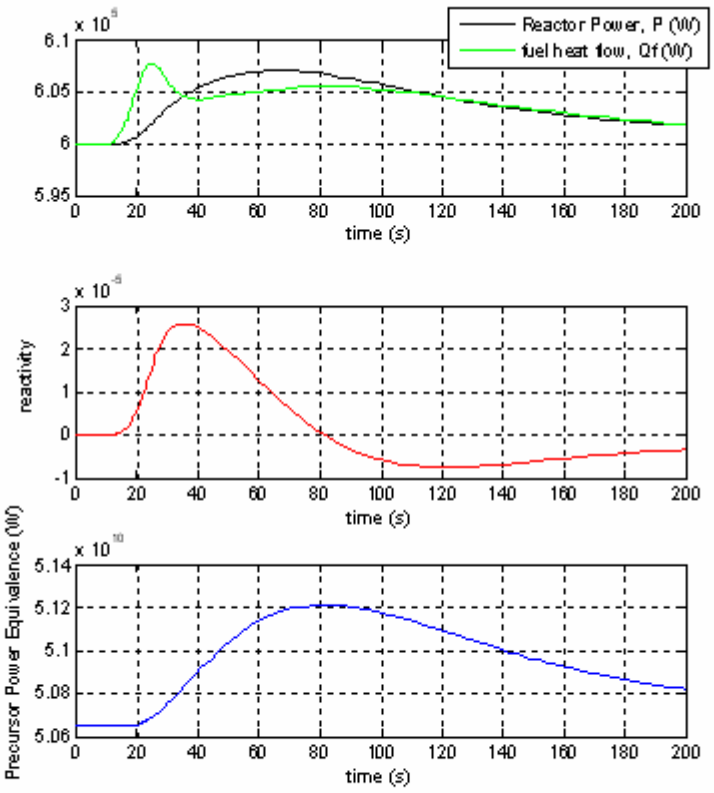

Figure 6-5. Reactor response to decreasing the secondary transfer loop sink temperature 1 Kelvin/second for 10 seconds. The reactivity and power of the reactor increase as colder NaK enters the reactor and they decrease as the NaK is heated above the equilibrium value.

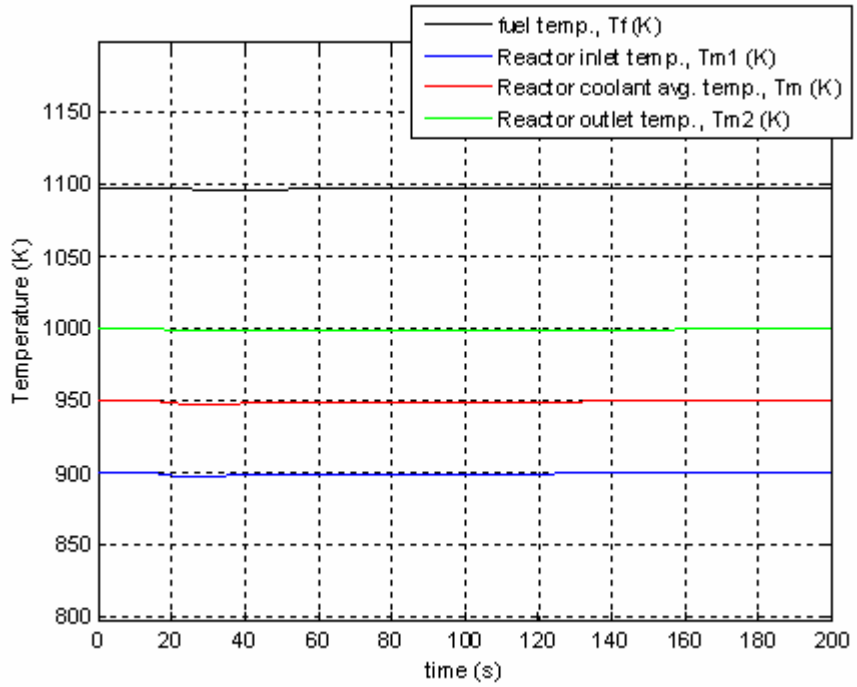

Figure 6-6. Reactor response to decreasing the secondary transfer loop sink temperature 1 Kelvin/second for 10 seconds. The coolant temperatures drop, resulting in a subsequent temperature drop in the fuel.

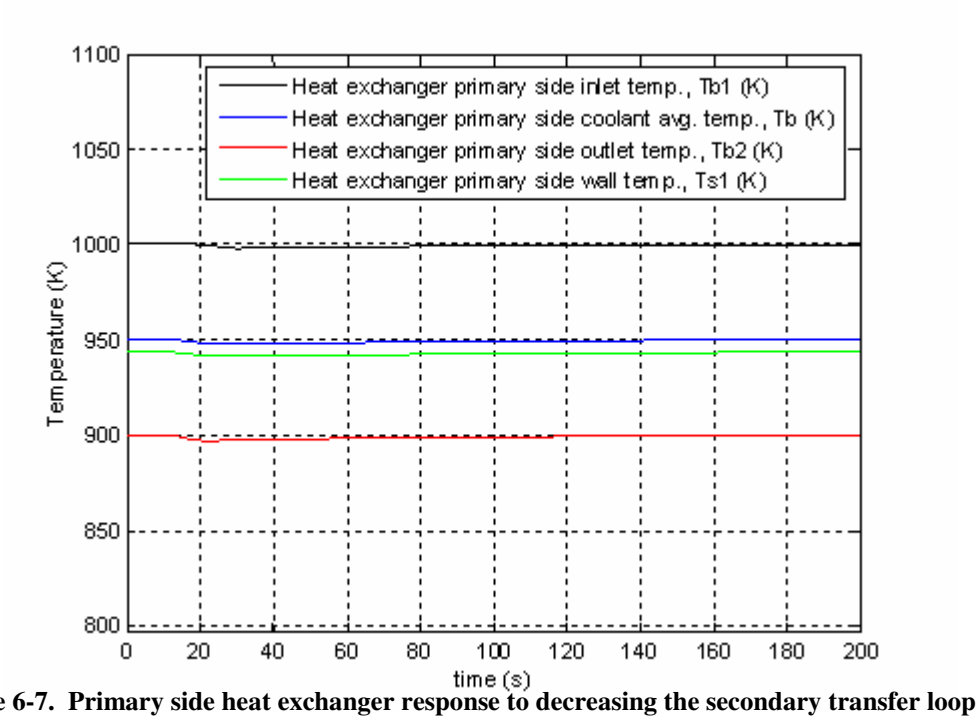

Figure 6-7. Primary side heat exchanger response to decreasing the secondary transfer loop sink temperature 1 Kelvin/second for 10 seconds. The outlet temperature responds earlier than the inlet temperature due to the transit time of NaK in the primary loop.

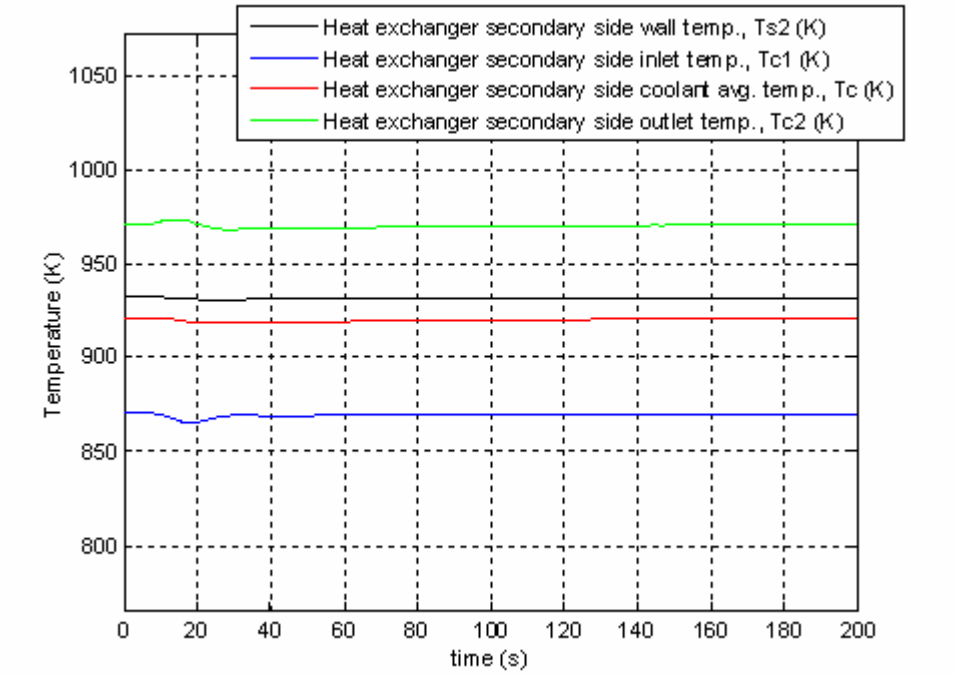

Figure 6-8. Secondary side heat exchanger response to decreasing the secondary transfer loop sink temperature 1 Kelvin/second for 10 seconds. The decrease in the inlet temperature draws more heat from the primary loop, resulting in the increase in outlet temperature. Both temperatures return to normal after the primary coolant temperature returns to its original value.

6.2 Partial Model Simulation Results for a Stirling Converter

A Stirling model was created using the method outlined in Section 4. Data provided by Glenn Research Center (GRC) was used as a guide (Appendix E). The model was tested by analyzing the steady state response when a constant heat input was added to the Stirling heater. The initial 0.3 seconds of this response is shown in Figures 6-9 and 6-10 (page 74). It is clear from counting the oscillations in these graphs that the Stirling is operating near the expected frequency of 96 Hz (slightly higher than the 90 Hz provided by GRC). As demonstrated in the left plot of Figure 6-9, the expansion and compression space temperatures are nearly identical. This validates the small pressure difference assumption made in Section 4-1. The magnitude of the pistons movement is just short of the expected 13 mm and the mean pressure is near the expected 13.6 MPa. Also, taking the area of the pressure-volume diagram (Figure 6-10) and multiplying by the frequency and electrical efficiency produces 45 kW(e). This value matches the electrical power provided by the simulation (Figure 6-11, page 75). This value can be obtained by subtracting the heat rejected from the heat added in Figure 6-11 and multiplying by the

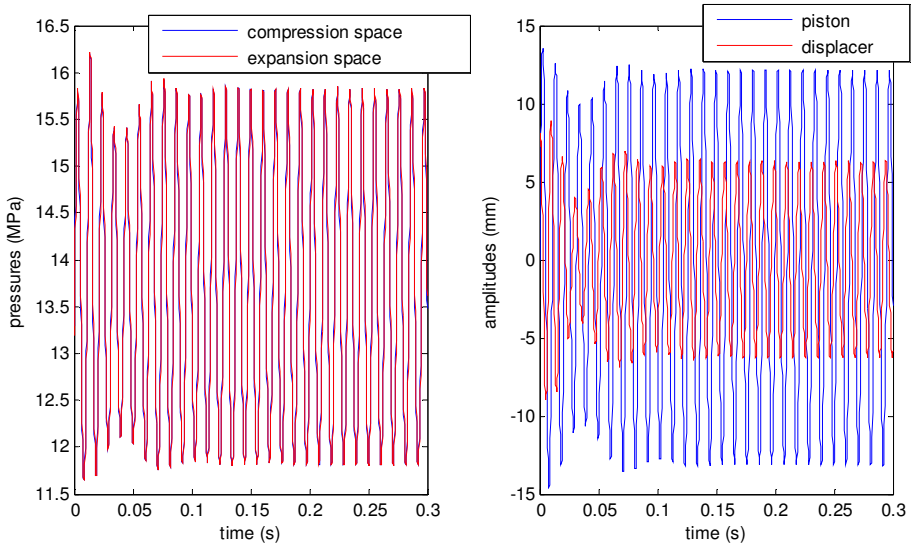

Figure 6-9. Stirling steady state response. The values initially varied as the model was started. This start-up transient ended within 0.13 seconds.

alternator electrical efficiency (93%). All of the preceding evidence proves that the Stirling model is working correctly and the simulation reveals that the model is stable. It is worth noting, however, that the simulations shown in this section are for one Stirling converter, while the completed system has four converters. Also, the Stirling electrical output is lower than the 50 kW(e) needed to produce 200 kW(e). This issue was resolved when the complete system model was created and it will be discussed in further detail in Section 6.4. The steady state values determined by the model are given in Table 6-3.

Sub-System Parameter	Steady State Value
Electrical Power, kW(e)	45
Heat Addition, kW(t)	143
Heat Rejection, kW(t)	94
Frequency, Hz	96
Mean Pressure, MPa	13.6
Piston Amplitude, mm	12.5
Displacer Amplitude, mm	6.5
Heater Temperature, K	925
Cooler Temperature, K	463
Alternator Constant, Vs/m	38.5
Alternator inductance, mH	0.2
Alternator resistance, Ω	0.028
Load resistance, Ω	0.878

Table 6-3. Steady state values for the Stirling converter sub-model.

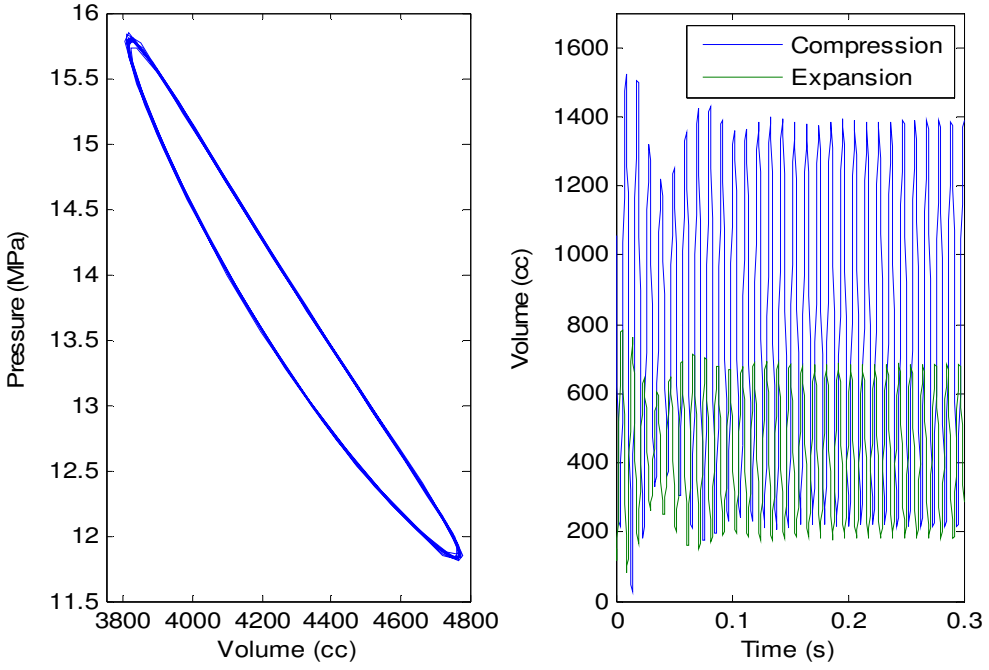

Figure 6-10. Steady state plots of the Stirling PV diagram and Volume versus time.

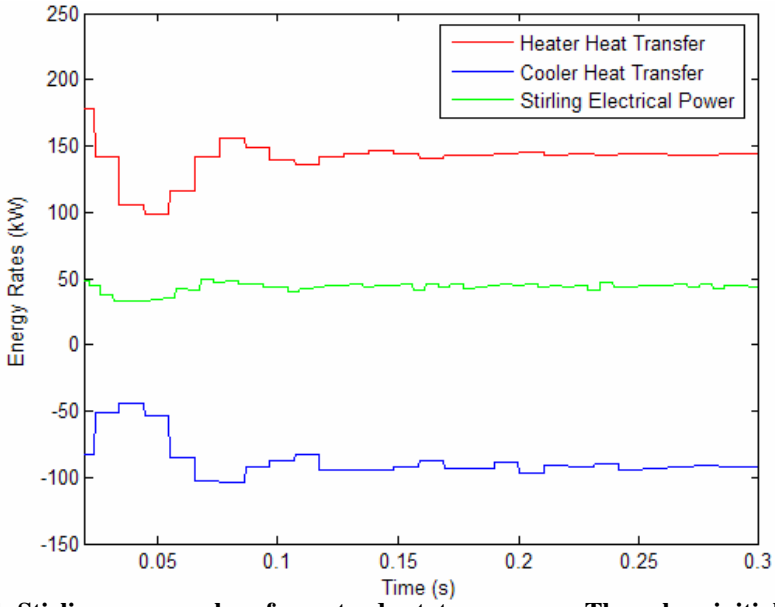

Figure 6-11. Stirling power values for a steady state response. The values initially varied as the model was started. This start-up transient ended within 0.13 seconds.

6.3 Heat Rejection System Model Simulation Results

The model of the heat rejection system described in Section 5 was also modeled and tested in Simulink. The steady state temperatures of the model agreed with theory. In order to simulate conditions similar to a reactivity insertion, the thermal power into the NaK channels of the Stirling coolers were increased from the steady state value by 20

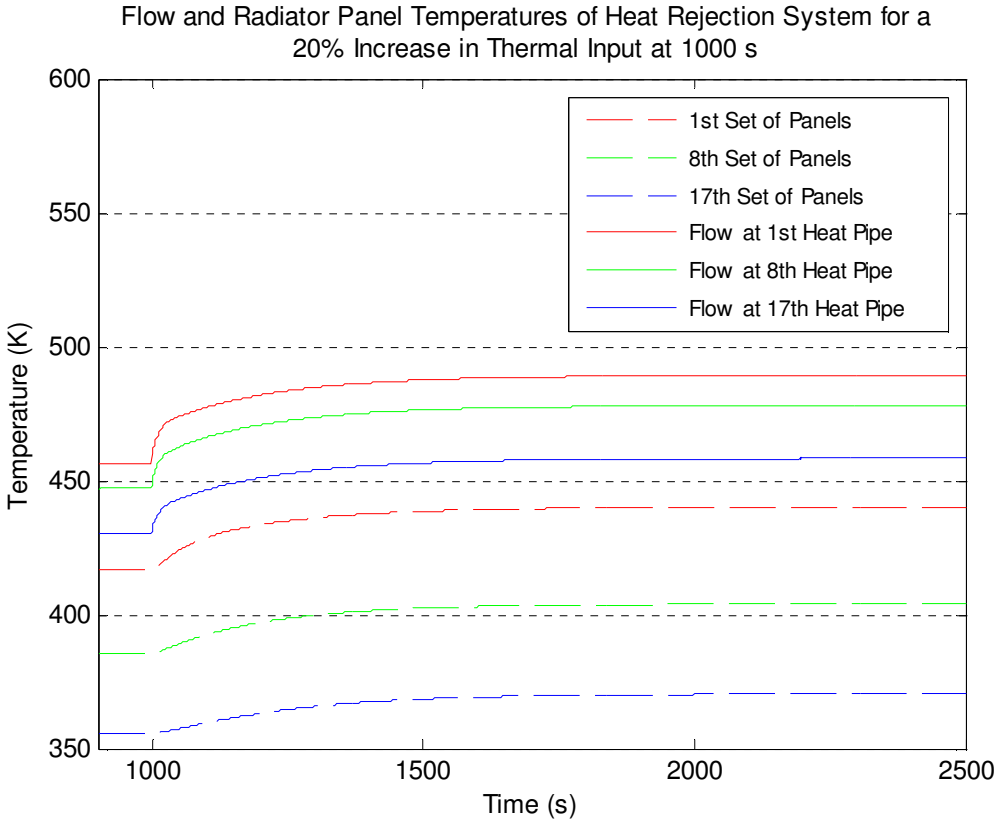

Figure 6-12. Transient Test of the Radiator Model

percent (600 to 720 kW(t)). The results of the transient test are shown in Figure 6-12. It is clear from this figure that the NaK channel flow has a smaller thermal capacitance since it increases in temperature so quickly (solid lines). Also, one can see the increase in thermal capacitance of the radiators as distance from the heat source increases along the pumped loop and the radiator size increases (the 17th set of panels heats up slower than the 1st set). This simulation suggests that the heat rejection model is working correctly

and that the model is stable. The steady state values calculated by this model are given in Table 6-4.

After the validation of the radiator model, it was linked with the Stirling and reactor models to create the model of the entire system. The simulation tests of the system model are displayed and analyzed in the next section.

Sub-System Parameter	Steady State Value
Number of radiator panels	36
Number of heat pipes	36
NaK temperature at 1st set of heat pipes, K	457
NaK temperature at 8th set of heat pipes, K	449
NaK temperature at 17th set of heat pipes, K	428
Temperature of 1st set of radiator panels, K	415
Temperature of 8th set of radiator panels, K	387
Temperature of 17th set of radiator panels, K	355
Heat Rejection, kW(t)	600

Table 6-4. Steady state values of the Heat Rejection System.

6.4 System Simulation Results

After the system model was created, tests (Table 6-5) were run to determine that the component models were linked together properly. This was accomplished by determining the initial conditions of the system analytically and then running the model and comparing the results to the expected results. Each simulation, including all of the previous simulations, were run using the variable-step ode45 (Dormand-Prince) as the numerical solver with a tolerance of 10^{-4}. This solver is a Runga-Kutta solver and is the most accurate option available in Simulink.

Initially, each model did not integrate smoothly due to small differences in the initial conditions created by using separate reference points. This problem was solved by taking the values of the Stirling heater and cooler temperatures and using them as a reference to determine the initial conditions of the reactor and radiator models. As mentioned in Section 6.2, the four Stirling converters were not producing the required electrical power (200 kW(e)), because their efficiency was slightly lower than that initially assumed (31.7% vice 33.3%). The effect of this lower efficiency was that reactor thermal power needed to be slightly greater than 600 kW(e) as shown in Figure 6-13.

As can be seen, the steady state condition of this system nearly produces the 200 kW(e) that is desired. The thickness of the electrical power plot is not due to erratic behavior of the electrical circuit, but due to the discrete jumps in the plot from the differences in the cycle averages. MATLAB connects all of the data points when plotting, so the transition between cycles produces vertical plot lines (this is shown clearly in Figure 6-11, which has a smaller time interval). These vertical lines can be eliminated with lower tolerances for the numerical solver, but some error was introduced as a sacrifice for simulation speed. This error was usually less than two percent but occasionally was slightly higher than three percent.

After the model was validated at steady state, perturbation scenarios were created for simulation tests. Table 6-5 lists the desired perturbation simulations from easiest to

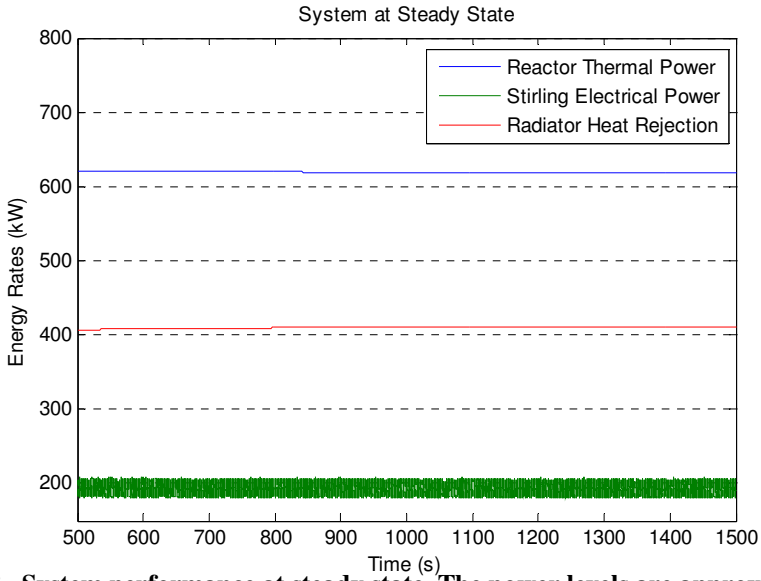

Figure 6-13. System performance at steady state. The power levels are approximately: reactor (618 kW(t)), Stirlings (195 kW(e)), radiators (408 kW(t)).

hardest. The scenarios were then completed in this order, with the exception of the last few which were not completed due to time constraints. The simulations required large amounts of time when they were run on a personal computer (22X simulation time), so all system simulations were run on a multi-node LINUX cluster in the Naval Academy's Computer Aided Design/Interactive Graphics (CADIG) laboratory (3X simulation time). The rest of this section describes the results of these simulations. Due to the large amount of data available from each simulation, the results of the simulations will only show the reactor power, Stirling electrical power, and the radiator heat rejection so that the overall system performance can be evaluated.

Simulation	System Perturbations	Variable Altered
0	Steady State	none
1	0.001 Reactivity Insertion	reactivity
2	-0.001 Reactivity Insertion	reactivity
3	Radiator efficiency decrease	background temperature
4	Stirling Failure	number of converters
5	0.5 Ohm Decrease in the Resistive Load	load resistance
6	1 Ohm increase in the Resistive Load	load resistance
7	Load short out **(run with errors)**	load resistance
8	Change from 10% to 100% power **(was not completed)**	reactor power
9	Change from 100% to 10% power **(was not completed)**	reactor power
10	System start up **(was not completed)**	reactor power
11	System shut down **(was not completed)**	reactor power

Table 6-5. List of planned system perturbation simulations.

Simulation 1 was a 0.001 reactivity insertion at 600 s with the system at equilibrium. This test is intended to show what the effects of partially removing a control rod are on the entire system. The system power values from the simulation are shown in Figure 6-14. At the time of the reactivity insertion, the reactor power rapidly increased by about 20%. As a result, an increased thermal load was added the Stirling converters. The Stirling converters responded by increasing their operating power and the radiators

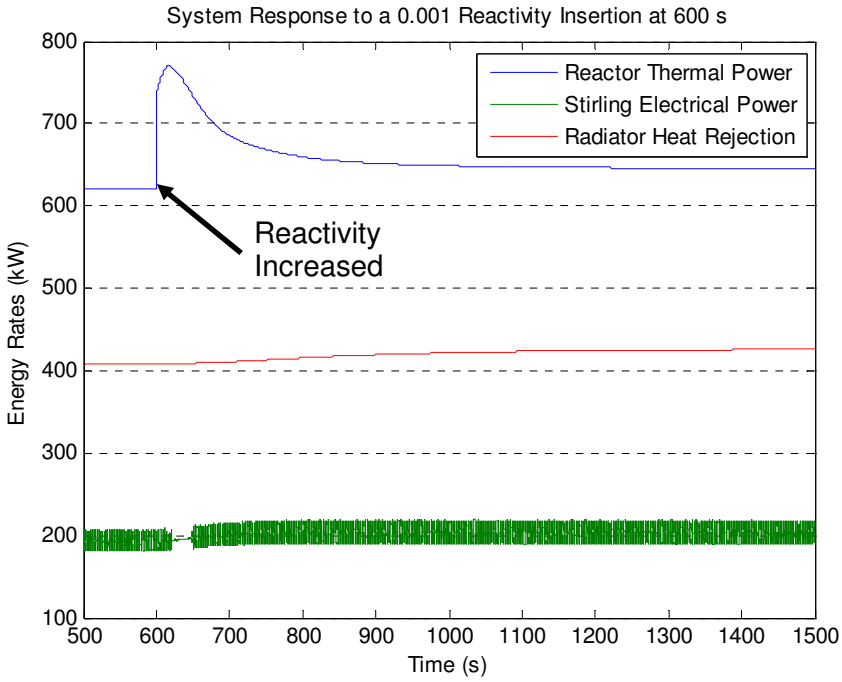

Figure 6-14. System response to a 0.001 reactivity insertion at 600s. The final power levels are approximately: reactor (640 kW(t)), Stirlings (205 kW(e)), radiators (420 kW(t)).

rejected more heat. The Stirling electrical power also seemed to stabilize at about 610 seconds. This is due to the fact the simulation step size decreased the most during this sharp change in the transient. This result showed that the model was numerically stable under transient conditions and predicts that such a system would be load following.

Following the reactivity insertion simulation, a similar simulation was run with a negative 0.001 reactivity insertion at 600 seconds with the system at equilibrium. The negative reactivity insertion is used to evaluate how partially inserting a control rod in the

reactor might affect the overall system. This simulation (Simulation 2) is displayed in Figure 6-15. Similar to the previous simulation, the reactor responded immediately. However, in this case the reactor power rapidly decreased by 20% due to the negative reactivity. The resultant decrease in thermal load on the Stirling converters caused them to operate at a lower power level (≈ 5% decrease) and the radiators rejected less heat (≈ 2.5% decrease). Again, the model was stable and predicted that the system would be load following.

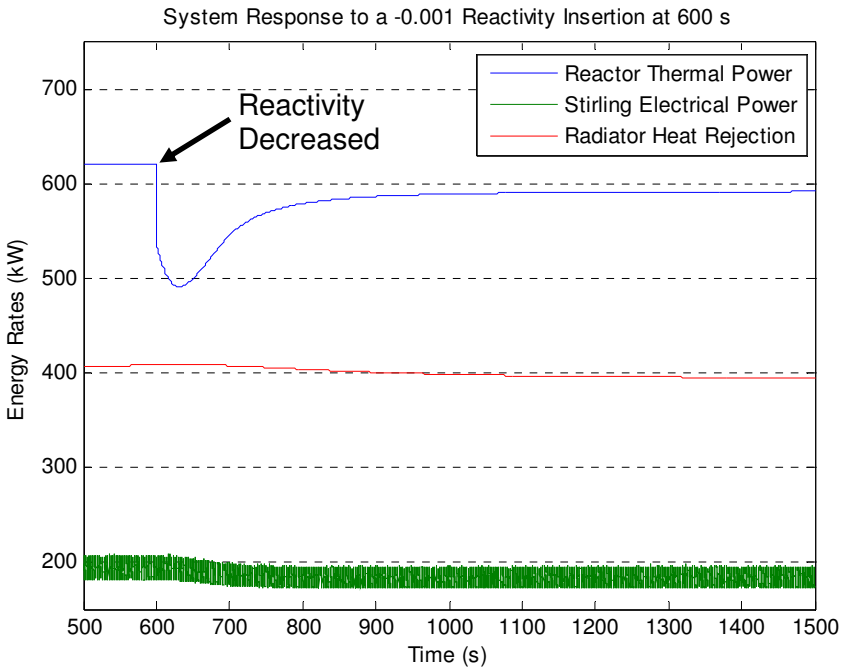

Figure 6-15. System response to a negative 0.001 reactivity insertion at 600 s. The final power levels are approximately: reactor (595 kW(t)), Stirlings (186 kW(e)), radiators (395 kW(t)).

Simulation 3 was a radiator efficiency induced perturbation. This perturbation simulates a loss in the radiators ability to reject heat, which could be caused by a change in the solar or albedo incident energy on the radiation panels. Albedo energy is solar energy that is reflected from a planet. This perturbation was modeled by increasing the ambient space temperature from 4 to 304 K (see Equation 5-5) for half of the radiator panels, which creates the effects of approximately 4 kW/m^2 of incident energy on the

radiation panels. This energy flux is similar to the solar flux the panels could receive if the system was on a spacecraft between Mercury and Venus. The results of the simulation are shown in Figure 6-16. The inability of the radiators to reject heat is shown by the sudden 20% drop in radiator heat rejection. The Stirling converters and the reactor both respond with decreases in power (≈ 3% and 2% decrease, respectively), which brings the system back into equilibrium.

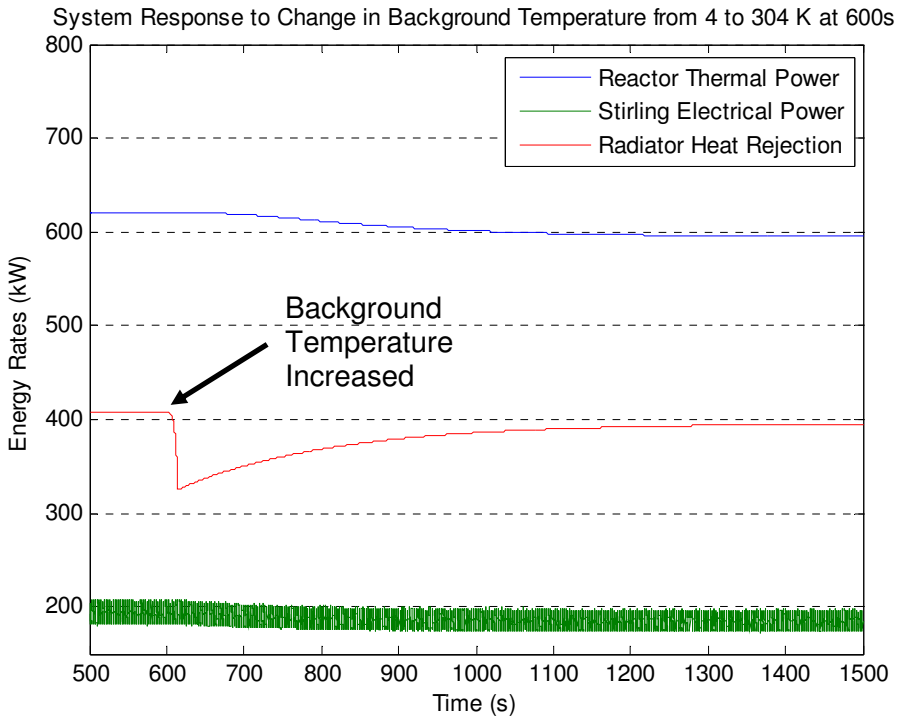

Figure 6-16. System response to a 4 to 304 K increase in ambient space temperature for one side of the radiator panels. The final power levels are approximately: reactor (596 kW(t)), Stirlings (186 kW(e)), radiators (396 kW(t)).

The next simulation run (Simulation 4) was a Stirling converter failure. Figure 6-17 illustrates how the reactor, electrical, and radiated power of the system responded to this perturbation. As the converter failed, the electrical power immediately dropped and the entire thermal load was placed on the three operating converters instead of the normal four. The three remaining converters almost accommodate for the lost converter by increasing power levels. The reactor and radiators responded to the drop in power by

decreasing power levels. As time increased to 700 seconds, the reactor power partially recovered in order to provide more heat to the converters operating at an increased power level. Similarly to the previous simulations, the model was stable and predicted that the system was load following.

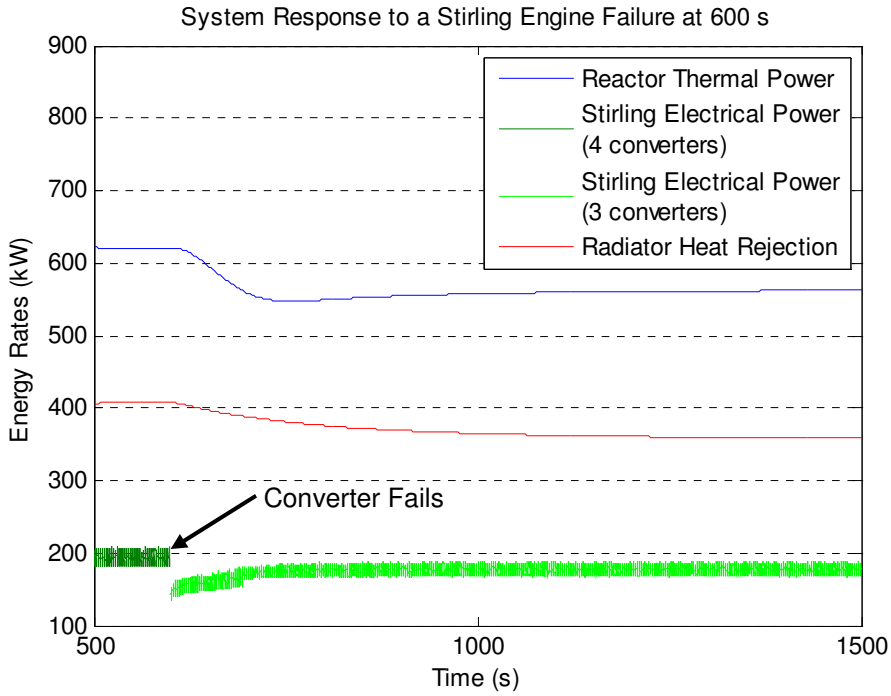

Figure 6-17. System response to a Stirling converter failure at 600 s. The final power levels are approximately: reactor (565 kW(t)), Stirlings (188 kW(e)), radiators (363 kW(t)).

Next, a load alteration simulation was run which involved cutting the resistive load approximately in half by removing half an ohm of resistance (R_{load} in Equation 4-65 was decreased by half an ohm). In this simulation, the perturbation simulates the effect of a significant decrease in the electrical resistance (possibly through short or turning instruments on). The result of this simulation on the reactor power, radiator heat rejection, and Stirling electrical power is shown in Figure 6-18. The decreased resistance causes an increase in current, which increases the damping on the piston. The increased damping on the piston caused a sudden drop in Stirling electrical power, but the higher current draw allowed the Stirling converters to become steady at 200 kW(e) while using

less thermal energy. In this case, both the reactor thermal power and the heat rejected from the radiator decreased (both ≈ 2%). While this result seems incorrect, it can be

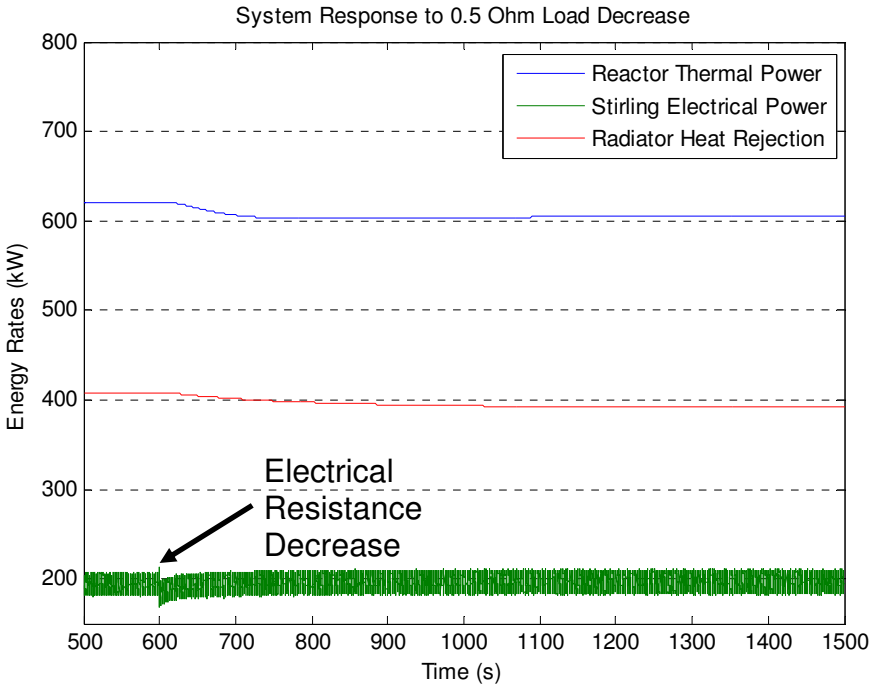

Figure 6-18. System response to halving the load resistance at 600 s. The final power levels are approximately: reactor (605 kW(t)), Stirlings (200 kW(e)), radiators (395 kW(t)).

explained by the changes in the Stirling converters' heater and cooler temperatures. This caused the converters to slightly increase power and have a higher efficiency (≈ 34.7%). This phenomenon will be explained further in the explanation of the next simulation.

The last simulation completed (Simulation 6) involved increasing the resistive load by adding one ohm of resistance (R_{load} in Equation 4-65 was increased by one ohm). This simulation was meant to replicate a scenario where the electrical resistance significantly increased (due to bad connections or suddenly turning off components). The increased resistance dramatically lowered the current in the electrical circuit and consequently reduces the electrical power produced by the system (Figure 6-19). The sudden loss in current led to a sudden loss in damping which allowed the piston to operate at a higher speed. However, the sudden increase (≈ 45% of original value) in electrical power from this perturbation is shortly followed by a decrease (≈ 25% of original value) as the

increase in heat addition from the Stirling heater to the working gas (Figure 6-20) causes the temperature of the heater to drop (Figure 6-21). This drop in heater temperature eventually causes the reactor to produce more power. However, as shown by the increase in temperature of the Stirling cooler (Figure 6-21), the Stirling converters are now operating less efficiently (≈ 21.7%). In others words, the converters are requiring more heat input to produce less electrical power, meaning the system is operating far from its optimum efficiency condition. Simulations 5 and 6 demonstrate that the electrical resistance of the alternator circuit affects the efficiency of the Stirling converters. Also, the current value in the alternator for Simulation 6 experienced a shift at the moment of the resistance increase. While all the electrical relationships held true during this shift (including electrical power), this phenomenon should be analyzed and better understood.

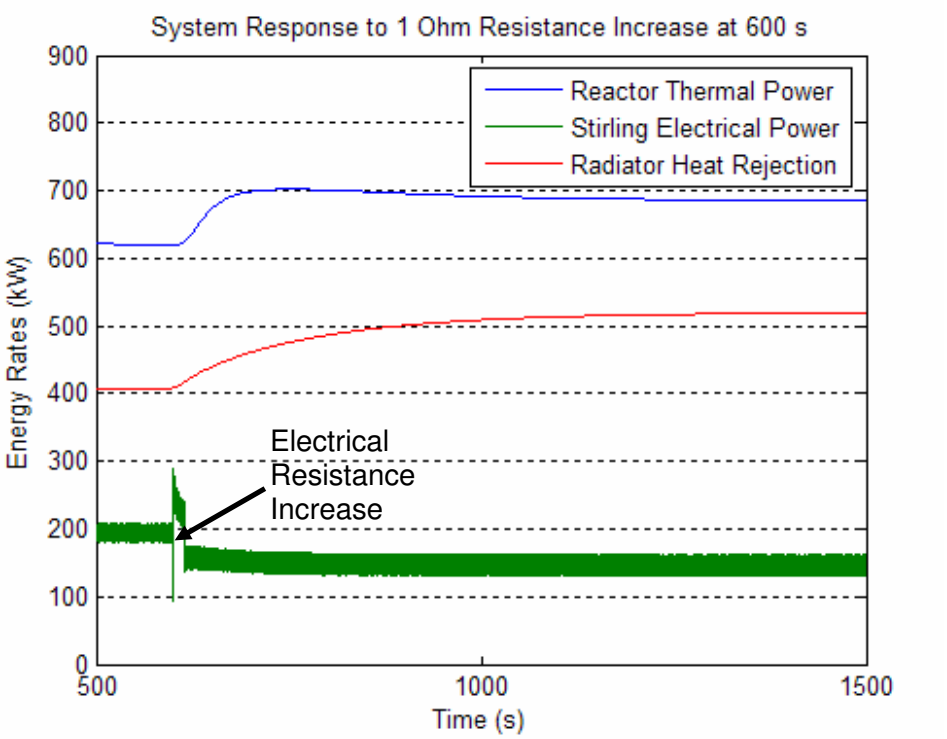

Figure 6-19. System response to doubling the load resistance at 600 s. The final power levels are approximately: reactor (690 kW(t)), Stirlings (150 kW(e)), radiators (515 kW(t)).

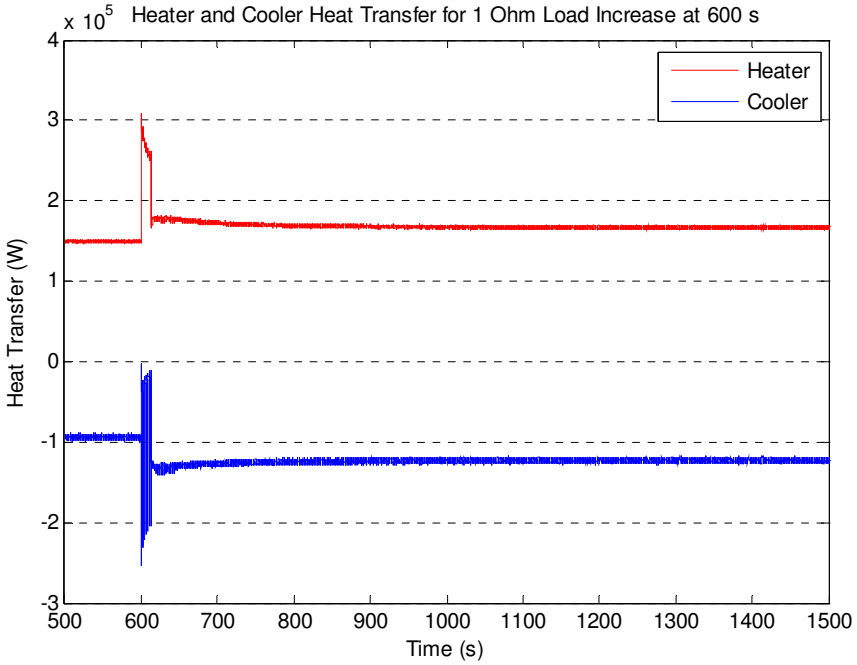

Figure 6-20. Stirling heater and cooler heat transfer values during a doubling of the electrical load resistance. The heat addition of the heater doubles but settles at a value 13% higher than the initial value. The heat rejection of the cooler increases by 250%, but settles at a value 20% larger.

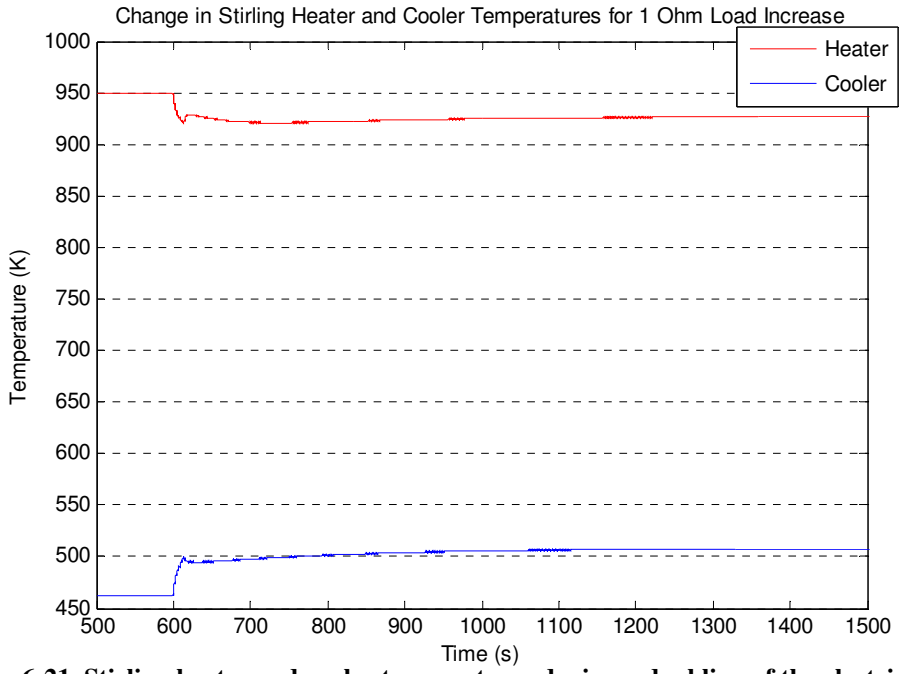

Figure 6-21. Stirling heater and cooler temperatures during a doubling of the electrical load resistance. The heater experiences a sudden drop in temperature while the cooler experiences a sudden rise in temperature at 600 s.

7. Project Conclusions

At the conclusion of this project, a model of a Stirling space nuclear power system consisting of detailed reactor, Stirling, and radiator submodels was developed. Simulations of the individual components of the system verified that the assumptions used were reasonable and that each component model was stable. According to the simulations presented in Section 6, it is evident that the system modeled tends to be a stable, load-following system, where load is based on the heat transferred and rejected by the Stirling heater and cooler to the working gas. A change in one component resulted in changes in the other components that lead the system to reach a steady state condition. It was also evident that each part of the system had a different time lag when responding to changes in the system. This time lag is inversely proportional to the components mass and size (thermal time constant), where the Stirling converters (smallest) respond the fastest and the radiators (largest) respond the slowest. For Simulations 1-4, the power level of each major component increased or decreased in the same direction as the other components. In Simulations 5 and 6, this was not the case. For the unregulated electrical system modeled, it was apparent that decreases in load increased thermal efficiency of the Stirling converters while increased load decreased thermal efficiency (Figures 6-18 and 6-19). However, in all cases, the reactor power matched the heat drawn by the Stirling converters and the radiators matched the heat rejected by the Stirling converters.

Conclusions

- **Completed model was stable**
- **Assumptions used were reasonable**
- **Model suggests a stable, load following system**
- **Each major components thermal capacity had a large effect on the systems dynamics**
- **Changing electrical load affects Stirling converter efficiency**

This project has much potential for future work. First, the systems individual elements should be optimized and system controls should be examined to provide a means for increasing the system's performance. This examination should include the creation of a detailed performance map of the Stirling converter as a function of electrical load. Second, the rest of the simulations listed in Table 6-5 should be run and further work examining the effects of the electrical circuit on the system is needed. This is especially true with regard to the current anomaly of Simulation 6 in Section 6.4. Future work should also study the effect of infinite impedance (opening the circuit). A test with infinite impedance would show the worst case scenario for the circuit resistance since it would cause the largest possible increase in reactor power. Third, a more detailed and thorough design of the whole system would provide a more realistic examination of the connections between the three main components and the performance/monetary merits of each of the alternatives. Fourth, the numerical solvers in Simulink should be examined further so that a thorough analysis of accuracy and simulation can be made. Fifth, the system should undergo a material analysis to make sure that all of the components can safely withstand operation or be improved with the selection of another material. Finally, it is recommended that the model be compared using other modeling software (such as Simplorer®). This would allow for comparisons between the performance of each software tool and it could serve to provide an assessment as to the adequacy of each model.

Future Work Suggestions

- **Further, in-depth sub-system study (including a Stirling converter performance map)**
- **Complete the planned simulations and conduct further simulations that examine changes in the alternator electrical circuit**
- **Develop the system design more thoroughly, especially where the main components connect**
- **Examine Simulink's numerical solvers with respect to accuracy and speed**
- **Conduct a material evaluation of the entire system**
- **Compare the model with different simulation software**

[1] Paul Kallender, "Japan's Adeos-2 Suffers Catastrophic Failure," *Spacenews.com,* 11 November 2003. Available at http://www.space.com/spacenews/archive03/adeosarch_111103.html.
[2] *Ultra Triple Junction Solar Cells*, www.spectrolab.com/DataSheets/TNJCell/utj3.pdf
[3] *Wikipedia,* online edition, 20 Nov 2005, s.v. "Solar Cell." Available at http://en.wikipedia.org/wiki/ Solar_cell.
[4] Conversation via phone with Mark Natale, Naval Reactors, 2005.
[5] Roger R. Bate, Donald D Mueller, and Jerry E. White, *Fundamentals of Astrodynamics,* (New York: Dover Publications, Inc., 1971), 360-361.
[6] Charles C. Babcock, "High Power for Space Systems," *Propulsion Techniques: Action and Reaction,* (AIAA: Reston, VA, 1998), 335.
[7] Tony Philips, "Happy Anniversary, Viking Lander," *Science at NASA,* 20 July 2001. Available at http://science.nasa.gov/headlines/y2001/ast20jul_1.htm.
[8] Vincent Pisacane, "Lecture 1: Power System Introduction," *EA365 Space Power and Communications,* (Pisacane, 2005), 1-7.
[9] Gerald L. Kulcinski, "Spring 2000 Lecture 3," *NEEP602 Nuclear Power in Space,* (University of Wisconsin, 2000), 2. Available at http://fti.neep.wisc.edu/neep602/SPRING00/lecture3.pdf
[10] Gerald L. Kulcinski, "Fall 1996 Lecture 25," *NEEP602 Nuclear Power in Space,* (University of Wisconsin, 1996), 6. Available at http://fti.neep.wisc.edu/neep602/LEC25/IMAGES/fig6.GIF.
[11] David Buden, "Nuclear Reactors for Space Power," *Propulsion Techniques: Action and Reaction,* (AIAA: Reston, VA, 1998), 341.
[12] Gerald L. Kulcinski, "Fall 1996 Lecture 25," *NEEP602 Nuclear Power in Space,* (University of Wisconsin: Madison, 1996), 21-22. Available at http://fti.neep.wisc.edu/neep602/lecture25.html.
[13] Jerry Grey, "Commentary," *Aerospace America*, Vol. 43, No. 6, June 2005.
[14] David Darling, "Project Prometheus," 9 Nov 2005. Available at http://www.daviddarling.info/ encyclopedia/P/PrometheusProj.html.
[15] Leonard David, "Prometheus Pre-empted? New Nuclear Fission Missions Evaluated," *Space.com*, 10 Dec 2004. Available at http://www.space.com/businesstechnology/technology/jimo_update_041210.html.
[16] Wayne Smith, "Project Prometheus: NASA's New Nuclear Rocket Program," *Nuclearspace.com*. Available at http://www.nuclearspace.com/a_project_prometheus.htm.
[17] "Atlas V 500 Series," International Launch Services, 2005. Available at http://www.ilslaunch.com/atlas/ atlasv/AtlasV500/
[18] Ronald W. Humble, Gary N. Henry, and Wiley J. Larson, *Space Propulsion Analysis and Design*, (McGraw-Hill: New York, 1995), 692.
[19] Blair P. Bromley, "Getting More Miles Per Gallon," Astrodigital.org, 2001. Available at http://www.astrodigital.org/space/nuclear.html.
[20] Picture found at http://www.qrg.northwestern.edu/projects/vss/docs/Propulsion/1-how-does-ds1s-engine-work.html.
[21] Vincent Pisacane, "Lecture 4," *EA365 Space Power and Communications,* (Pisacane, 2005).

[22] *NASA Contractor Report CR-191023: Lunar Electric Power Systems Utilizing the SP-100 Reactor Coupled to Dynamic Conversion Systems*, (Washington, D.C.: NASA, 1993), 55.
[23] Matt Forsbacka, "Nuclear Safety Philosophy: A Risk Management Strategy and Building Block,"
[24] C.R. Nave, "Uranium-235 Fission," *Hyperphysics,* (C.R. Nave, 2005). Available at http://hyperphysics.phy-astr.gsu.edu/hbase/nucene/u235chn.html#c1.
[25] John R. Lamarsh and Anthony J. Baratta, *Introduction to Nuclear Engineering*, 3rd Ed., (Prentice Hall: Upper Saddle River, 2001).
[26] L. Barry Penswick, *1050K Stirling Space Engine Design,* (Mechanical Technology, Inc: 1988).
[27] Jerry John Sellers, *Understanding Space,* 2nd Ed., (McGraw-Hill: New York, 2000), 574.
[28] G. Walker and J.R. Senft, "Free Piston Stirling Engines," (Stirling Machine World: Los Olivos, CA, 1985), 9.
[29] Israel, Urieli, "Ideal Isothermal Analysis," *ME422 Stirling Cycle Machine Analysis*, (Ohio University, 2005). Available at www.ent.ohiou.edu/~urieli/stirling/isothermal/pvplot.jpg.
[30] Brent H. Van Arsdell, "Stirling Engines," Reprinted from *MacMillan Encyclopedia of Energy,* (MacMillan Reference USA, 2000).
[31] Clip from video at http://prometheus.jpl.nasa.gov. No longer available.
[32] Donald C. Hailey, *User Manual for the Multi-Purpose Heat Pipe Space Radiator Design and Analysis Code (HEPSPARC) Code Version 1.0,* (Lewis Research Center Group; Brookpark, OH, 1990).
[33] R.J. Onego, "Reactor Dynamic Module, PD-2 Reactor Kinetics with Feedback," 1973.
[34] Charles E. Tominson, *Nuclear Power Plant Thermodynamics and Heat Transfer*, (Iowa State University: Ames, IA, 1989).
[35] Frank P. Incropera and David P. DeWitt, *Fundamentals of Heat and Mass Transfer,* 4th Ed., (John Wiley & Sons: New York, 1996), 215.
[36] J. Weisman, *Elements of Nuclear Reactor Design,* (Elsevier: New York, 1977), 230.
[37] Peter M. Dussinger, William G. Anderson, and Eric T. Sunada, *Design and Testing of Titanium/Cesium and Titanium/Potassium Heat Pipes*, AIAA, http://www.1-act.com/13.pdf.
[38] G. P. Peterson, "Chapter 12: Heat Pipes," *Handbook of Heat Transfer*, 3rd Ed. (McGraw Hill: New York, 1998).
[39] David Berchowitz, *Stirling Cycle Engine Design and Optimization*, (University of Witwatersrund: Johannesburg, South Africa, 1986).
[40] Israel Urieli and David Berchowitz, *Stirling Cycle Engine Analysis*, (Adam Hilger Ltd: Bristol, GB, 1984).
[41] Norman S. Nise, *Control Systems Engineering,* 4th Ed. (California State Polytechnic Univ.: Pomona, 2004).
[42] Barry Penswick, "Navy 50 kW Stirling," Provided through NASA Glenn Research Center, December 2005.
[43] Israel Urieli, *Heater and Cooler Simple Analysis*, Ohio University, 2006. Found at http://www.ent.ohiou.edu/~urieli/stirling/simple/htx_simple.html.

[44] W. M. Kays and A. L. London, *Compact Heat Exchangers*, 3rd Ed. (Krieger Publishing Co.: Malabar, FL, 1998).
[45] Lanny G. Thieme, *Friction Factor Characterization for High-Porosity Random Fiber Regenerators.* (Glenn Research Center: Cleveland, OH, 2001), 7.
[46] David Gedeon, *SAGE: Stirling-Cycle Model-Class Reference Guide*, 3rd Ed. (Gedeon Associates: Athens, OH, 1999).
[47] William G. Anderson, David Sarraf, and Peter M. Dussinger, *Development of a High Temperature Water Heat Pipe Radiator,* 3rd International Energy Conversion Engineering Conference, (AIAA, 2005).
[48] Lee S. Mason, A Power Conversion Concept for the Jupiter Icy Moons Orbiter, (Glenn Research Center: Cleveland, OH, 2003), 6.

Bibliography

Anderson, William G., David Sarraf, and Peter M. Dussinger. *Development of a High Temperature Water Heat Pipe Radiator.* 3rd International Energy Conversion Engineering Conference. (AIAA, 2005).

"Atlas V 500 Series." International Launch Services. 2005. Available at http://www.ilslaunch.com/atlas/ atlasv/AtlasV500/.

Babcock, Charles C. "High Power for Space Systems." *Propulsion Techniques: Action and Reaction.* (AIAA: Reston, VA, 1998).

Bate, Roger R., Donald D Mueller, and Jerry E. White. *Fundamentals of Astrodynamics.* (New York: Dover Publications, Inc., 1971).

Berchowitz, David. *Stirling Cycle Engine Design and Optimization.* (University of Witwatersrund: Johannesburg, South Africa, 1986).

Bromley, Blair P. "Getting More Miles Per Gallon." Astrodigital.org. 2001. Available at http://www.astrodigital.org/space/nuclear.html.

Buden, David. "Nuclear Reactors for Space Power." *Propulsion Techniques: Action and Reaction.* (AIAA: Reston, VA, 1998).

Clip from video at http://prometheus.jpl.nasa.gov. No longer available.

Darling, David. "Project Prometheus." 9 Nov 2005. Available at http://www.daviddarling.info/encyclopedia/P/PrometheusProj.html.

David, Leonard. "Prometheus Pre-empted? New Nuclear Fission Missions Evaluated." *Space.com.* 10 Dec 2004. Available at http://www.space.com/businesstechnology/ technology/jimo_update_041210.html.

Dussinger, Peter M., William G. Anderson, and Eric T. Sunada. *Design and Testing of Titanium/Cesium and Titanium/Potassium Heat Pipes*. AIAA. http://www.1-act.com/13.pdf.

Forsbacka, Matt. "Nuclear Safety Philosophy: A Risk Management Strategy and Building Block."

Gedeon, David. *SAGE: Stirling-Cycle Model-Class Reference Guide.* 3rd Ed. (Gedeon Associates: Athens, OH, 1999).

Grey, Jerry. "Commentary." *Aerospace America.* Vol. 43. No. 6. June 2005.

Hailey, Donald C. *User Manual for the Multi-Purpose Heat Pipe Space Radiator Design and Analysis Code (HEPSPARC) Code Version 1.0.* (Lewis Research Center Group; Brookpark, OH, 1990).

Humble, Ronald W., Gary N. Henry, and Wiley J. Larson. *Space Propulsion Analysis and Design.* (McGraw-Hill: New York, 1995).

Incropera, Frank P., and David P. DeWitt. *Fundamentals of Heat and Mass Transfer.* 4th Ed. (John Wiley & Sons: New York, 1996).

Kallender, Paul. "Japan's Adeos-2 Suffers Catastrophic Failure." *Spacenews.com.* 11 November 2003. Available at http://www.space.com/spacenews/archive03/ adeosarch_111103.html.

Kays, W. M., and A. L. London. *Compact Heat Exchangers.* 3rd Ed. (Krieger Publishing Co.: Malabar, FL, 1998).

Kulcinski, Gerald L. "Fall 1996 Lecture 25." *NEEP602 Nuclear Power in Space.* (University of Wisconsin, 1996). Available at http://fti.neep.wisc.edu/neep602/ LEC25/IMAGES/fig6.GIF.

Kulcinski, Gerald L. "Fall 1996 Lecture 25." *NEEP602 Nuclear Power in Space.* (University of Wisconsin: Madison, 1996). Available at http://fti.neep.wisc.edu/neep602/lecture25.html.

Kulcinski, Gerald L. "Spring 2000 Lecture 3." *NEEP602 Nuclear Power in Space.* (University of Wisconsin, 2000). Available at http://fti.neep.wisc.edu/neep602/SPRING00/lecture3.pdf.

Lamarsh, John R., and Anthony J. Baratta. *Introduction to Nuclear Engineering.* 3rd Ed. (Prentice Hall: Upper Saddle River, 2001).

Mason, Lee S. *A Power Conversion Concept for the Jupiter Icy Moons Orbiter.* (Glenn Research Center: Cleveland, OH, 2003).

NASA Contractor Report CR-191023: Lunar Electric Power Systems Utilizing the SP-100 Reactor Coupled to Dynamic Conversion Systems. (Washington, D.C.: NASA, 1993).

Natale, Mark. Conversation via phone. Naval Reactors. 2005.

Nave, C. R. "Uranium-235 Fission." *Hyperphysics.* (C.R. Nave, 2005). Available at http://hyperphysics.phy-astr.gsu.edu/hbase/nucene/u235chn.html#c1.

Nise, Norman S. *Control Systems Engineering.* 4th Ed. (California State Polytechnic Univ.: Pomona, 2004).

Onego, R.J. "Reactor Dynamic Module, PD-2 Reactor Kinetics with Feedback." 1973.

Tominson, Charles E. *Nuclear Power Plant Thermodynamics and Heat Transfer.* (Iowa State University: Ames, IA, 1989).

Penswick, L. Barry. *1050K Stirling Space Engine Design.* (Mechanical Technology, Inc: 1988).

Penswick, L. Barry. "Navy 50 kW Stirling." Provided through NASA Glenn Research Center. December 2005.

Peterson, G. P. "Chapter 12: Heat Pipes." *Handbook of Heat Transfer.* 3rd Ed. (McGraw Hill: New York, 1998).

Philips, Tony. "Happy Anniversary, Viking Lander." *Science at NASA.* 20 July 2001. Available at http://science.nasa.gov/headlines/y2001/ast20jul_1.htm.

Picture found at http://www.qrg.northwestern.edu/projects/vss/docs/Propulsion/1-how-does-ds1s-engine-work.html.

Pisacane, Vincent. "Lecture 1: Power System Introduction." *EA365 Space Power and Communications.* (Pisacane, 2005).

Pisacane, Vincent. "Lecture 4." *EA365 Space Power and Communications.* (Pisacane, 2005).

Sellers, Jerry John. *Understanding Space.* 2nd Ed. (McGraw-Hill: New York, 2000).

Smith, Wayne. "Project Prometheus: NASA's New Nuclear Rocket Program." *Nuclearspace.com.* Available at http://www.nuclearspace.com/a_project_prometheus.htm.

Ultra Triple Junction Solar Cells. www.spectrolab.com/DataSheets/TNJCell/utj3.pdf.

Urieli, Israel. *Heater and Cooler Simple Analysis.* Ohio University. 2006. Found at http://www.ent.ohiou.edu/~urieli/stirling/simple/htx_simple.html.

Urieli, Israel. "Ideal Isothermal Analysis." *ME422 Stirling Cycle Machine Analysis.* (Ohio University, 2005). Available at www.ent.ohiou.edu/~urieli/stirling/isothermal/pvplot.jpg.

Urieli, Israel, and David Berchowitz. *Stirling Cycle Engine Analysis.* (Adam Hilger Ltd:

Bristol, GB, 1984).
Van Arsdell, Brent H. “Stirling Engines.” Reprinted from *MacMillan Encyclopedia of Energy.* (MacMillan Reference USA, 2000).
Walker, G., and J.R. Senft. “Free Piston Stirling Engines.” (Stirling Machine World: Los Olivos, CA, 1985).
Weisman, J. *Elements of Nuclear Reactor Design.* (Elsevier: New York, 1977).
Wikipedia. online edition, 20 Nov 2005, s.v. “Solar Cell.” Available at http://en.wikipedia.org/wiki/Solar_cell.

Appendix A: Reactivity Insertion of 0.001 at the 5 Second Mark. Constant 600 kWt Heat Flow Out of the Stirling Hot End.

This appendix shows all the output values for the title simulation from the partial model of the reactor, heat transfer loops, and heat exchanger.

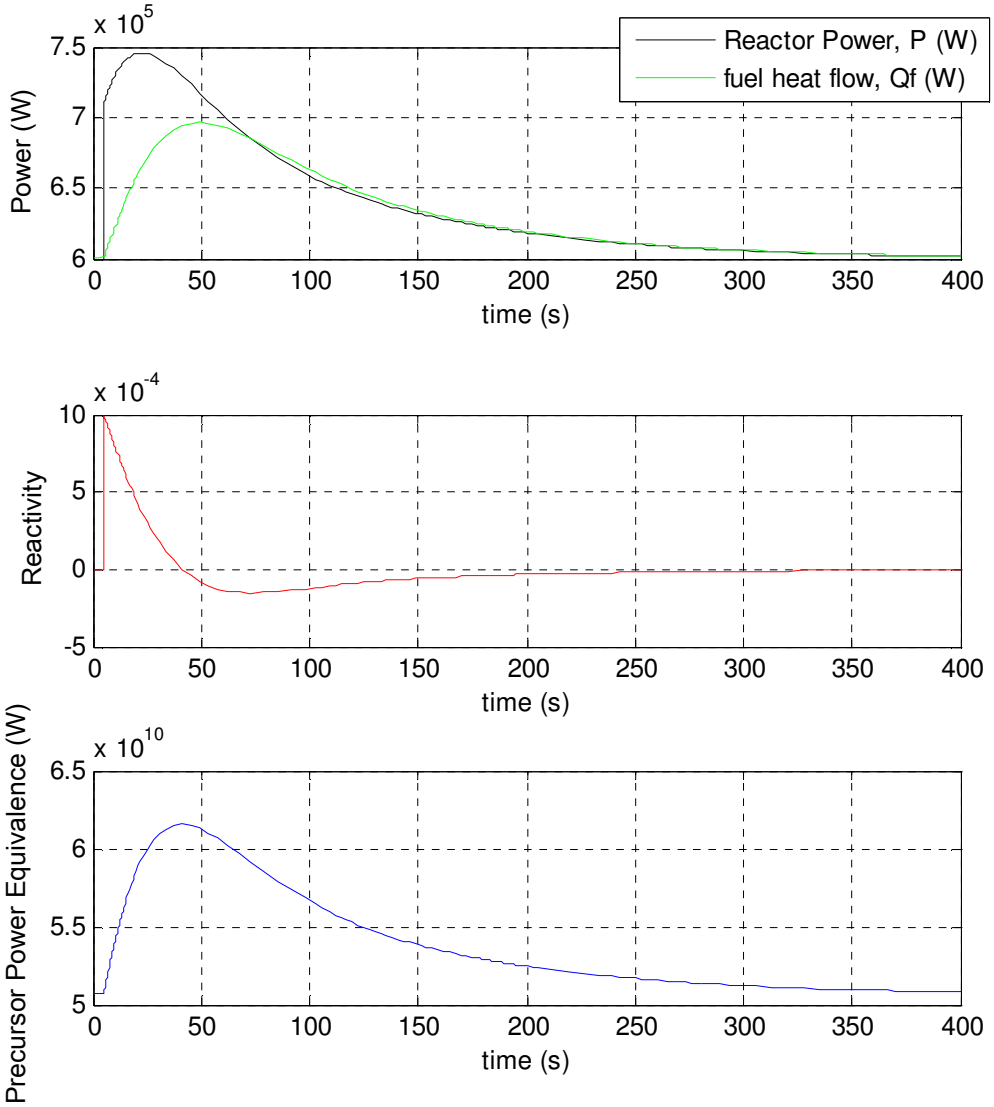

Appendix A: Reactivity Insertion of 0.001 at the 5 Second Mark.

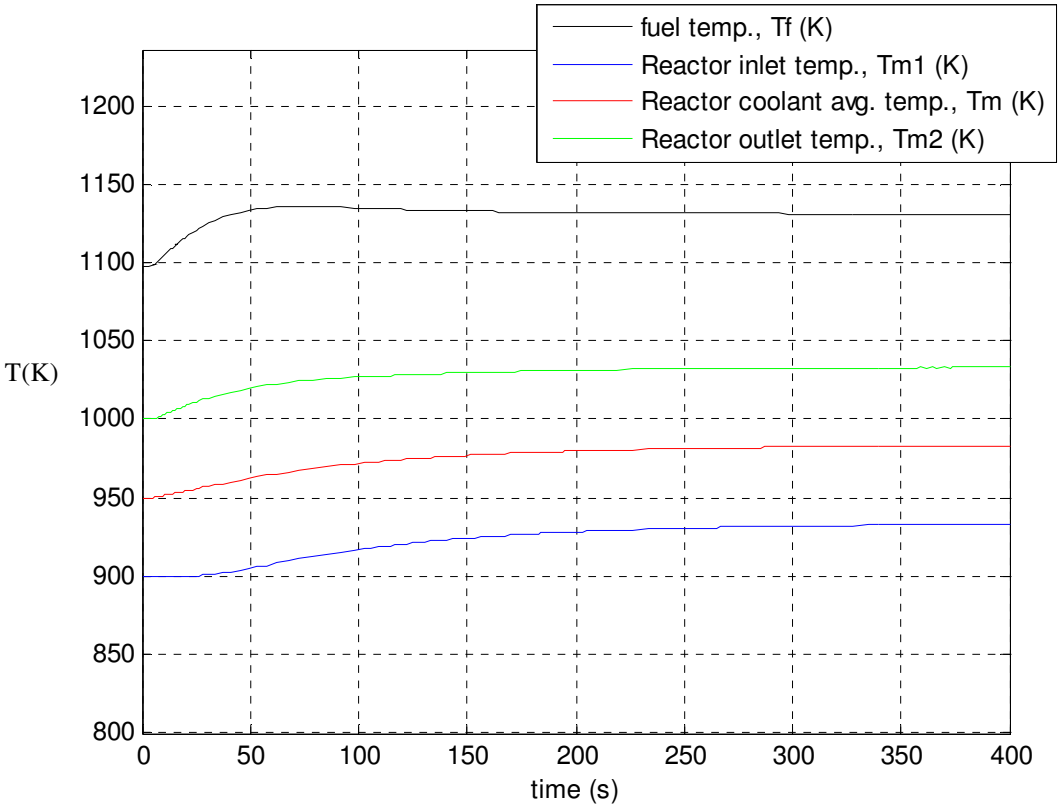

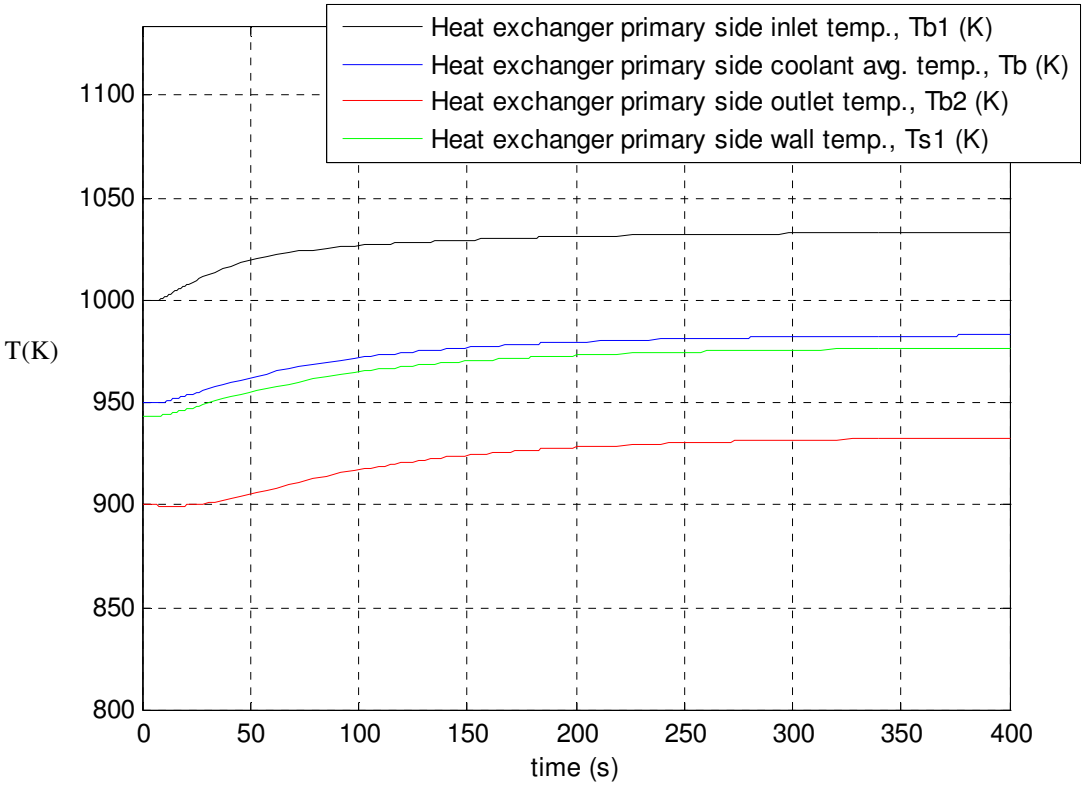

Appendix A: Reactivity Insertion of 0.001 at the 5 Second Mark.

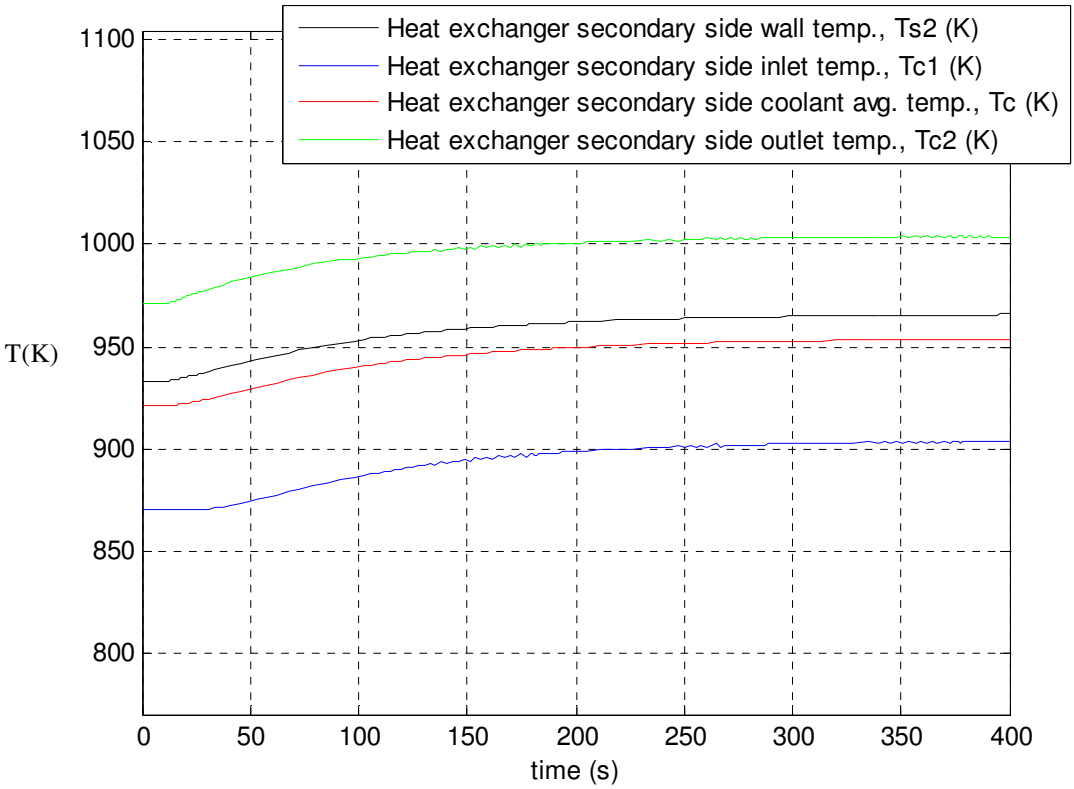

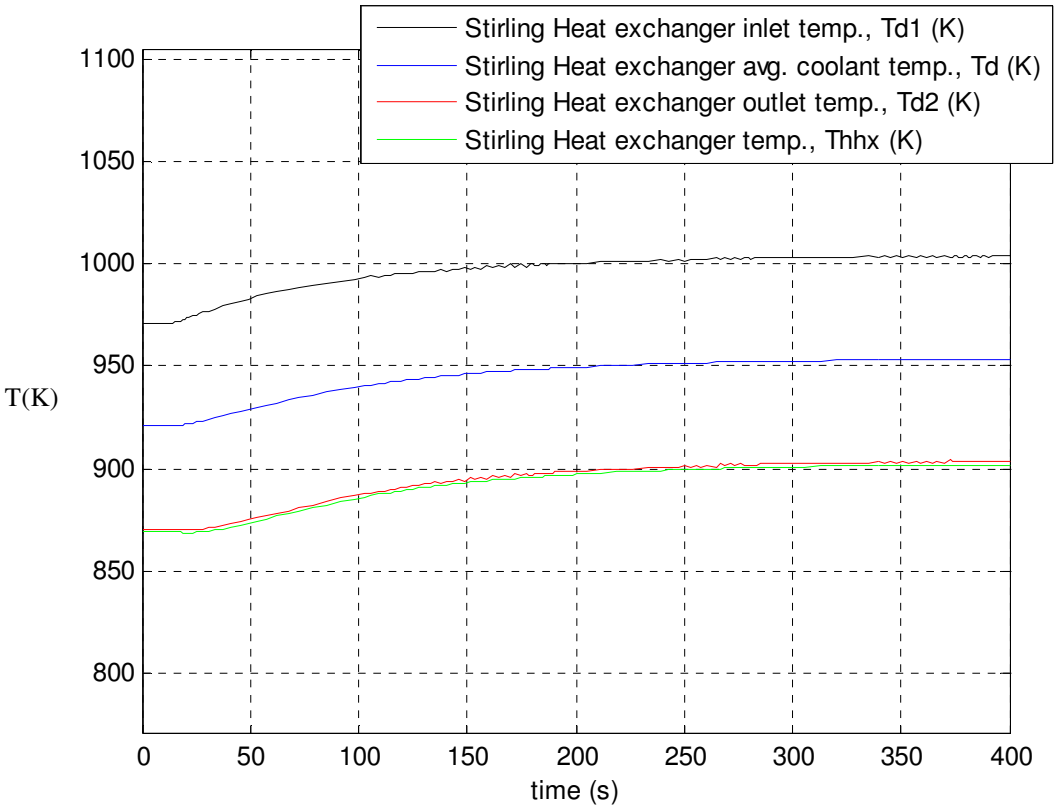

Appendix B: Reactivity Insertion of -0.001 at the 5 Second mark. Constant 600 kWt Heat Flow Out of the Stirling Hot End.

This appendix shows all the output values for the title simulation from the partial model of the reactor, heat transfer loops, and heat exchanger.

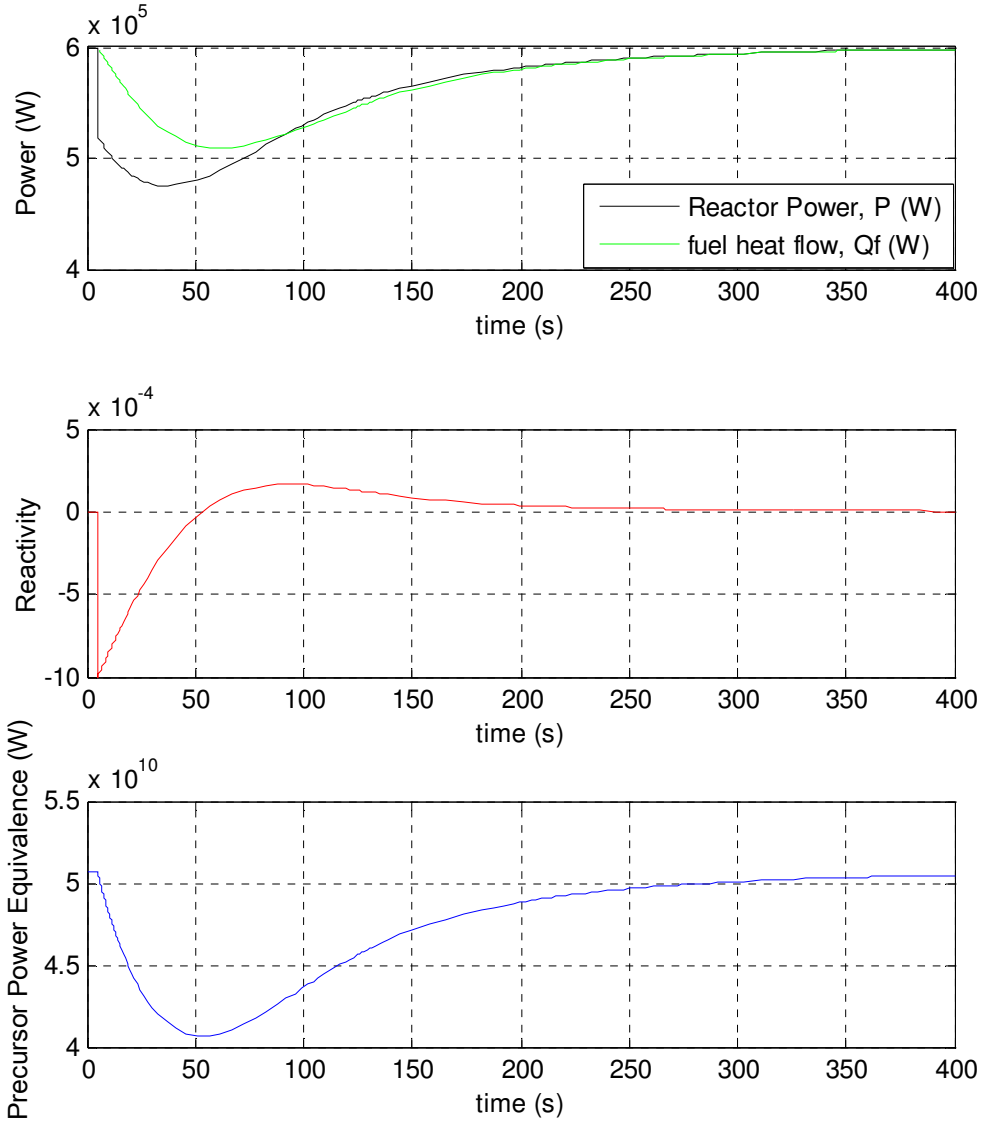

Appendix B: Reactivity Insertion of -0.001 at the 5 Second mark.

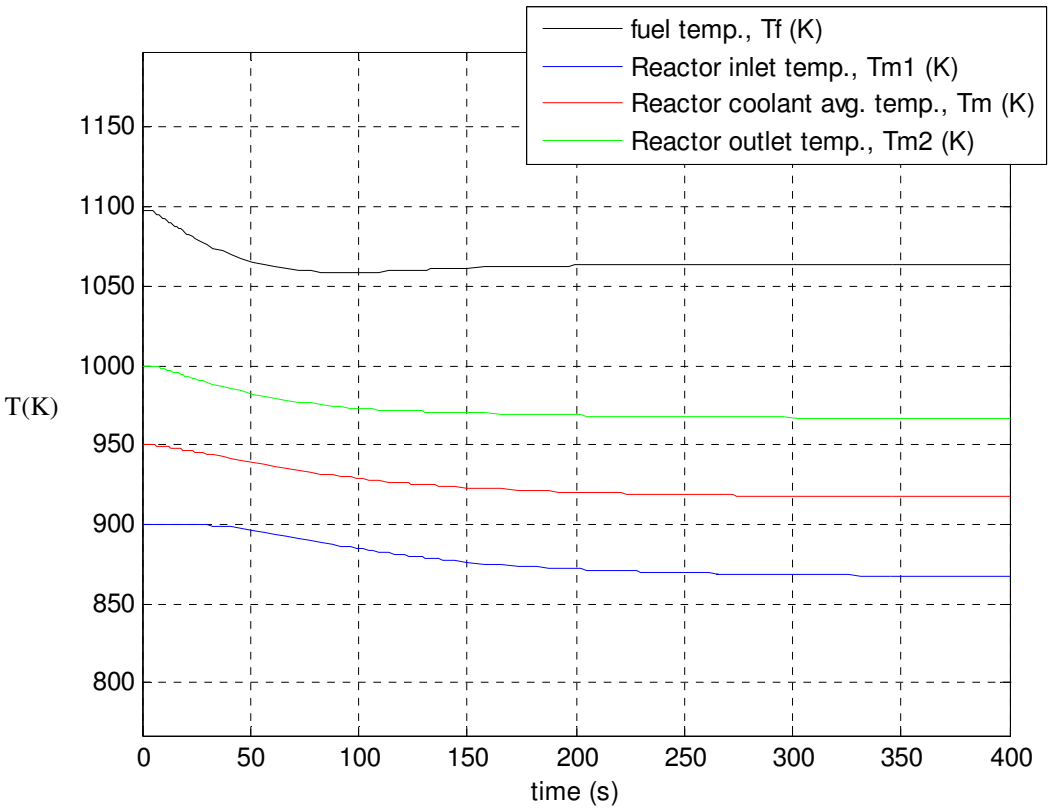

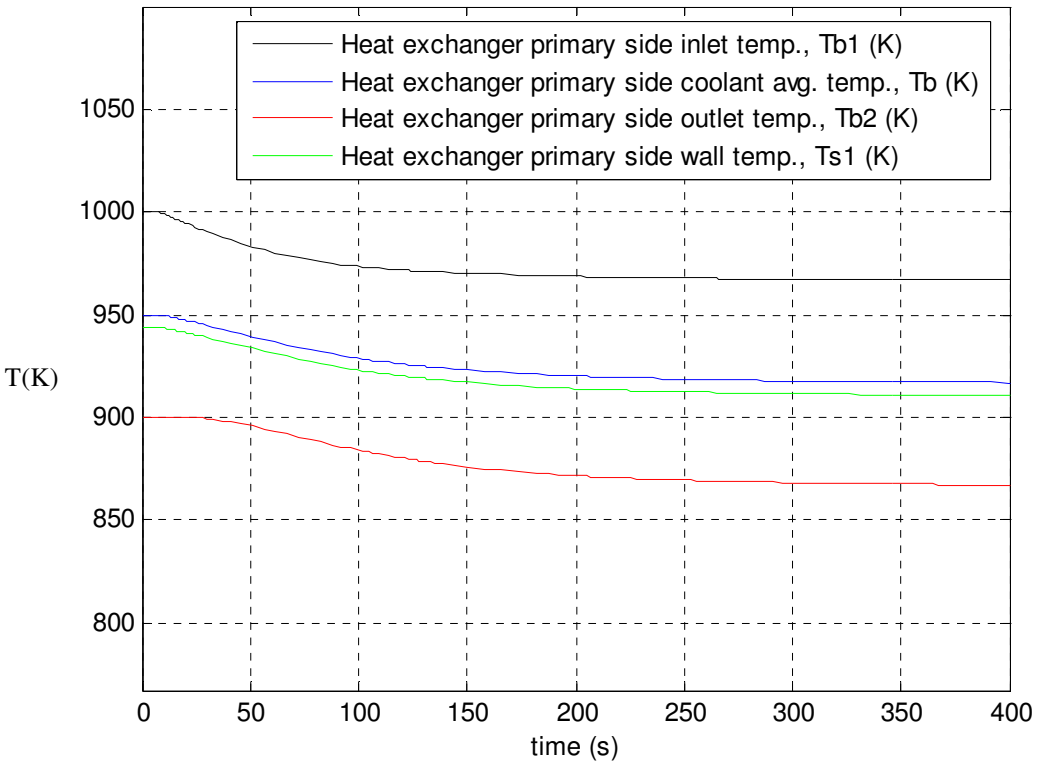

Appendix B: Reactivity Insertion of -0.001 at the 5 Second mark.

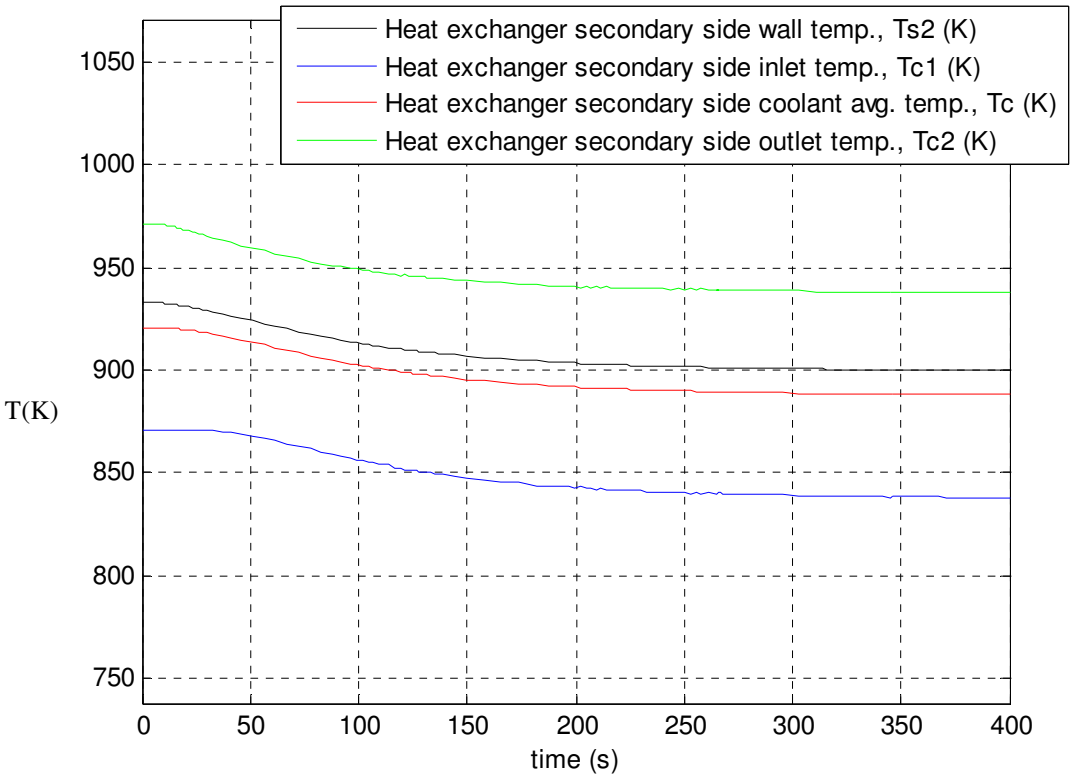

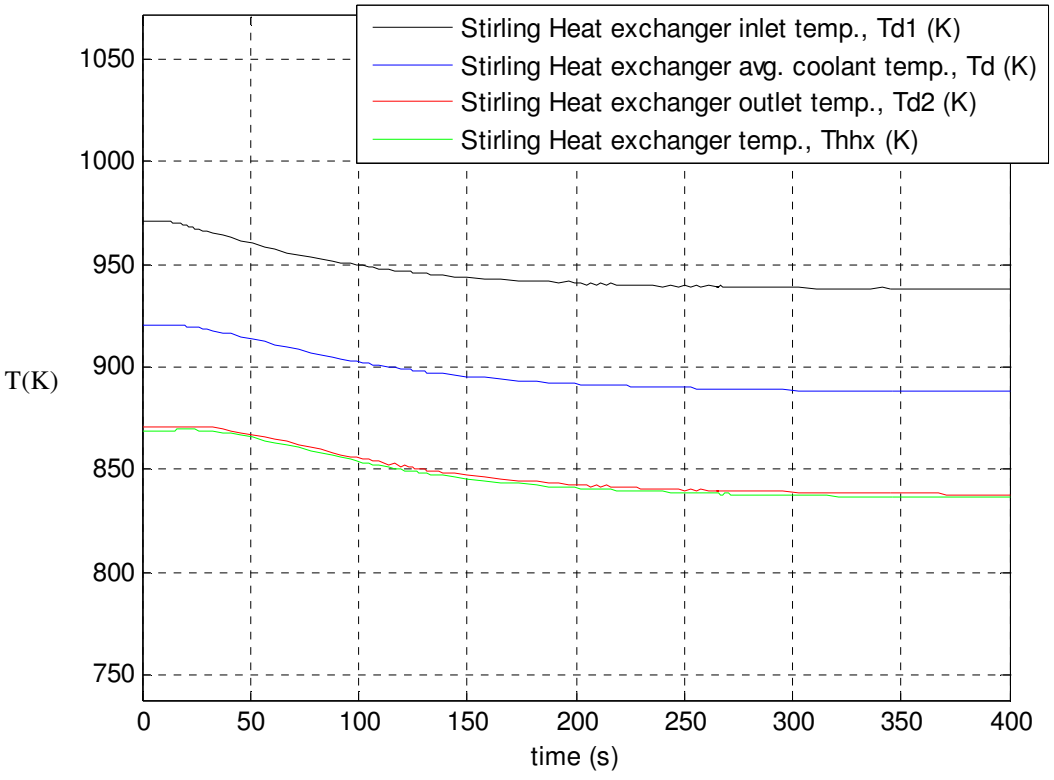

Appendix C: Ten Degree Temperature Drop for Stirling Hot End Heat Exchanger.

This appendix shows all the output values for the title simulation from the partial model of the reactor, heat transfer loops, and heat exchanger.

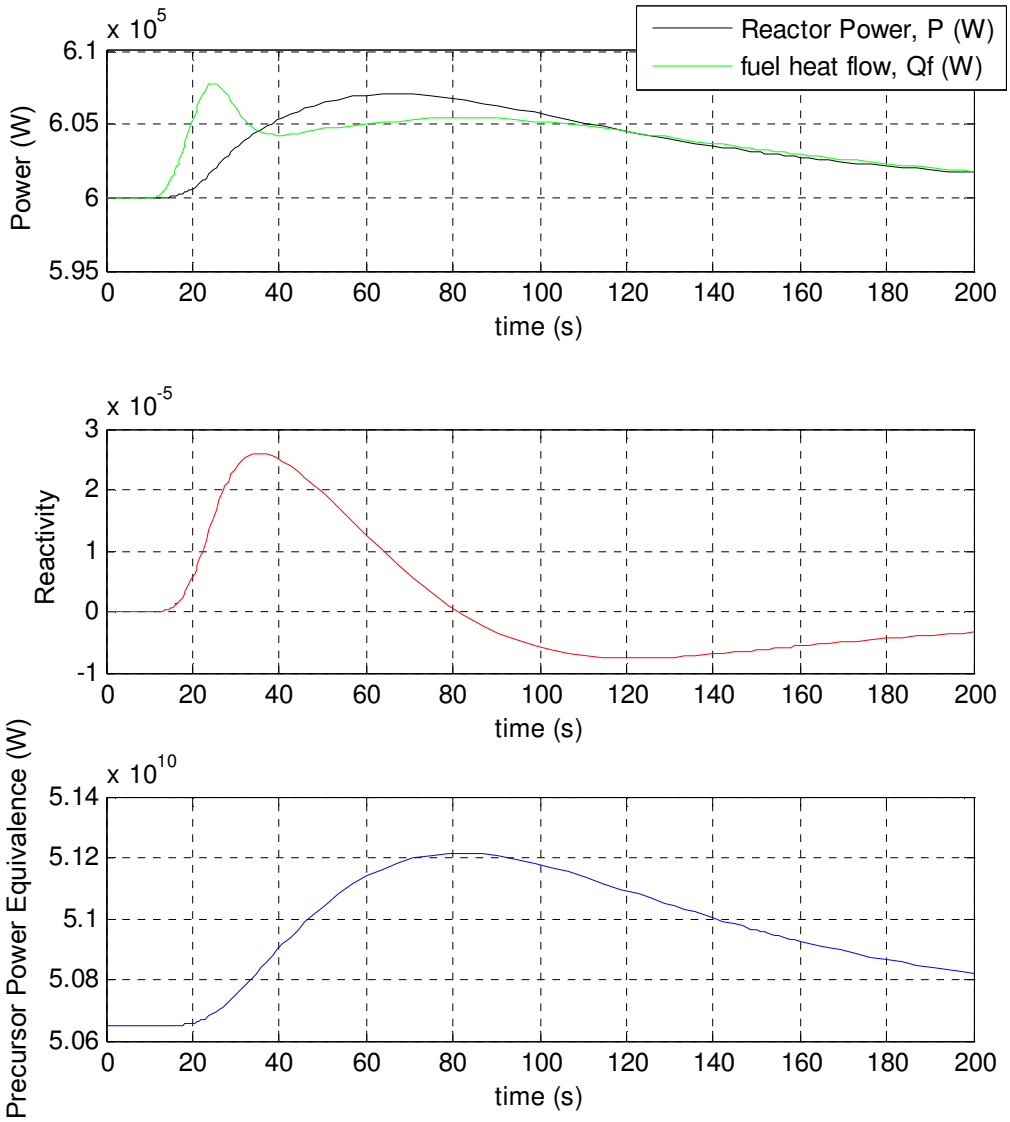

Appendix C: Ten Degree Temperature Drop for Stirling Hot End Heat Exchanger.

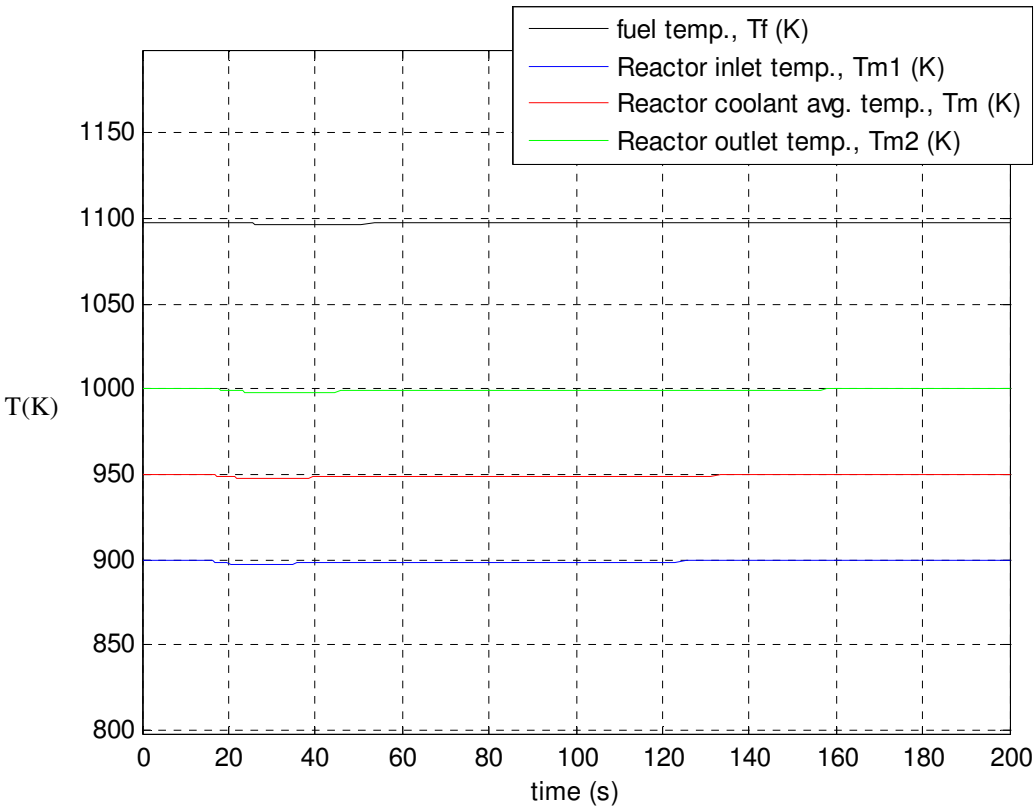

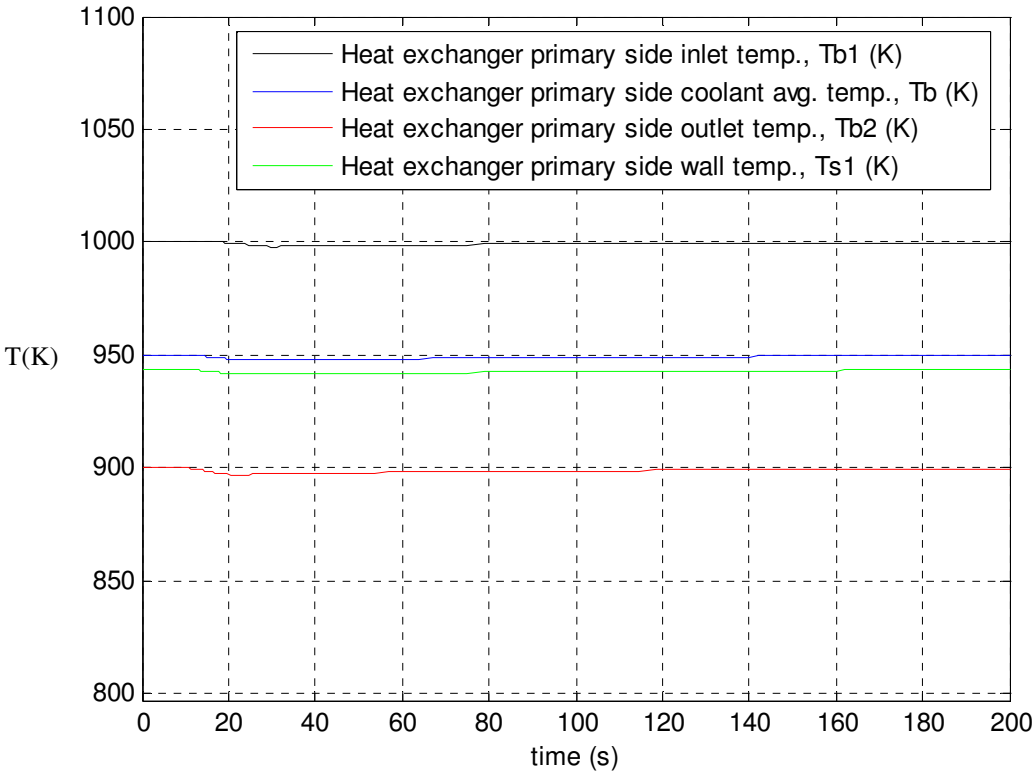

Appendix C: Ten Degree Temperature Drop for Stirling Hot End Heat Exchanger.

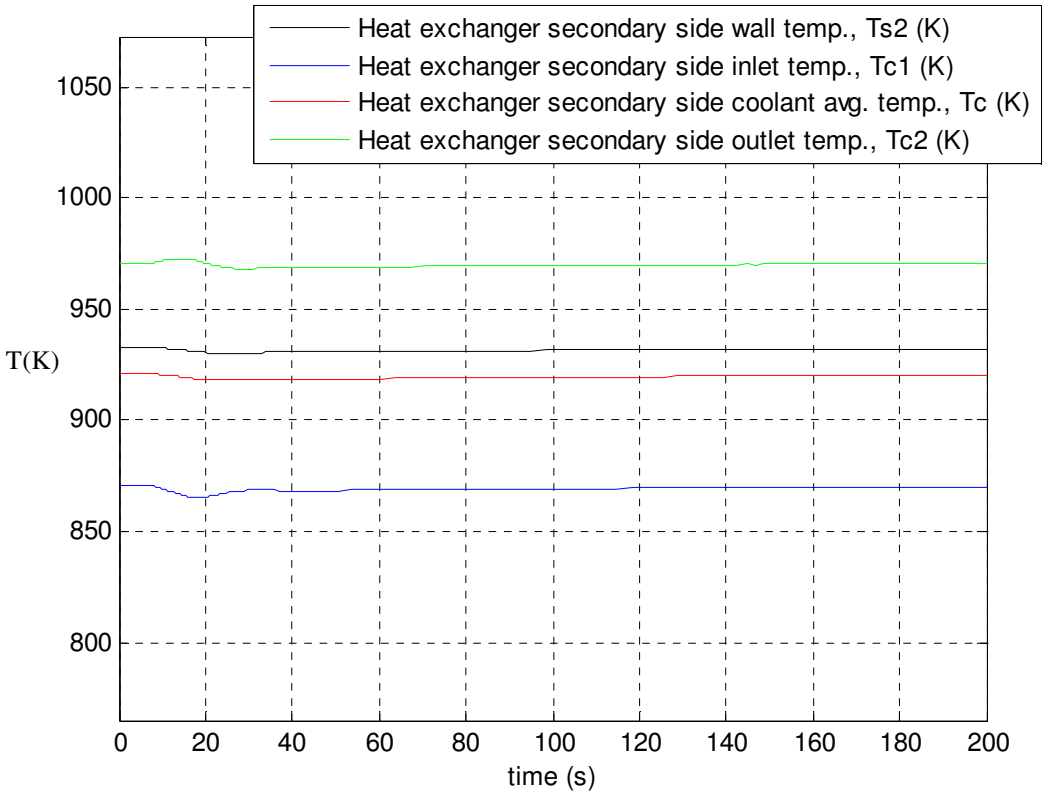

Appendix D: Ten Degree Temperature Rise for Stirling Hot End Heat Exchanger.

This appendix shows all the output values for the title simulation from the partial model of the reactor, heat transfer loops, and heat exchanger.

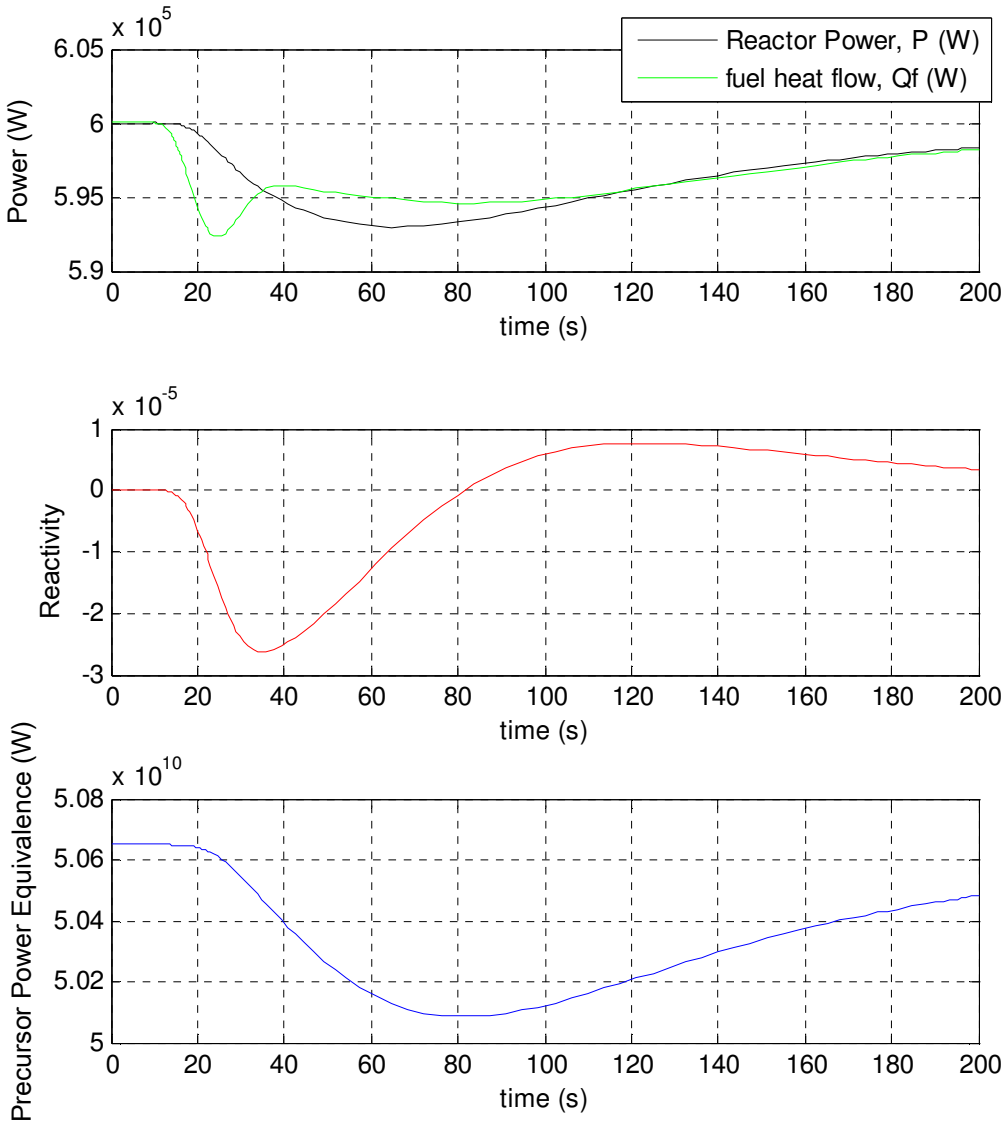

Appendix D: Ten Degree Temperature Rise for Stirling Hot End Heat Exchanger.

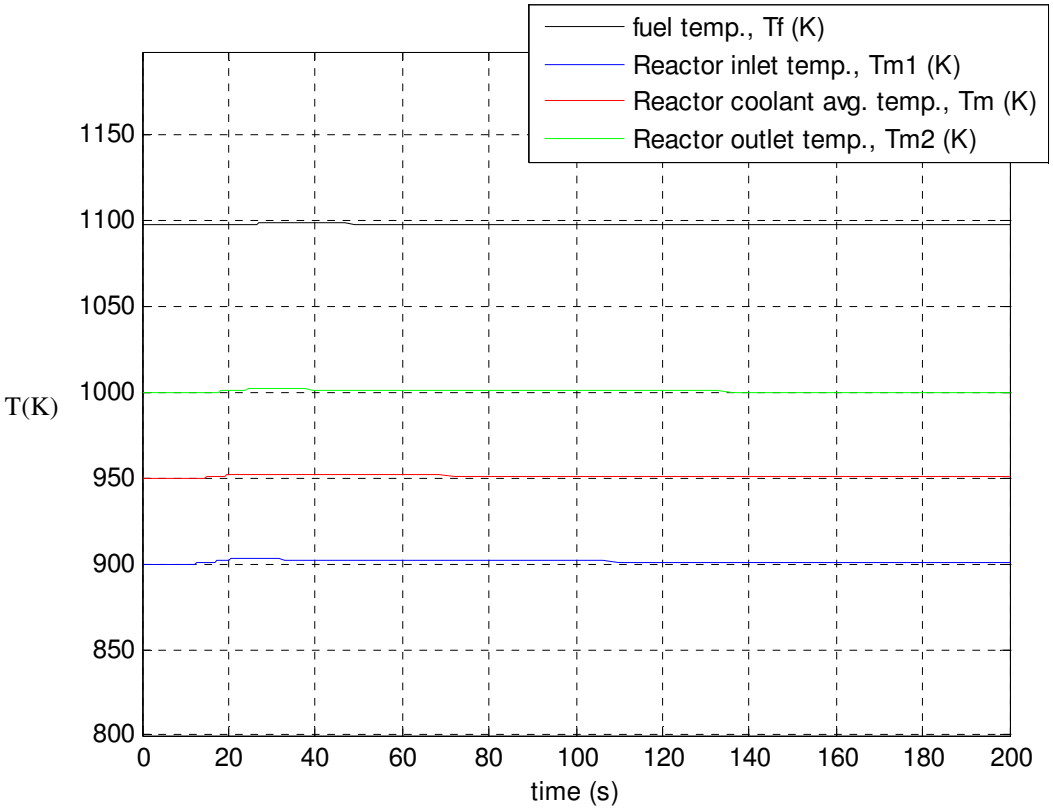

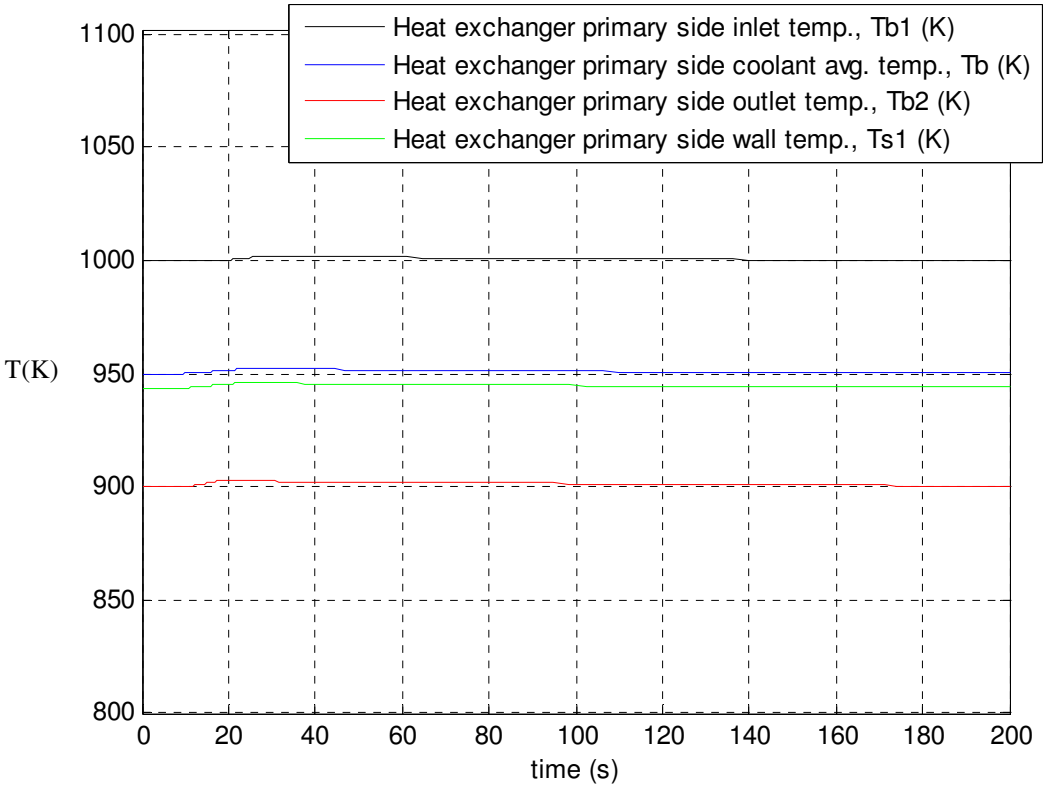

Appendix D: Ten Degree Temperature Rise for Stirling Hot End Heat Exchanger.

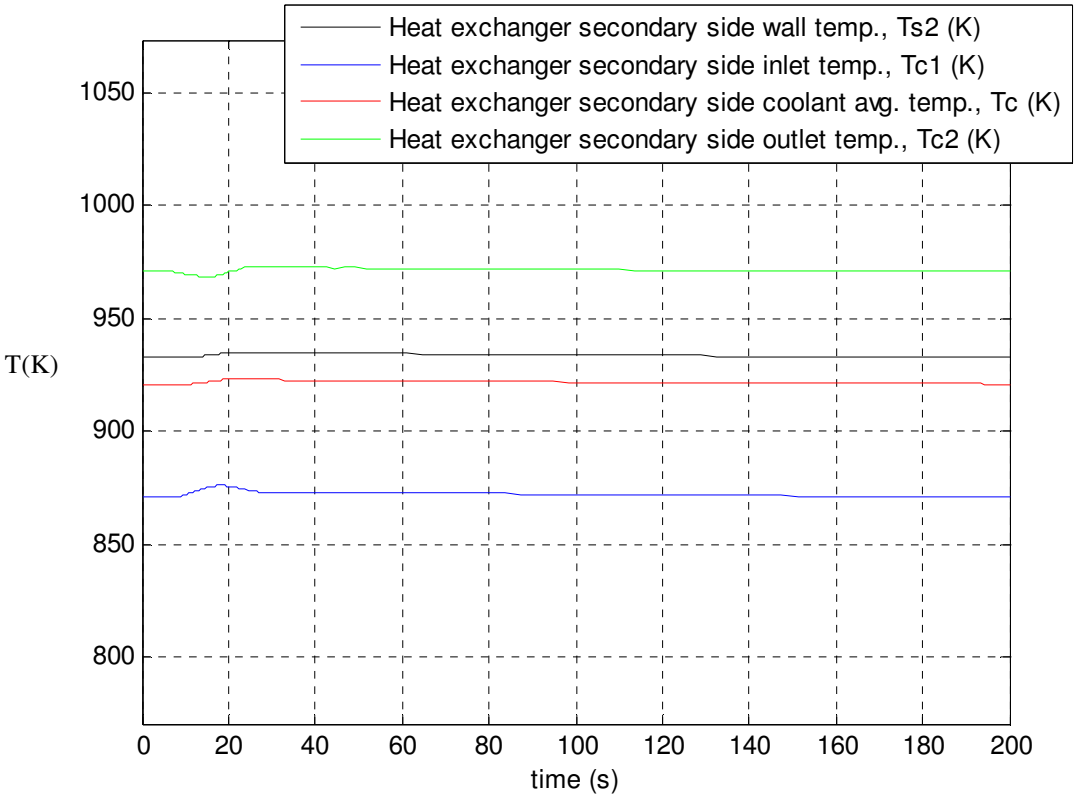

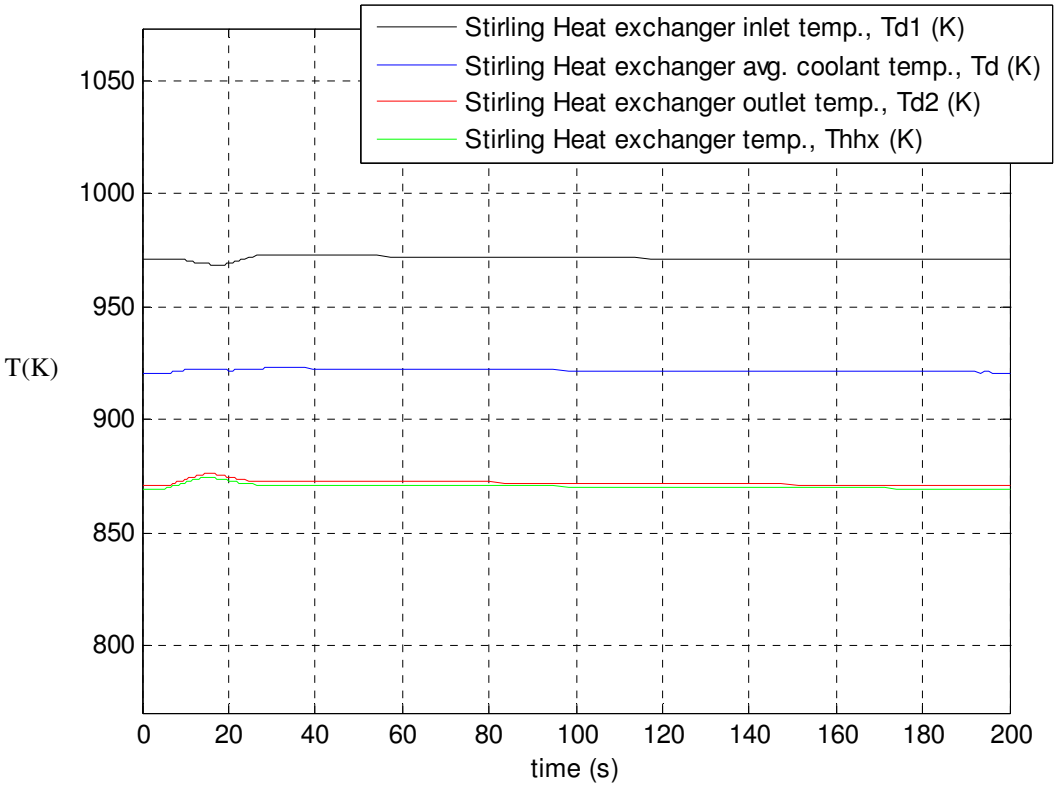

Appendix E: Stirling Model Data Provided by NASA

TO: Justin Langlois

FROM: Barry Penswick

SUBJECT: 50 KW Stirling convertor model

DATE: 6 Dec 05

The following material describes the parameters of a hypothetical 50 KW Stirling cycle convertor that hopefully will meet your system modeling requirements. Some of the generic convertor characteristics can be related back to a relatively recent review carried out at NASA / GRC concerning high power space systems. As such the operating point employed in the model may not match potential operating conditions that may evolve from your ongoing work, however modifying the model to meet your specific requirements is a straightforward process.

Configuration Issues

The reference configuration of the 50 KW system is a conventional piston / displacer arrangement with a linear alternator attached to the power piston. The basic external configuration of the convertor is shown in the following sketch. It is important to note that as configured the 50 KW convertor is NOT balanced. I've assumed that you will have to address this issue and would recommend that you simply assume that the two convertors are operated in a "hot end to hot end" opposed configuration and are electrically coupled so as to provide the proper synchronization of the pistons and in turn effective vibration balancing the pair of 50 KW convertors.

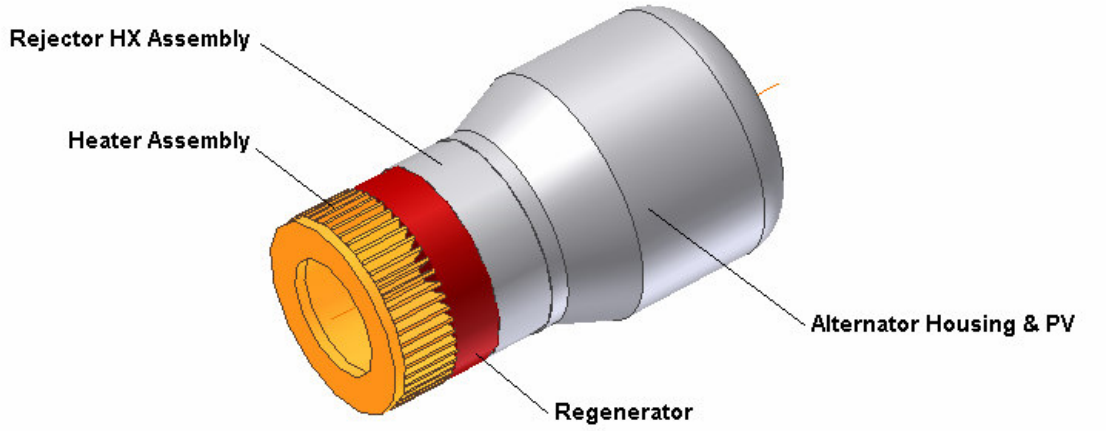

Figure 1. Convertor configuration

From the viewpoint of the internal component configuration it is assumed that the conventional common cylinder diameter with the displacer rod through the power piston is employed. The regenerator is of an annular configuration surrounding the displacer. Both the accepter and rejecter heat exchangers are of the tubular type. This fundamental configuration is currently employed by SunPower Inc. and other groups and represents a logical configuration for this sized convertor. Terminology employed in the model is noted on the following sketch where applicable and values provided in the next table.

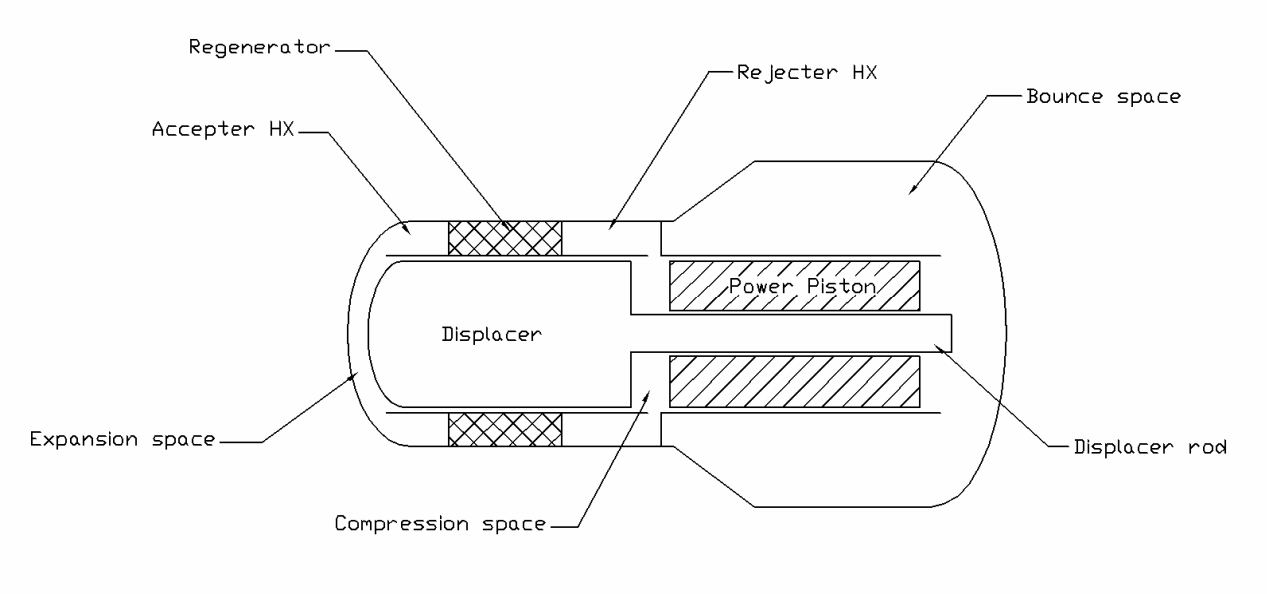

Figure 2. Convertor internal component configuration and terminology

Table 1 - Convertor parameters

Parameter	Nominal Value / Comment
General	
Operating frequency	90 Hz
Charge pressure	136 Bar
Effective hot end temperature	925 K (652 C)
Effective rejecter temperature	463 K (190 C)
Total convertor mass	270 Kg
Net electrical out put power	50 KW
Convertor cycle efficiency	.316
Convertor over all efficiency	.294
Power piston related	
Piston frontal area	.0381 m^2
Piston amplitude	13 mm
Power piston / alternator moving mass	25 Kg

Compression space volume	6.0E-4 m^3
Bounce space volume	14.5E-3 m^3
Piston / displacer phase angle	59.3 degrees
Piston PV power	53.6 KW
Displacer related	
Displacer hot end frontal area	3.892E-2
Displacer cold end frontal area	3.81E-2
Displacer rod diameter	32 mm
Displacer amplitude	8.4 mm
Displacer effective moving mass	8.5 Kg
Expansion space volume	4.34E-4 m^3
Rejecter HX related	
Length	75 mm
Tube ID	1.4 mm
Tube number	3100
Regenerator related	
Frontal area	5.017E-2
Length	55 mm
Porosity	88 %
Wire diameter	25 micron
Accepter HX related	
Length	75 mm
Tube ID	1.3 mm
Tube number	2750

Linear Alternator

A simplified alternator modeling technique was employed to develop a reference alternator. Since there was no definition of the alternator requirements the values noted in the following table represent the parameters of the reference alternator. As noted previously it is a relatively straightforward process to adapt the model alternator to your specific operating requirements.

Table 2 - Linear alternator parameters

Alternator Characteristics	Nominal Value / Comments
Design output power	50 KW
Terminal voltage	200 Vrms
Design efficiency	93%
Operating temperature (apx.)	490 K (215 C)
Piston amplitude	13 mm
Alternator constant	38.5 V sec/m
Coil resistance (est.)	.028 ohm
Coil inductance (est.)	.2 mH

Appendix F: MATLAB® Code for System Constants and Initial Conditions

```
% Fuel Properties (UN)
beta=0.0065; %delayed neutron fraction (dl)
lamda=0.077; %one group precursor decay constant (1/s)
ng=10^(-6); %neutron generation time (s)
rowo=0; %initial reactivity (dl)
Lf=0.25; %fuel pin length (m)
kf=14; %fuel conductivity UN (W/(m*K))
mU235=180; %U-235 mass (kg)
mUN=2*mU235*(235+15)/235; %UN mass (kg)
pf=14320; %fuel density UN (kg/m^3)
N=108;   %number of fuel pins (dl)
vf=mUN/pf; %fuel volume (m^3)
rf=round(10000*sqrt(vf/(pi*Lf*N)))/10000; %fuel pin radius (m)
cpf=219.4; %fuel specific heat UN (W*s/(kg*K))
alphaf=-3*10^(-5); %fuel temperature coefficient UO2 (1/K)

% Power level
Po=6.9*10^5; %initial power level (Wt)
PEo=Po*beta/(lamda*ng); %initial power equivalence (Wt)

% Moderator Properties (NaK)
pm=725;     %moderator density (kg/m^3)
cpm1=875;  %mod. spec. heat at reactor inlet (W*s/(kg*K))
cpm2=875;  %mod. spec. heat at reactor outlet (W*s/(kg*K))
cpm=(cpm1+cpm2)/2; %avg. mod. spec. heat (W*s/(kg*K))
mdotm=Po/(2*cpm*25); %mod. mass flow (kg/s)
pc=sqrt(2*pi)*rf;  %pitch (m)
Acell=pc^2-pi*rf^2; %cell mod. area (m^2)
pw=pi*2*rf; %wetted perimeter (m)
vm=Acell*Lf*N; %moderator volume (m^3)
de=4*Acell/pw; %equivalent diameter (m)
alpham=0; %mod. temp. coeff. (1/K)
velm=mdotm/(pm*Acell*N); %mod. velocity (m/s)
um=1.59*10^(-4); %mod. viscosity (kg/(m*s))
km=25.6;       %mod. thermal conductivity (W/(m*K))
Re=de*velm*pm/um; %mod. Reynolds number (dl)
Pr=cpm*um/km; %mod. Prandtl number (dl)
Pe=Re*Pr; %Peclet Number (dl)
ht=(km/de)*(7+4.24*(pc/(2*rf))^1.52); %mod. heat transfer coeff. (W/(m^2*K))

% Primary Loop Outside the Reactor
dp=0.04; %pipe diameter (m)
Ap=pi*dp^2/4; %pipe cross-section area (m^2)
tau3=2.5; %time delay from reactor outlet to heat exchanger inlet (s)
tau4=2.5; %time delay from heat exchanger outlet to reactor inlet (s)
lg3=mdotm*tau3/(pm*Ap); %pipe length from reactor outlet to hx1 (m)
lg4=mdotm*tau4/(pm*Ap); %pipe length from hx1 to reactor inlet (m)

% Primary to Secondary Heat Exchanger Properties (steel)
dt=0.0095; %diameter of hx tubes
tt=0.003; %hx tube thickness
odt=dt+2*tt; %outer diameter tube
At=pi*dt^2/4; %area cs of hx tubes
n=18; %hx size
Nt=n^2+4*n; %number of hx tubes
Lt=0.5; %tube length
vhx1=At*Nt*Lt; %volume of coolant in heat exchanger (m^3)
ahx1=pi*dt*Lt*Nt;   %primary side heat exchanger wall area (m^2)
Rem=mdotm*dt/(At*Nt*um); %hx1 Reynolds number
Prm=cpm*um/km; %hx1 Prandtl number
Pem=Rem*Prm; %hx1 Peclet number
hx1=(km/dt)*(4.82+0.697*odt/dt);  %primary side heat transfer coeff. (W/(m^2*K))
ahx2=Lt*pi*odt*Nt; %wall area loop 2
phx2=1.25*odt; %hx pitch
pw=8000;   %wall density (kg/m^3)
vw=pi/4*(odt^2-dt^2)*Lt*Nt; %wall volume (m^3)
mw=vw*pw; %wall mass (kg)
cpw=500; %wall spec. heat steel (W*s/(kg*K))
```

```
kw=21.5; %wall conductivity
Bix1=hx1*Lt/kw; %tube Biot number
mdots=mdotm; %mass flow rate of coolant in secondary loop (kg/s)
ps=pm; %density of sec. coolant (kg/m^3)
cps=cpm; %avg. spec. heat of sec. coolant (W*s/(kg*K))
cps1=cpm; %avg. spec. heat of sec. coolant at exch. inlet (W*s/(kg*K))
cps2=cpm; %avg. spec. heat of sec. coolant at exch. outlet (W*s/(kg*K))
ks=km; %sec. coolant conductivity
us=um; %sec. coolant viscosity
ds=2*n*phx2; % shell diameter (m)
As=pi/4*ds^2-Nt*pi/4*odt^2; %shell area (m^2)
dsh=4*As/(Nt*pi*odt); %hydraulic diameter of shell
Res=mdots*ds/(ahx2*us); %hx2 Reynolds number
Prs=cps*us/ks; %hx2 Prandtl number
Pes=Res*Prs; %hx2 Peclet number
hx2=(ks/dsh)*(7+4.24*(phx2/odt)^1.52); %secondary side heat tranfer coeff. (W/(m^2*K))
Bix2=hx2*Lt/kw; %shell Biot number
vhx2=Lt*As; %volume of sec. coolant in heat exch. (m^3)
UAhx=1/(1/(hx1*ahx1)+log(odt/dt)/(2*pi*kw*Lt*Nt)+1/(hx2*ahx2)); %hx total resistance
dThx=Po/UAhx; %temperature drop across heat exch. (K)

% Secondary Loop
tau6=2.5; %time delay from heat exchanger outlet to stirling engine heat source (s)
tau5=2.5; %time delay from stirling heat sink to heat exchanger inlet (s)

% Stirling Heat Source
%Heat Pipe - CP Grade 2 Titanium
HHxLg=0.075; %Length of the Stirling Hot Heat Exchanger (m)
HHxA=5.017*10^(-2); %Hot Heat Exchanger Cross Section Area (m^2)
nht=2750*4; %number of hot heat exchanger gas tubes
htd=0.0013/2; %Hot Heat Exchanger gas tube diameter (m)
htA=nht*pi*htd^2/4; %Hot Heat Exchanger gas tubes area (m^2)
sf=0.5; %heat pipe area safety factor
hpid=sf*0.05; %heat pipe inner diameter (m)
hpt=sf*7.11*10^(-4); %heat pipe thickness (m)
hpod=hpid+2*hpt; %heat pipe outer diameter (m)
hpwt=sf*0.0015; %heat pipe wick thickness (m)
hpwid=hpid-2*hpwt; %heat pipe wick inner diameter (m)
hpposs=(HHxA-htA)/(pi*hpod^2/4); %number of heat pipes possible
Le=1; %heat pipe evaporator length (m)
Lc=HHxLg; %heat pipe condenser lenght (m)
kp=22; %heat pipe conductivity - titanium (W/(m^2*K))
Cp=540; %heat pipe specific heat - titanium (J/(kg*K))
rowp=4510; %heat pipe density - titanium (kg/m^2)
porp=0.65; %heat pipe porosity
kl=32.3; %heat pipe fluid conductivity - potassium (W/(m*K))
keff=kl*((kl+kp)-(1-porp)*(kl-kp))/((kl+kp)+(1-porp)*(kl-kp)); %heat pipe wick effective
thermal conductivity (W/(m*K))
Rpe=log(hpod/hpid)/(2*pi*Le*kp); %heat pipe evaporator thermal resistance (K/W)
Rwe=log(hpid/hpwid)/(2*pi*Le*keff); %heat pipe evaporator wick thermal resistanc (K/W)
Rpc=log(hpod/hpid)/(2*pi*Lc*kp); %heat pipe condenser thermal resistance (K/W)
Rwc=log(hpid/hpwid)/(2*pi*Lc*keff); %heat pipe condenser thermal resistance (K/W)
Rtot=Rpe+Rwe+Rpc+Rwc; %heat pipe total thermal resistance (K/W)
Nhp=floor(hpposs); %number of heat pipes
NSE=4; %number of Stirling engines
Apxs=pi*(hpod^2-hpid^2)/4; %heat pipe cross section area (m^2)
Vpe=Apxs*Le*Nhp*NSE; %heat pipe condenser volume (m^3)
Aevap=pi*hpod*Le*Nhp*NSE; %heat pipe evaporator transfer area (m^2)
hppitch=2*hpod; %heat pipe matrix pitch (m)
hpflowarea=(hppitch^2-pi*hpod^2/4); %heat pipe unit cell flow area (m^2)
hpwetper=pi*hpod; %heat pipe unit cell wetted perimeter (m)
ahx3=hpflowarea*Nhp; %total flow area (m^2)
vhx3=ahx3*Le; %flow volume (m^3)
hphyddiam=4*hpflowarea/hpwetper; %heat pipe unit cell hydraulic diameter (m)
uflow=mdots/(hpflowarea*ps*4); %flow velocity (m/s)
Red=ps*uflow*hphyddiam/um; %flow Reynolds number
Nux3=7+4.24*(2)^1.52; %flow Nusselt number
hx3=Nux3*ks/hphyddiam; %heat xfer coef. between flow and heat pipes (W/(m^2*K))
deltaT=Po*Rtot/(Nhp*NSE); %temperature difference between flow and Stirling hot heat
exchanger (K)
mh=20; %heater mass - TeCu (kg)
```

```
cph=393.5; %heater specific heat - TeCu (J/(kg*K))

%Temperatures (K)
Twh=925; %Stirling heater
Tpe=Twh+deltaT; %heat pipe evaporator
Td2o=Tpe+(Po/(mdots*cps))/(exp(hx3*Aevap/(mdots*cps))-1); %init. coolant temp. at heat
source outlet (K)
Td2=Tpe+(Po/(mdots*cps))/(exp(hx3*Aevap/(mdots*cps))-1); %coolant temp. at heat source
outlet (K)
Td1o=Td2o+Po/(mdots*cps); %init. avg. coolant temp. at heat source (K)
Td1=Td2+Po/(mdots*cps); %avg. coolant temp. at heat source (K)
Tc1o=Td2; %init. temp. of sec. fluid entering exch. (K)
Tc1=Td2; %temp. of sec. fluid entering exch. (K)
Tco=(Td1o+Tc1o)/2; %initial avg. temp. of secondary fluid at exch.(K)
Tc=(Td1+Tc1)/2; %avg. temp. of secondary fluid at exch.(K)
Tc2=Tc+Po/(2*mdots*cps); %temp. of sec. fluid leaving exch. (K)
Tbo=Tco+Po/UAhx; %init. avg. temp. of heat exchanger primary coolant (K)
Tb=Tc+Po/UAhx; %avg. temp. of heat exchanger primary coolant (K)
Tb2o=Tbo-Po/(2*mdotm*cpm); %init. heat exchanger primary coolant outlet temp. (K)
Tb2=Tb-Po/(2*mdotm*cpm); %heat exchanger primary coolant outlet temp. (K)
Ts1=Tbo-(1/(hx1*ahx1))*UAhx*dThx; %initial wall temp. (K)
Ts2=Tco+(1/(hx2*ahx2))*UAhx*dThx;  %wall temp. (K)
Tb1o=2*Tbo-Tb2;%init. coolant temp. at heat exchanger inlet (K)
Tb1=2*Tb-Tb2;%coolant temp. at heat exchanger inlet (K)
Tm1o=2*Tbo-Tb1o;%init. mod. temp. at reactor outlet (K)
Tm1=2*Tb-Tb1; %mod. temp. at reactor outlet (K)
Tmo=Tm1o+Po/(2*mdotm*cpm);%initial avg. mod. temp.(K)
Tm=Tm1+Po/(2*mdotm*cpm); %mod. avg. temp. (K)
Tm2=2*Tm-Tm1; %reactor outlet coolant temp. (K)
Tfo=Tmo+(1+2*kf/(rf*ht))*Po/(4*pi*Lf*kf*N);%initial fuel temperature (K)
Tf=Tm+(1+2*kf/(rf*ht))*Po/(4*pi*Lf*kf*N);%fuel temperature (K)

%Stirling Parameters and IC's
vc=1.3; %compression space volume factor - multiple of volume given by NASA
ve=1; %expansion space volume factor - multiple of volume given by NASA
Xp=0.013; %piston displacement amplitude (m)
Xd=0.0084; %displacer displacement amplitude (m)
mp=20.3; %piston mass (kg)
md=8.5; %displacer mass (kg)
Dd=0; %displacer damping (kg/s)
kdisp=3.1*10^6; %displacer spring constant (N/m)
kd3=0*10^10; %third order displacer spring constant (N/m^3)
kd=kdisp-kd3*Xd^2; %adjusted first order spring constant (N/m)
kalt=38.5; %alternator constant (V*s/m)
freq=sqrt(kd/md)/(2*pi); %expected operating frequency (Hz)
Vmax=kalt*Xp*(2*pi*freq); %max voltage expected (V)
kWe=50000; %design power output per Stirling (kWe)
Zalt=Vmax^2/(2*kWe); %alternator impedance (ohms)
Apist=0.0381; %piston area (m^2)
xpo=0;  %initial piston position (m)
vpo=Xp*2*pi*freq; %initial piston velocity (m/s)
kalt=38.5; %alternator constant (Vs/m)
Ralt=0.028; %alternator resistance (ohm)
Halt=0.0002; %alternator inductance (H)
Calt=0; %circuit capacitance (F) - power corrected value = 1/((2*pi*freq)^2*Halt);
Rload=sqrt(Zalt^2-(2*pi*freq*Halt)^2)-Ralt; %electric load resistance (ohms)
Ialt=kalt*vpo/Zalt; %max expected current (A)
Dp=kalt^2/Zalt; %piston damping (kg/s)
drd=0.032; %displacer rod diameter (m)
Arod=pi*drd^2/4; %displacer rod area (m^2)
Ade=0.03892; %displacer area-exp. side (m^2)
Adc=Apist; %displacer area-comp. side (m^2)
dpist=sqrt(4*Ade/pi); %piston diameter (m)
phase=60; %expected piston-displacer phase angle (deg)
xdo=Xd*sin(pi*phase/180); %displacer initial position (m)
vdo=Xd*2*pi*freq*cos(pi*phase/180); %displacer initial velocity (m/s)
pmean=13.6*10^6; %piston mean pressure (Pa)
Twk=463; %cooler temperature (K)
Twh=925; %heater temperature (K)
Twr=(Twh+Twk)/2; %regenerator temp. (K)
Vcso=vc*6*10^(-4); %compression space volume (m^3)
```

```
Nkchan=3100*4; %number cold exchanger channels (dl)
CHxLg=0.075; %cold exch. length (m)
dtk=0.0014/2; %cooler channel diameter (m)
CHxpw=(pi*dtk)*Nkchan; %cooler wetted perimeter (m)
Awk=CHxpw*CHxLg; %cooler wall area (m^2)
ACHx=Nkchan*pi*dtk^2/4; %cooler cross-sectional area (m^2)
CHxDh=4*ACHx/CHxpw; %cooler hydraulic diameter (m)
Vk=ACHx*CHxLg; %cooler volume (m^3)
rLg=0.055; %regen. 1 length (m)
por=0.88; %regen. porosity (dl)
Acr=5.017*10^(-2); %regen. area (m^2)
Ar=Acr*por; %regen. flow area (m^2)
dr=2/pi*(pi*(Apist+Acr))^(1/2); %outer regen. diameter (m)
dir=sqrt(4*Ade/pi); %inner regen. diameter (m)
Awr=pi*(dr+dir)*rLg; %regen. 1 wall area (m^2)
rwd=25*10^(-6); %regen. wire diameter (m)
rpw=4*(1-por)*Acr/rwd; %reg. wetted perimeter (m)
rDh=4*Ar/rpw; %regen. hyd. diameter (m)
Amr=rpw*rLg; %regen. 1 matrix area (m^2)
Vr=rLg*Ar; %regen. 1 volume (m^3)
HHxLg=0.075; %heater length (m)
htd=.0013/2; %heater tube diameter (m)
Nht=2750*4; %number heater tubes (dl)
AHHx=Nht*pi/4*htd^2; %heater cross-sectional area (m^2)
Vh=AHHx*HHxLg; %heater volume (m^3)
HHxpw=Nht*pi*htd; %heater wetted perimeter (m)
HHxDh=4*AHHx/HHxpw; %heater diameter hyd. (m)
Awh=HHxpw*HHxLg; %heater wall area (m^2)
Veo=ve*4.34*10^(-4); %expansion space volume (m^3)
Vbso=14.5*10^(-3); %bounce space volume (m^3)
Vt=Vcso+Veo+Vh+Vr+Vk; %total volume (m^3)
gammaHe=1.667; %helium ratio of specific heats (dl)
Rgas=2077; %helium gas constant (J/(kg*K))
kHe=0.14; %helium conductivity (J/(kg*K))
cp=5230; %helium specific heat-const. press. (J/(kg*K))
cv=cp-Rgas; %helium specific heat-const. vol. (J/(kg*K))
cs=500; %steel specific heat (J/(kg*K))
CSutherland=1.286e-6; %Sutherland's law constant
SSutherland=8.63; %Sutherland's law constant
Diss=0; %initial total Stirling gas energy dissipation (W)
Dissk=0; %initial Stirling cooler gas energy dissipation (W)
Dissr=0; %initial Stirling regen. gas energy dissipation (W)
Dissh=0; %initial Stirling heater gas energy dissipation (W)
pcso=1.3243e+007; %initial compression space pressure (Pa)
peo=1.3174e+007; %initial expansion space pressure (Pa)
pko=pmean; %initial cooler pressure (Pa)
pro=pmean; %initial regen. pressure (Pa)
pho=pmean; %initial heater pressure (Pa)
WpV=53.6*10^3; %expected Stirling cycle PV power (W)
cyceff=0.316; %expected cycle efficiency
dQhss=WpV/cyceff; %expected cycle avg. heat addition (W)
dQkss=WpV-dQhss; %expected cycle avg. heat rejection (W)
Nuh=3.66; %initial Stirling heater Nusselt number
Nuk=3.66; %initial Stirling cooler Nusselt number
hAk=Nuk*kHe*Awk/CHxDh; %initial Stirling cooler heat transfer coefficient (W/(m^2*K))
hAh=Nuh*kHe*Awh/HHxDh; %initial Stirling heater heat transfer coefficient (W/(m^2*K))
hAr=por^2.61*kHe*Awr/rDh; %initial Stirling regen. heat transfer coefficient (W/(m^2*K))
Th=Twh-dQhss/hAh; %initial heater space temp. (K)
Tk=Twk-dQkss/hAk; %initial cooler space temp. (K)
Tcs=Tk; %initial compression space temperature (K)
Te=Th; %initial expansion space temperature (K)
Tr=(Th-Tk)/log(Th/Tk); %initial regen. temp. (K)
Tmr=Tr; %initial regen. matrix temp. (K)
muk=CSutherland*Tk^1.5/(Tk+SSutherland); %initial cooler viscosity
muh=CSutherland*Th^1.5/(Th+SSutherland); %initial heater viscosity
mur=CSutherland*Tr^1.5/(Tr+SSutherland); %initial regenerator viscosity
meo=peo*(Veo-xdo*Ade)/(Rgas*Twh); %initial expansion space gas mass (kg)
mho=pho*Vh/(Rgas*Th); %initial heater space gas mass (kg)
mro=pro*Vr/(Rgas*Tr); %initial regen. space gas mass (kg)
mko=pko*Vk/(Rgas*Tk); %initial cooler space gas mass (kg)
mcso=pcso*(Vcso+(xdo-xpo)*Apist)/(Rgas*Twk); %initial compression space gas mass (kg)
```

```
mbo=pmean*(Vbso+xdo*Arod+xpo*Apist)/(Rgas*Twk); %initial bounce space gas mass (kg)
mwork=(meo+mho+mro+mko+mcso); %total gas mass of the working spaces (kg)
dQh=hAh*(Twh-Th); %initial heater heat transfer (W)
dQk=hAk*(Twk-Tk); %initial cooler heat transfer (W)
dQr=hAr*(Twr-Tr); %initial regen. heat transfer (W)
dQ=dQh+dQr+dQk; %initial total heat transfer (W)

%Radiator Panels
Chanht=0.0725; %cooler NaK channel height (m)
Chanwd=0.1; %cooler NaK channel width (m)
ChanLg=pi*dpist+2*(dr-dpist); %cooler NaK channel length (m)
NChan=2; %number of cooler NaK channels
ptl=840; %NaK density in rejection loop (kg/m^3)
cptl=915; %NaK specific heat in rejection loop (J/(kg*K))
ktl=25; %NaK conductivity in rejection loop (W/(m*K))
AChan=Chanht*Chanwd; %NaK channel cross sectional area (m^2)
VChan=NChan*AChan*ChanLg; %NaK channel volume (m^3)
PChan=2*Chanht+2*Chanwd; %NaK channel wetted perimeter (m)
ChanDh=4*AChan/PChan; %NaK channel hydraulic diameter (m)
AwChan=NChan*PChan*ChanLg; %NaK channel wetted area (m^2)
mdotChan=mdotm/4; %NaK channel mass flow (kg/s)
mdott=mdotm; %rejection loop mass flow (kg/s)
Arlp=NChan*AChan*4; %rejection loop pipe cross sectional area (m^2)
drlp=sqrt(4*(Arlp)/pi); %rejection loop pipe diameter (m)
dradhp=0.0254; %radiator heat pipe diameter (m)
idradhp=dradhp-2*0.049*0.0254; %radiator heat pipe inner diameter (m)
idhpw=idradhp-2*0.049*0.0254; %radiator heat pipe wick inner diameter (m)
utl=3.81*10^(-4); %NaK viscosity in rejection loop (kg/(m*s))
PrChan=utl*cptl/ktl; %NaK channel Prandtl number
velChan=mdotChan/(ptl*AChan*NChan); %NaK channel flow velocity (m/s)
veltl=mdott/(ptl*Arlp); %rejection loop flow velocity (m/s)
ReChan=ptl*velChan*ChanDh/utl; %NaK channel Reynolds number
PeChan=PrChan*ReChan; %NaK channel Peclet number
hChan=ktl/ChanDh*(9.49+0.0596*PeChan^0.86); %NaK channel heat transfer coefficient
(W/(m^2*K))
dQChan=4.06e+005/4; %NaK channel heat transfer (W)
dTChan=dQChan/(hChan*AwChan); %temperature difference between cooler and NaK channel (K)
dTax=dQChan/(mdotChan*cptl); %temperature drop across NaK channel (K)
Rehp=ptl*veltl*dradhp/utl; %flow Reynolds number at radiator heat pipes
Pehp=PrChan*Rehp; %flow Peclet number at radiator heat pipes
hradhp=(ktl/dradhp)*(5+0.025*Pehp^0.8); %heat transfer coefficient at radiator heat pipes
(W/(m^2*K))
Lerhp=drlp*2; %radiator heat pipe evaporator length (m)
dwrhp=0.0027*0.0254; %radiator heat pipe wetted diameter (m)
erhp=0.2738; %radiator heat pipe wick porosity
kwhp=0.678; %radiator heat pipe water conductivity (W/(m*K))
keffrhp=kl*((kwhp+kp)-(1-erhp)*(kwhp-kp))/((kwhp+kp)+(1-erhp)*(kwhp-kp)); %radiator heat
pipe effective wick conductivity (W/(m*K))
Aerhp=Lerhp*dradhp*pi; %radiator heat pipe evaporator area (m^2)
sigmasb=5.67*10^(-8); %Stephan-Boltzman constant (W/(m^2*K^4))
emiss=0.9; %radiator panel emissivity
trad=0.018; %radiator panel thickness (m)
wrad=1.5; %radiator panel width (m)
Lrad12=9*sin(10*pi/180); %radiator panels 1&2 length (m)
Arad12=4*wrad*Lrad12; %radiator panels 1&2 area (m^2)
Lrad34=(9+1.6)*sin(10*pi/180);%radiator panels 3&4 length (m)
Arad34=4*wrad*Lrad34;%radiator panels 3&4 area (m^2)
Lrad56=(9+2*1.6)*sin(10*pi/180);%radiator panels 5&6 length (m)
Arad56=4*wrad*Lrad56;%radiator panels 5&6 area (m^2)
Lrad78=(9+3*1.6)*sin(10*pi/180);%radiator panels 7&8 length (m)
Arad78=4*wrad*Lrad78;%radiator panels 7&8 area (m^2)
Lrad910=(9+4*1.6)*sin(10*pi/180);%radiator panels 9&10 length (m)
Arad910=4*wrad*Lrad910;%radiator panels 9&10 area (m^2)
Lrad1112=(9+5*1.6)*sin(10*pi/180);%radiator panels 11&12 length (m)
Arad1112=4*wrad*Lrad1112;%radiator panels 11&12 area (m^2)
Lrad1314=(9+6*1.6)*sin(10*pi/180);%radiator panels 13&14 length (m)
Arad1314=4*wrad*Lrad1314;%radiator panels 13&14 area (m^2)
Lrad1516=(9+7*1.6)*sin(10*pi/180);%radiator panels 15&16 length (m)
Arad1516=4*wrad*Lrad1516;%radiator panels 15&16 area (m^2)
Lrad1718=(9+8*1.6)*sin(10*pi/180);%radiator panels 17&18 length (m)
Arad1718=4*wrad*Lrad1718;%radiator panels 17&18 area (m^2)
```

```
Lrad1920=(9+9*1.6)*sin(10*pi/180);%radiator panels 19&20 length (m)
Arad1920=4*wrad*Lrad1920;%radiator panels 19&20 area (m^2)
Lrad2122=(9+10*1.6)*sin(10*pi/180);%radiator panels 21&22 length (m)
Arad2122=4*wrad*Lrad2122;%radiator panels 21&22 area (m^2)
Lrad2324=(9+11*1.6)*sin(10*pi/180);%radiator panels 23&24 length (m)
Arad2324=4*wrad*Lrad2324;%radiator panels 23&24 area (m^2)
Lrad2526=(9+12*1.6)*sin(10*pi/180);%radiator panels 25&26 length (m)
Arad2526=4*wrad*Lrad2526;%radiator panels 25&26 area (m^2)
Lrad2728=(9+13*1.6)*sin(10*pi/180);%radiator panels 27&28 length (m)
Arad2728=4*wrad*Lrad2728;%radiator panels 27&28 area (m^2)
Lrad2930=(9+14*1.6)*sin(10*pi/180);%radiator panels 29&30 length (m)
Arad2930=4*wrad*Lrad2930;%radiator panels 29&30 area (m^2)
Lrad3132=(9+15*1.6)*sin(10*pi/180);%radiator panels 31&32 length (m)
Arad3132=4*wrad*Lrad3132;%radiator panels 31&32 area (m^2)
Lrad3334=(9+16*1.6)*sin(10*pi/180);%radiator panels 33&34 length (m)
Arad3334=4*wrad*Lrad3334;%radiator panels 33&34 area (m^2)
Lrad3536=(9+5.64*1.6)*sin(10*pi/180);%radiator panels 35&36 length (m)
Arad3536=4*wrad*Lrad3536;%radiator panels 35&36 area (m^2)
Aradtot=Arad12+Arad34+Arad56+Arad78+Arad910+Arad1112+Arad1314+Arad1516+Arad1718+Arad1920+
Arad2122+Arad2324+Arad2526+Arad2728+Arad2930+Arad3132+Arad3334+Arad3536;%radiator panels
total area (m^2)
Rpc12=log(dradhp/idradhp)/(4*pi*Lrad12*kp); %Heat pipes for panels 1&2 condenser thermal
resistance (K/W)
Rpc34=log(dradhp/idradhp)/(4*pi*Lrad34*kp); %Heat pipes for panels 3&4 condenser thermal
resistance (K/W)
Rpc56=log(dradhp/idradhp)/(4*pi*Lrad56*kp); %Heat pipes for panels 5&6 condenser thermal
resistance (K/W)
Rpc78=log(dradhp/idradhp)/(4*pi*Lrad78*kp); %Heat pipes for panels 7&8 condenser thermal
resistance (K/W)
Rpc910=log(dradhp/idradhp)/(4*pi*Lrad910*kp); %Heat pipes for panels 9&10 condenser
thermal resistance (K/W)
Rpc1112=log(dradhp/idradhp)/(4*pi*Lrad1112*kp); %Heat pipes for panels 11&12 condenser
thermal resistance (K/W)
Rpc1314=log(dradhp/idradhp)/(4*pi*Lrad1314*kp); %Heat pipes for panels 13&14 condenser
thermal resistance (K/W)
Rpc1516=log(dradhp/idradhp)/(4*pi*Lrad1516*kp);%Heat pipes for panels 15&16 condenser
thermal resistance (K/W)
Rpc1718=log(dradhp/idradhp)/(4*pi*Lrad1718*kp);%Heat pipes for panels 17&18 condenser
thermal resistance (K/W)
Rpc1920=log(dradhp/idradhp)/(4*pi*Lrad1920*kp);%Heat pipes for panels 19&20 condenser
thermal resistance (K/W)
Rpc2122=log(dradhp/idradhp)/(4*pi*Lrad2122*kp);%Heat pipes for panels 21&22 condenser
thermal resistance (K/W)
Rpc2324=log(dradhp/idradhp)/(4*pi*Lrad2324*kp);%Heat pipes for panels 23&24 condenser
thermal resistance (K/W)
Rpc2526=log(dradhp/idradhp)/(4*pi*Lrad2526*kp);%Heat pipes for panels 25&26 condenser
thermal resistance (K/W)
Rpc2728=log(dradhp/idradhp)/(4*pi*Lrad2728*kp);%Heat pipes for panels 27&28 condenser
thermal resistance (K/W)
Rpc2930=log(dradhp/idradhp)/(4*pi*Lrad2930*kp);%Heat pipes for panels 29&30 condenser
thermal resistance (K/W)
Rpc3132=log(dradhp/idradhp)/(4*pi*Lrad3132*kp);%Heat pipes for panels 31&32 condenser
thermal resistance (K/W)
Rpc3334=log(dradhp/idradhp)/(4*pi*Lrad3334*kp);%Heat pipes for panels 33&34 condenser
thermal resistance (K/W)
Rpc3536=log(dradhp/idradhp)/(4*pi*Lrad3536*kp);%Heat pipes for panels 35&36 condenser
thermal resistance (K/W)
Rpwc12=log(idradhp/idhpw)/(4*pi*Lrad12*keffrhp);%Heat pipes for panels 1&2 condenser wick
thermal resistance (K/W)
Rpwc34=log(idradhp/idhpw)/(4*pi*Lrad34*keffrhp);%Heat pipes for panels 3&4 condenser wick
thermal resistance (K/W)
Rpwc56=log(idradhp/idhpw)/(4*pi*Lrad56*keffrhp);%Heat pipes for panels 5&6 condenser wick
thermal resistance (K/W)
Rpwc78=log(idradhp/idhpw)/(4*pi*Lrad78*keffrhp);%Heat pipes for panels 7&8 condenser wick
thermal resistance (K/W)
Rpwc910=log(idradhp/idhpw)/(4*pi*Lrad910*keffrhp);%Heat pipes for panels 9&10 condenser
wick thermal resistance (K/W)
Rpwc1112=log(idradhp/idhpw)/(4*pi*Lrad1112*keffrhp);%Heat pipes for panels 11&12
condenser wick thermal resistance (K/W)
Rpwc1314=log(idradhp/idhpw)/(4*pi*Lrad1314*keffrhp);%Heat pipes for panels 13&14
condenser wick thermal resistance (K/W)
```

```
Rpwc1516=log(idradhp/idhpw)/(4*pi*Lrad1516*keffrhp);%Heat pipes for panels 15&16
condenser wick thermal resistance (K/W)
Rpwc1718=log(idradhp/idhpw)/(4*pi*Lrad1718*keffrhp);%Heat pipes for panels 17&18
condenser wick thermal resistance (K/W)
Rpwc1920=log(idradhp/idhpw)/(4*pi*Lrad1920*keffrhp);%Heat pipes for panels 19&20
condenser wick thermal resistance (K/W)
Rpwc2122=log(idradhp/idhpw)/(4*pi*Lrad2122*keffrhp);%Heat pipes for panels 21&22
condenser wick thermal resistance (K/W)
Rpwc2324=log(idradhp/idhpw)/(4*pi*Lrad2324*keffrhp);%Heat pipes for panels 23&24
condenser wick thermal resistance (K/W)
Rpwc2526=log(idradhp/idhpw)/(4*pi*Lrad2526*keffrhp);%Heat pipes for panels 25&26
condenser wick thermal resistance (K/W)
Rpwc2728=log(idradhp/idhpw)/(4*pi*Lrad2728*keffrhp);%Heat pipes for panels 27&28
condenser wick thermal resistance (K/W)
Rpwc2930=log(idradhp/idhpw)/(4*pi*Lrad2930*keffrhp);%Heat pipes for panels 29&30
condenser wick thermal resistance (K/W)
Rpwc3132=log(idradhp/idhpw)/(4*pi*Lrad3132*keffrhp);%Heat pipes for panels 31&32
condenser wick thermal resistance (K/W)
Rpwc3334=log(idradhp/idhpw)/(4*pi*Lrad3334*keffrhp);%Heat pipes for panels 33&34
condenser wick thermal resistance (K/W)
Rpwc3536=log(idradhp/idhpw)/(4*pi*Lrad3536*keffrhp);%Heat pipes for panels 35&36
condenser wick thermal resistance (K/W)
Rpe12=log(dradhp/idradhp)/(4*pi*Lerhp*kp);%Heat pipes for panels 1&2 evaporator thermal
resistance (K/W)
Rpe34=log(dradhp/idradhp)/(4*pi*Lerhp*kp);%Heat pipes for panels 3&4 evaporator thermal
resistance (K/W)
Rpe56=log(dradhp/idradhp)/(4*pi*Lerhp*kp);%Heat pipes for panels 5&6 evaporator thermal
resistance (K/W)
Rpe78=log(dradhp/idradhp)/(4*pi*Lerhp*kp);%Heat pipes for panels 7&8 evaporator thermal
resistance (K/W)
Rpe910=log(dradhp/idradhp)/(4*pi*Lerhp*kp);%Heat pipes for panels 9&10 evaporator thermal
resistance (K/W)
Rpe1112=log(dradhp/idradhp)/(4*pi*Lerhp*kp);%Heat pipes for panels 11&12 evaporator
thermal resistance (K/W)
Rpe1314=log(dradhp/idradhp)/(4*pi*Lerhp*kp);%Heat pipes for panels 13&14 evaporator
thermal resistance (K/W)
Rpe1516=log(dradhp/idradhp)/(4*pi*Lerhp*kp);%Heat pipes for panels 15&16 evaporator
thermal resistance (K/W)
Rpe1718=log(dradhp/idradhp)/(4*pi*Lerhp*kp);%Heat pipes for panels 17&18 evaporator
thermal resistance (K/W)
Rpe1920=log(dradhp/idradhp)/(4*pi*Lerhp*kp);%Heat pipes for panels 19&20 evaporator
thermal resistance (K/W)
Rpe2122=log(dradhp/idradhp)/(4*pi*Lerhp*kp);%Heat pipes for panels 21&22 evaporator
thermal resistance (K/W)
Rpe2324=log(dradhp/idradhp)/(4*pi*Lerhp*kp);%Heat pipes for panels 23&24 evaporator
thermal resistance (K/W)
Rpe2526=log(dradhp/idradhp)/(4*pi*Lerhp*kp);%Heat pipes for panels 25&26 evaporator
thermal resistance (K/W)
Rpe2728=log(dradhp/idradhp)/(4*pi*Lerhp*kp);%Heat pipes for panels 27&28 evaporator
thermal resistance (K/W)
Rpe2930=log(dradhp/idradhp)/(4*pi*Lerhp*kp);%Heat pipes for panels 29&30 evaporator
thermal resistance (K/W)
Rpe3132=log(dradhp/idradhp)/(4*pi*Lerhp*kp);%Heat pipes for panels 31&32 evaporator
thermal resistance (K/W)
Rpe3334=log(dradhp/idradhp)/(4*pi*Lerhp*kp);%Heat pipes for panels 33&34 evaporator
thermal resistance (K/W)
Rpe3536=log(dradhp/idradhp)/(4*pi*Lerhp*kp);%Heat pipes for panels 35&36 evaporator
thermal resistance (K/W)
Rpwe12=log(idradhp/idhpw)/(4*pi*Lerhp*keffrhp);%Heat pipes for panels 1&2 evaporator wick
thermal resistance (K/W)
Rpwe34=log(idradhp/idhpw)/(4*pi*Lerhp*keffrhp);%Heat pipes for panels 3&4 evaporator wick
thermal resistance (K/W)
Rpwe56=log(idradhp/idhpw)/(4*pi*Lerhp*keffrhp);%Heat pipes for panels 5&6 evaporator wick
thermal resistance (K/W)
Rpwe78=log(idradhp/idhpw)/(4*pi*Lerhp*keffrhp);%Heat pipes for panels 7&8 evaporator wick
thermal resistance (K/W)
Rpwe910=log(idradhp/idhpw)/(4*pi*Lerhp*keffrhp);%Heat pipes for panels 9&10 evaporator
wick thermal resistance (K/W)
Rpwe1112=log(idradhp/idhpw)/(4*pi*Lerhp*keffrhp);%Heat pipes for panels 11&12 evaporator
wick thermal resistance (K/W)
```

```
Rpwe1314=log(idradhp/idhpw)/(4*pi*Lerhp*keffrhp);%Heat pipes for panels 13&14 evaporator
wick thermal resistance (K/W)
Rpwe1516=log(idradhp/idhpw)/(4*pi*Lerhp*keffrhp);%Heat pipes for panels 15&16 evaporator
wick thermal resistance (K/W)
Rpwe1718=log(idradhp/idhpw)/(4*pi*Lerhp*keffrhp);%Heat pipes for panels 17&18 evaporator
wick thermal resistance (K/W)
Rpwe1920=log(idradhp/idhpw)/(4*pi*Lerhp*keffrhp);%Heat pipes for panels 19&20 evaporator
wick thermal resistance (K/W)
Rpwe2122=log(idradhp/idhpw)/(4*pi*Lerhp*keffrhp);%Heat pipes for panels 21&22 evaporator
wick thermal resistance (K/W)
Rpwe2324=log(idradhp/idhpw)/(4*pi*Lerhp*keffrhp);%Heat pipes for panels 23&24 evaporator
wick thermal resistance (K/W)
Rpwe2526=log(idradhp/idhpw)/(4*pi*Lerhp*keffrhp);%Heat pipes for panels 25&26 evaporator
wick thermal resistance (K/W)
Rpwe2728=log(idradhp/idhpw)/(4*pi*Lerhp*keffrhp);%Heat pipes for panels 27&28 evaporator
wick thermal resistance (K/W)
Rpwe2930=log(idradhp/idhpw)/(4*pi*Lerhp*keffrhp);%Heat pipes for panels 29&30 evaporator
wick thermal resistance (K/W)
Rpwe3132=log(idradhp/idhpw)/(4*pi*Lerhp*keffrhp);%Heat pipes for panels 31&32 evaporator
wick thermal resistance (K/W)
Rpwe3334=log(idradhp/idhpw)/(4*pi*Lerhp*keffrhp);%Heat pipes for panels 33&34 evaporator
wick thermal resistance (K/W)
Rpwe3536=log(idradhp/idhpw)/(4*pi*Lerhp*keffrhp);%Heat pipes for panels 35&36 evaporator
wick thermal resistance (K/W)
Rtot12=1/(2*hradhp*Aerhp)+Rpe12+Rpwe12+Rpc12+Rpwc12;%Heat pipes for panels 1&2 total
thermal resistance (K/W)
Rtot34=1/(2*hradhp*Aerhp)+Rpe34+Rpwe34+Rpc34+Rpwc34;%Heat pipes for panels 3&4 total
thermal resistance (K/W)
Rtot56=1/(2*hradhp*Aerhp)+Rpe56+Rpwe56+Rpc56+Rpwc56;%Heat pipes for panels 5&6 total
thermal resistance (K/W)
Rtot78=1/(2*hradhp*Aerhp)+Rpe78+Rpwe78+Rpc78+Rpwc78;%Heat pipes for panels 7&8 total
thermal resistance (K/W)
Rtot910=1/(2*hradhp*Aerhp)+Rpe910+Rpwe910+Rpc910+Rpwc910;%Heat pipes for panels 9&10
total thermal resistance (K/W)
Rtot1112=1/(2*hradhp*Aerhp)+Rpe1112+Rpwe1112+Rpc1112+Rpwc1112;%Heat pipes for panels
11&12 total thermal resistance (K/W)
Rtot1314=1/(2*hradhp*Aerhp)+Rpe1314+Rpwe1314+Rpc1314+Rpwc1314;%Heat pipes for panels
13&14 total thermal resistance (K/W)
Rtot1516=1/(2*hradhp*Aerhp)+Rpe1516+Rpwe1516+Rpc1516+Rpwc1516;%Heat pipes for panels
15&16 total thermal resistance (K/W)
Rtot1718=1/(2*hradhp*Aerhp)+Rpe1718+Rpwe1718+Rpc1718+Rpwc1718;%Heat pipes for panels
17&18 total thermal resistance (K/W)
Rtot1920=1/(2*hradhp*Aerhp)+Rpe1920+Rpwe1920+Rpc1920+Rpwc1920;%Heat pipes for panels
19&20 total thermal resistance (K/W)
Rtot2122=1/(2*hradhp*Aerhp)+Rpe2122+Rpwe2122+Rpc2122+Rpwc2122;%Heat pipes for panels
21&22 total thermal resistance (K/W)
Rtot2324=1/(2*hradhp*Aerhp)+Rpe2324+Rpwe2324+Rpc2324+Rpwc2324;%Heat pipes for panels
23&24 total thermal resistance (K/W)
Rtot2526=1/(2*hradhp*Aerhp)+Rpe2526+Rpwe2526+Rpc2526+Rpwc2526;%Heat pipes for panels
25&26 total thermal resistance (K/W)
Rtot2728=1/(2*hradhp*Aerhp)+Rpe2728+Rpwe2728+Rpc2728+Rpwc2728;%Heat pipes for panels
27&28 total thermal resistance (K/W)
Rtot2930=1/(2*hradhp*Aerhp)+Rpe2930+Rpwe2930+Rpc2930+Rpwc2930;%Heat pipes for panels
29&30 total thermal resistance (K/W)
Rtot3132=1/(2*hradhp*Aerhp)+Rpe3132+Rpwe3132+Rpc3132+Rpwc3132;%Heat pipes for panels
31&32 total thermal resistance (K/W)
Rtot3334=1/(2*hradhp*Aerhp)+Rpe3334+Rpwe3334+Rpc3334+Rpwc3334;%Heat pipes for panels
33&34 total thermal resistance (K/W)
Rtot3536=1/(2*hradhp*Aerhp)+Rpe3536+Rpwe3536+Rpc3536+Rpwc3536;%Heat pipes for panels
35&36 total thermal resistance (K/W)
Tarl=459.559434565575;%Initial flow temperature before heat pipes 1&2 (K)
Tbrl=458.408559003126;%Initial flow temperature before heat pipes 3&4 (K)
Tcrl=457.121046878194;%Initial flow temperature before heat pipes 5&6 (K)
Tdrl=455.710508440862;%Initial flow temperature before heat pipes 7&8 (K)
Terl=454.188962155437;%Initial flow temperature before heat pipes 9&10 (K)
Tfrl=452.567094253402;%Initial flow temperature before heat pipes 11&12 (K)
Tgrl=450.854431195112;%Initial flow temperature before heat pipes 13&14 (K)
Thrl=449.059638655476;%Initial flow temperature before heat pipes 15&16 (K)
Tirl=447.190372373182;%Initial flow temperature before heat pipes 17&18 (K)
Tjrl=445.253895198845;%Initial flow temperature before heat pipes 19&20 (K)
Tkrl=443.256291491480;%Initial flow temperature before heat pipes 21&22 (K)
```

```
Tlrl=441.203969658223;%Initial flow temperature before heat pipes 23&24 (K)
Tmrl=439.101556561924;%Initial flow temperature before heat pipes 25&26 (K)
Tnrl=436.954984860839;%Initial flow temperature before heat pipes 27&28 (K)
Torl=434.767616817067;%Initial flow temperature before heat pipes 29&30 (K)
Tprl=432.544985917627;%Initial flow temperature before heat pipes 31&32 (K)
Tqrl=430.289569923276;%Initial flow temperature before heat pipes 33&34 (K)
Trrl=428.006331796269;%Initial flow temperature before heat pipes 35&36 (K)
Tsrl=427.730225305744;%Initial flow temperature after heat pipes 35&36 (K)
Tx=427.730225305744;%Initial flow temperature before the NaK channels (K)
Tabrl=(Tarl+Tbrl)/2;%Initial average flow temperature at heat pipes 1&2 (K)
Tbcrl=(Tbrl+Tcrl)/2;%Initial average flow temperature at heat pipes 3&4 (K)
Tcdrl=(Tcrl+Tdrl)/2;%Initial average flow temperature at heat pipes 5&6 (K)
Tderl=(Tdrl+Terl)/2;%Initial average flow temperature at heat pipes 7&8 (K)
Tef=(Terl+Tfrl)/2;%Initial average flow temperature at heat pipes 9&10 (K)
Tfg=(Tfrl+Tgrl)/2;%Initial average flow temperature at heat pipes 11&12 (K)
Tgh=(Tgrl+Thrl)/2;%Initial average flow temperature at heat pipes 13&14 (K)
Thi=(Thrl+Tirl)/2;%Initial average flow temperature at heat pipes 15&16 (K)
Tij=(Tirl+Tjrl)/2;%Initial average flow temperature at heat pipes 17&18 (K)
Tjk=(Tjrl+Tkrl)/2;%Initial average flow temperature at heat pipes 19&20 (K)
Tkl=(Tkrl+Tlrl)/2;%Initial average flow temperature at heat pipes 21&22 (K)
Tlm=(Tlrl+Tmrl)/2;%Initial average flow temperature at heat pipes 23&24 (K)
Tmn=(Tmrl+Tnrl)/2;%Initial average flow temperature at heat pipes 25&26 (K)
Tno=(Tnrl+Torl)/2;%Initial average flow temperature at heat pipes 27&28 (K)
Top=(Torl+Tprl)/2;%Initial average flow temperature at heat pipes 29&30 (K)
Tpq=(Tprl+Tqrl)/2;%Initial average flow temperature at heat pipes 31&32 (K)
Tqr=(Tqrl+Trrl)/2;%Initial average flow temperature at heat pipes 33&34 (K)
Trs=(Trrl+Tsrl)/2;%Initial average flow temperature at heat pipes 35&36 (K)
Tax=(Tarl+Tx)/2;%Initial average flow temperature at NaK channels (K)
dQp12e=mdott*cptl*(Tarl-Tbrl);%heat transfer into heat pipes 1&2 (W)
dQp34e=mdott*cptl*(Tbrl-Tcrl);%heat transfer into heat pipes 3&4 (W)
dQp56e=mdott*cptl*(Tcrl-Tdrl);%heat transfer into heat pipes 5&6 (W)
dQp78e=mdott*cptl*(Tdrl-Terl);%heat transfer into heat pipes 7&8 (W)
dQp910e=mdott*cptl*(Terl-Tfrl);%heat transfer into heat pipes 9&10 (W)
dQp1112e=mdott*cptl*(Tfrl-Tgrl);%heat transfer into heat pipes 11&12 (W)
dQp1314e=mdott*cptl*(Tgrl-Thrl);%heat transfer into heat pipes 13&14 (W)
dQp1516e=mdott*cptl*(Thrl-Tirl);%heat transfer into heat pipes 15&16 (W)
dQp1718e=mdott*cptl*(Tirl-Tjrl);%heat transfer into heat pipes 17&18 (W)
dQp1920e=mdott*cptl*(Tjrl-Tkrl);%heat transfer into heat pipes 19&20 (W)
dQp2122e=mdott*cptl*(Tkrl-Tlrl);%heat transfer into heat pipes 21&22 (W)
dQp2324e=mdott*cptl*(Tlrl-Tmrl);%heat transfer into heat pipes 23&24 (W)
dQp2526e=mdott*cptl*(Tmrl-Tnrl);%heat transfer into heat pipes 25&26 (W)
dQp2728e=mdott*cptl*(Tnrl-Torl);%heat transfer into heat pipes 27&28 (W)
dQp2930e=mdott*cptl*(Torl-Tprl);%heat transfer into heat pipes 29&30 (W)
dQp3132e=mdott*cptl*(Tprl-Tqrl);%heat transfer into heat pipes 31&32 (W)
dQp3334e=mdott*cptl*(Tqrl-Trrl);%heat transfer into heat pipes 33&34 (W)
dQp3536e=mdott*cptl*(Trrl-Tsrl);%heat transfer into heat pipes 35&36 (W)
Tabp=Tabrl-dQp12e*Rtot12;%temperature of radiator panels 1&2 (K)
Tbcp=Tbcrl-dQp34e*Rtot34;%temperature of radiator panels 3&4 (K)
Tcdp=Tcdrl-dQp56e*Rtot56;%temperature of radiator panels 5&6 (K)
Tdep=Tderl-dQp78e*Rtot78;%temperature of radiator panels 7&8 (K)
Tefp=Tef-dQp910e*Rtot910;%temperature of radiator panels 9&10 (K)
Tfgp=Tfg-dQp1112e*Rtot1112;%temperature of radiator panels 11&12 (K)
Tghp=Tgh-dQp1314e*Rtot1314;%temperature of radiator panels 13&14 (K)
Thip=Thi-dQp1516e*Rtot1516;%temperature of radiator panels 15&16 (K)
Tijp=Tij-dQp1718e*Rtot1718;%temperature of radiator panels 17&18 (K)
Tjkp=Tjk-dQp1920e*Rtot1920;%temperature of radiator panels 19&20 (K)
Tklp=Tkl-dQp2122e*Rtot2122;%temperature of radiator panels 21&22 (K)
Tlmp=Tlm-dQp2324e*Rtot2324;%temperature of radiator panels 23&24 (K)
Tmnp=Tmn-dQp2526e*Rtot2526;%temperature of radiator panels 25&26 (K)
Tnop=Tno-dQp2728e*Rtot2728;%temperature of radiator panels 27&28 (K)
Topp=Top-dQp2930e*Rtot2930;%temperature of radiator panels 29&30 (K)
Tpqp=Tpq-dQp3132e*Rtot3132;%temperature of radiator panels 31&32 (K)
Tqrp=Tqr-dQp3334e*Rtot3334;%temperature of radiator panels 33&34 (K)
Trsp=Trs-dQp3536e*Rtot3536;%temperature of radiator panels 35&36 (K)
Tamb=4; %ambient space temperature (K)
dQp12=emiss*sigmasb*Arad12*(Tabp^4-Tamb^4); %heat rejected by panels 1&2 (W)
dQp34=emiss*sigmasb*Arad34*(Tbcp^4-Tamb^4);%heat rejected by panels 3&4 (W)
dQp56=emiss*sigmasb*Arad56*(Tcdp^4-Tamb^4);%heat rejected by panels 5&6 (W)
dQp78=emiss*sigmasb*Arad78*(Tdep^4-Tamb^4);%heat rejected by panels 7&8 (W)
dQp910=emiss*sigmasb*Arad910*(Tefp^4-Tamb^4);%heat rejected by panels 9&10 (W)
dQp1112=emiss*sigmasb*Arad1112*(Tfgp^4-Tamb^4);%heat rejected by panels 11&12 (W)
```

```
dQp1314=emiss*sigmasb*Arad1314*(Tghp^4-Tamb^4);%heat rejected by panels 13&14 (W)
dQp1516=emiss*sigmasb*Arad1516*(Thip^4-Tamb^4);%heat rejected by panels 15&16 (W)
dQp1718=emiss*sigmasb*Arad1718*(Tijp^4-Tamb^4);%heat rejected by panels 17&18 (W)
dQp1920=emiss*sigmasb*Arad1920*(Tjkp^4-Tamb^4);%heat rejected by panels 19&20 (W)
dQp2122=emiss*sigmasb*Arad2122*(Tklp^4-Tamb^4);%heat rejected by panels 21&22 (W)
dQp2324=emiss*sigmasb*Arad2324*(Tlmp^4-Tamb^4);%heat rejected by panels 23&24 (W)
dQp2526=emiss*sigmasb*Arad2526*(Tmnp^4-Tamb^4);%heat rejected by panels 25&26 (W)
dQp2728=emiss*sigmasb*Arad2728*(Tnop^4-Tamb^4);%heat rejected by panels 27&28 (W)
dQp2930=emiss*sigmasb*Arad2930*(Topp^4-Tamb^4);%heat rejected by panels 29&30 (W)
dQp3132=emiss*sigmasb*Arad3132*(Tpqp^4-Tamb^4);%heat rejected by panels 31&32 (W)
dQp3334=emiss*sigmasb*Arad3334*(Tqrp^4-Tamb^4);%heat rejected by panels 33&34 (W)
Lrad3536=dQp3536e/(4*emiss*sigmasb*wrad*sin(1/18*pi)*(Trsp^4-Tamb^4));%length of
radiators 35&36 (m)
Arad3536=4*wrad*Lrad3536*sin(10*pi/180);%area of radiators 35&36 (m^2)
dQp3536=emiss*sigmasb*Arad3536*(Trsp^4-Tamb^4);%heat rejection of radiators 35&36 (W)
dQptot=dQp12+dQp34+dQp56+dQp78+dQp910+dQp1112+dQp1314+dQp1516+dQp1718+dQp1920+dQp2122+dQp
2324+dQp2526+dQp2728+dQp2930+dQp3132+dQp3334+dQp3536;%total radiator heat rejection (W)
wsad=0.0032; %graphite heat pipe saddle thickness (m)
ssad=dradhp+2*wsad; %graphite heat pipe saddle outer diameter (m)
psad=550; %graphite heat pipe density (kg/m^3)
pfin=180; %radiator panel density (kg/m^3)
cpg=720; %graphite heat pipe saddle specific heat (J/(kg*K))
Vrad12=Arad12*trad+Lrad12*(ssad^2-pi*dradhp^2/4);%volume of radiators 1&2 (m^3)
Vrad34=Arad34*trad+Lrad34*(ssad^2-pi*dradhp^2/4);%volume of radiators 3&4 (m^3)
Vrad56=Arad56*trad+Lrad56*(ssad^2-pi*dradhp^2/4);%volume of radiators 5&6 (m^3)
Vrad78=Arad78*trad+Lrad78*(ssad^2-pi*dradhp^2/4);%volume of radiators 7&8 (m^3)
Vrad910=Arad910*trad+Lrad910*(ssad^2-pi*dradhp^2/4);%volume of radiators 9&10 (m^3)
Vrad1112=Arad1112*trad+Lrad1112*(ssad^2-pi*dradhp^2/4);%volume of radiators 11&12 (m^3)
Vrad1314=Arad1314*trad+Lrad1314*(ssad^2-pi*dradhp^2/4);%volume of radiators 13&14 (m^3)
Vrad1516=Arad1516*trad+Lrad1516*(ssad^2-pi*dradhp^2/4);%volume of radiators 15&16 (m^3)
Vrad1718=Arad1718*trad+Lrad1718*(ssad^2-pi*dradhp^2/4);%volume of radiators 17&18 (m^3)
Vrad1920=Arad1920*trad+Lrad1920*(ssad^2-pi*dradhp^2/4);%volume of radiators 19&20 (m^3)
Vrad2122=Arad2122*trad+Lrad2122*(ssad^2-pi*dradhp^2/4);%volume of radiators 21&22 (m^3)
Vrad2324=Arad2324*trad+Lrad2324*(ssad^2-pi*dradhp^2/4);%volume of radiators 23&24 (m^3)
Vrad2526=Arad2526*trad+Lrad2526*(ssad^2-pi*dradhp^2/4);%volume of radiators 25&26 (m^3)
Vrad2728=Arad2728*trad+Lrad2728*(ssad^2-pi*dradhp^2/4);%volume of radiators 27&28 (m^3)
Vrad2930=Arad2930*trad+Lrad2930*(ssad^2-pi*dradhp^2/4);%volume of radiators 29&30 (m^3)
Vrad3132=Arad3132*trad+Lrad3132*(ssad^2-pi*dradhp^2/4);%volume of radiators 31&32 (m^3)
Vrad3334=Arad3334*trad+Lrad3334*(ssad^2-pi*dradhp^2/4);%volume of radiators 33&34 (m^3)
Vrad3536=Arad3536*trad+Lrad3536*(ssad^2-pi*dradhp^2/4);%volume of radiators 35&36 (m^3)
mrad12=pfin*Arad12*trad+psad*Lrad12*(ssad^2-pi*dradhp^2/4);%mass of radiators 1&2 (m^3)
mrad34=pfin*Arad34*trad+psad*Lrad34*(ssad^2-pi*dradhp^2/4);%mass of radiators 3&4 (m^3)
mrad56=pfin*Arad56*trad+psad*Lrad56*(ssad^2-pi*dradhp^2/4);%mass of radiators 5&6 (m^3)
mrad78=pfin*Arad78*trad+psad*Lrad78*(ssad^2-pi*dradhp^2/4);%mass of radiators 7&8 (m^3)
mrad910=pfin*Arad910*trad+psad*Lrad910*(ssad^2-pi*dradhp^2/4);%mass of radiators 9&10
(m^3)
mrad1112=pfin*Arad1112*trad+psad*Lrad1112*(ssad^2-pi*dradhp^2/4);%mass of radiators 11&12
(m^3)
mrad1314=pfin*Arad1314*trad+psad*Lrad1314*(ssad^2-pi*dradhp^2/4);%mass of radiators 13&14
(m^3)
mrad1516=pfin*Arad1516*trad+psad*Lrad1516*(ssad^2-pi*dradhp^2/4);%mass of radiators 15&16
(m^3)
mrad1718=pfin*Arad1718*trad+psad*Lrad1718*(ssad^2-pi*dradhp^2/4);%mass of radiators 17&18
(m^3)
mrad1920=pfin*Arad1920*trad+psad*Lrad1920*(ssad^2-pi*dradhp^2/4);%mass of radiators 19&20
(m^3)
mrad2122=pfin*Arad2122*trad+psad*Lrad2122*(ssad^2-pi*dradhp^2/4);%mass of radiators 21&22
(m^3)
mrad2324=pfin*Arad2324*trad+psad*Lrad2324*(ssad^2-pi*dradhp^2/4);%mass of radiators 23&24
mrad2526=pfin*Arad2526*trad+psad*Lrad2526*(ssad^2-pi*dradhp^2/4);%mass of radiators 25&26
mrad2728=pfin*Arad2728*trad+psad*Lrad2728*(ssad^2-pi*dradhp^2/4);%mass of radiators 27&28
mrad2930=pfin*Arad2930*trad+psad*Lrad2930*(ssad^2-pi*dradhp^2/4);%mass of radiators 29&30
(m^3)
mrad3132=pfin*Arad3132*trad+psad*Lrad3132*(ssad^2-pi*dradhp^2/4);%mass of radiators 31&32
(m^3)
mrad3334=pfin*Arad3334*trad+psad*Lrad3334*(ssad^2-pi*dradhp^2/4);%mass of radiators 33&34
(m^3)
mrad3536=pfin*Arad3536*trad+psad*Lrad3536*(ssad^2-pi*dradhp^2/4);%mass of radiators 35&36
(m^3)
Vhpx=Arlp*dradhp-2*drlp*pi*dradhp^2/4; %flow volume at radiator heat pipe condensers
(m^3)
```

Appendix G: Simulink Model

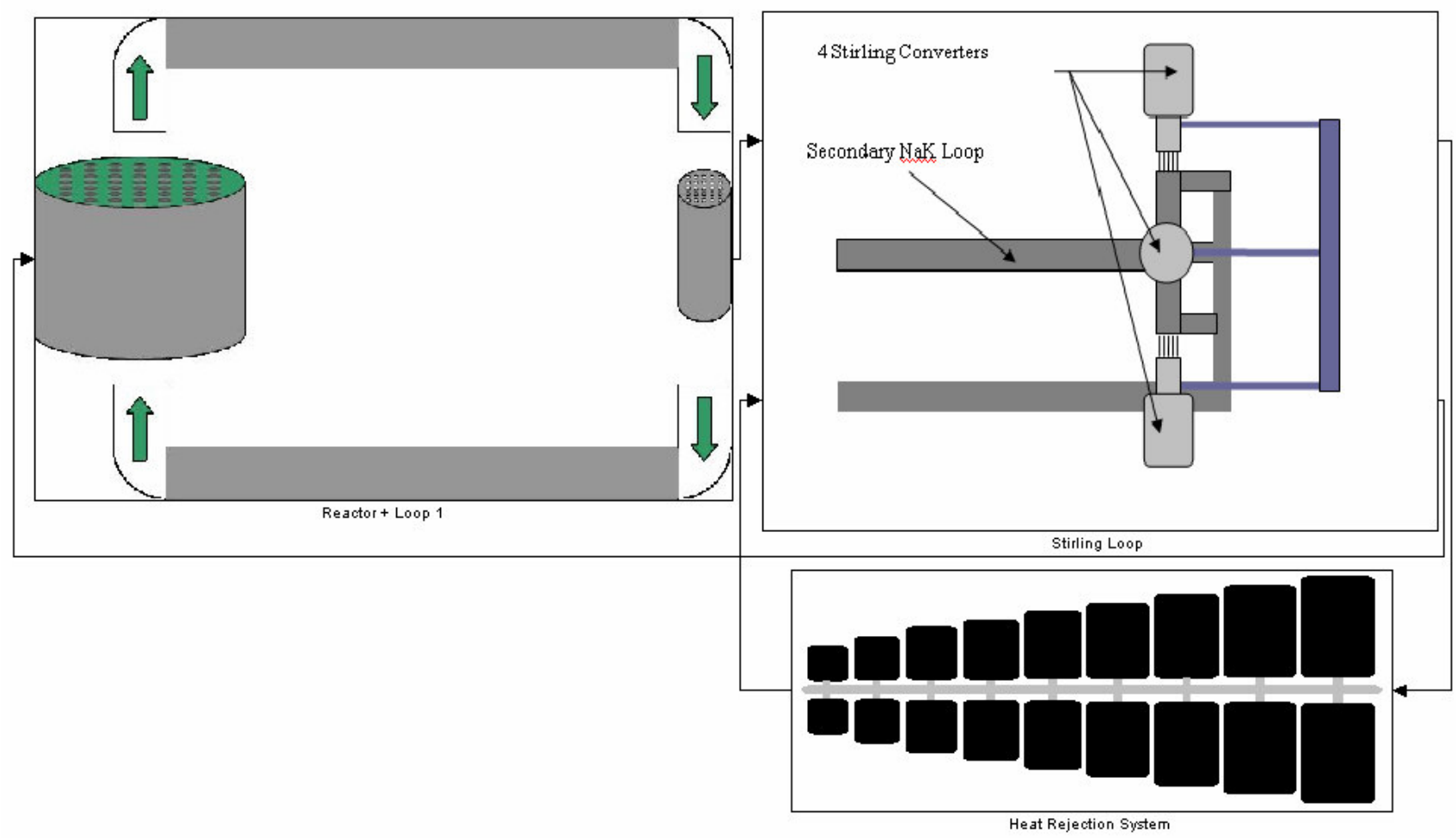

Appendix G: Simulink Model

Reactor + 1st Loop

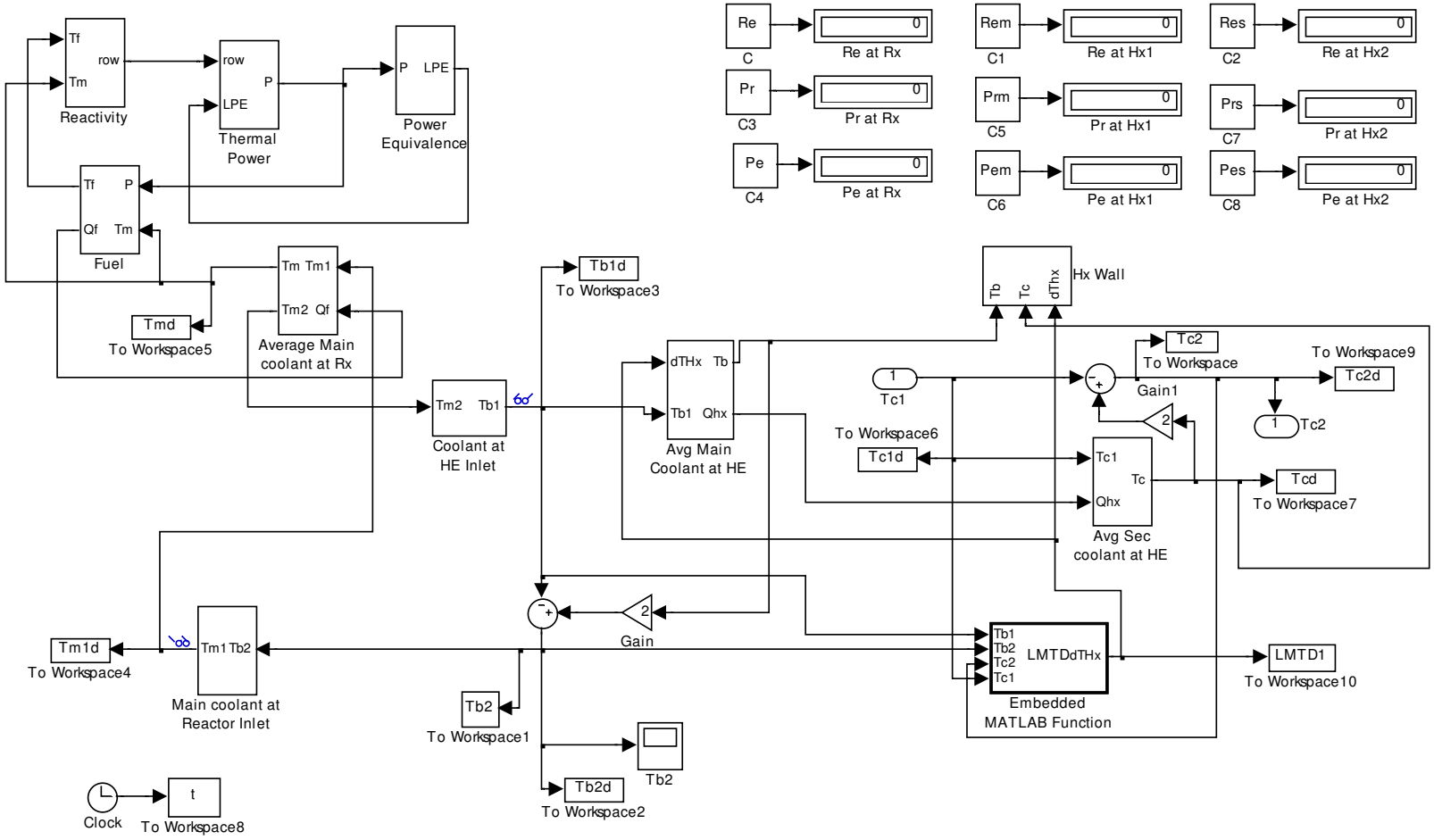

Appendix G: Simulink Model

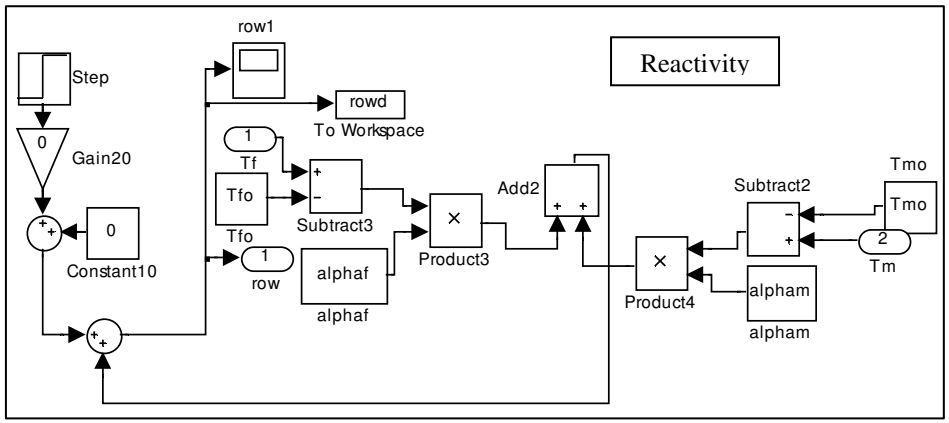

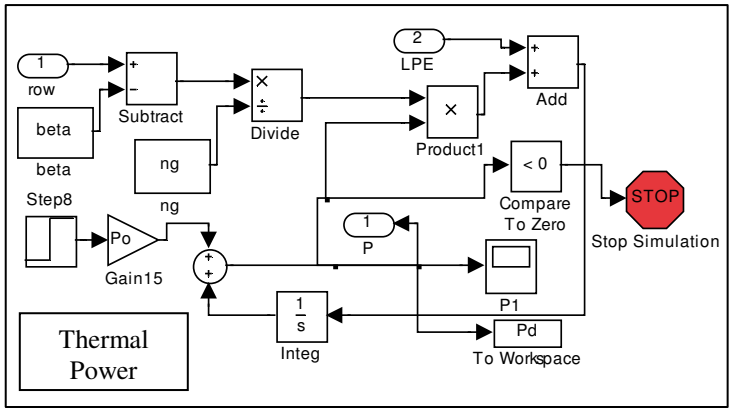

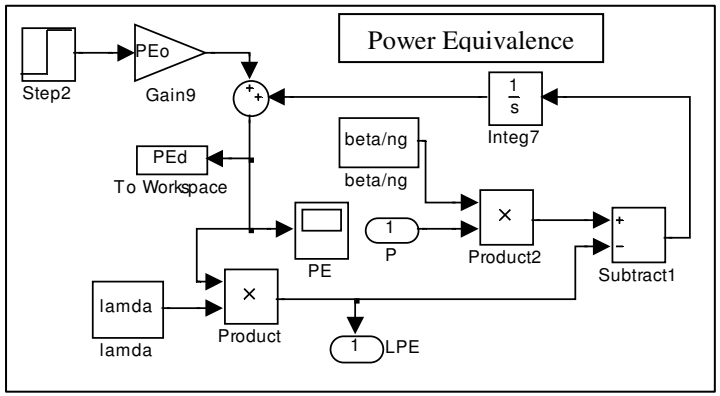

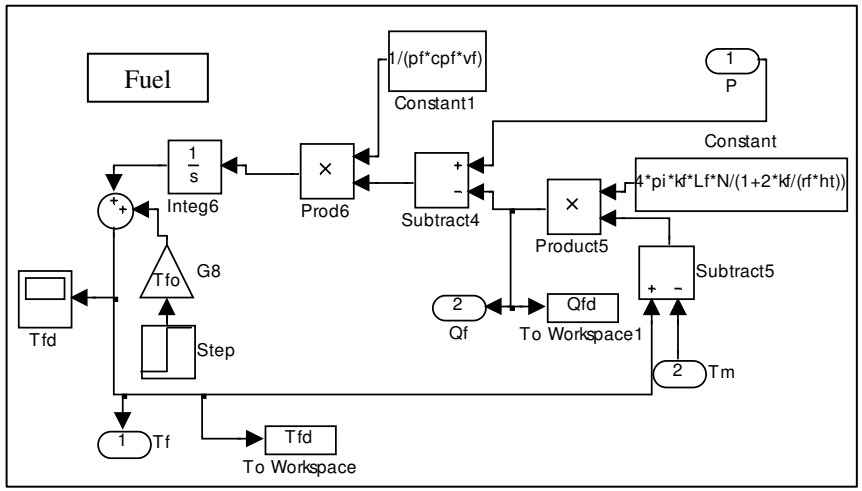

Appendix G: Simulink Model

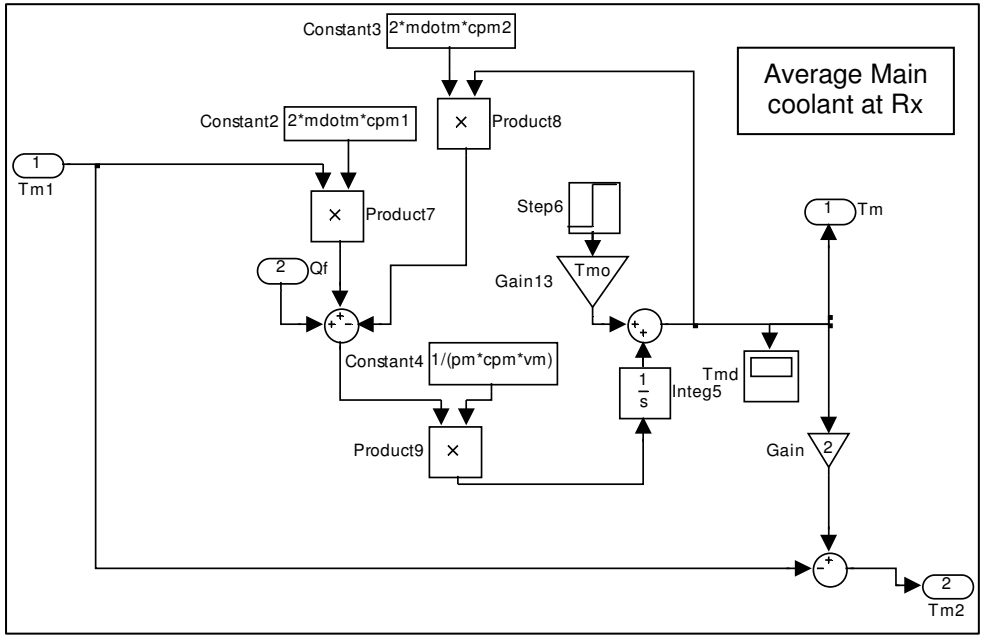

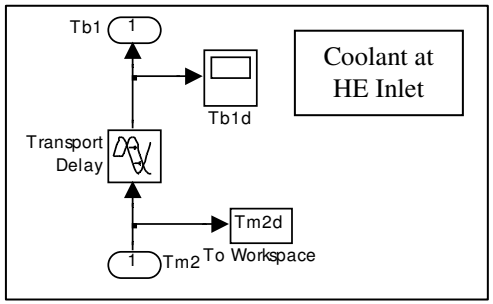

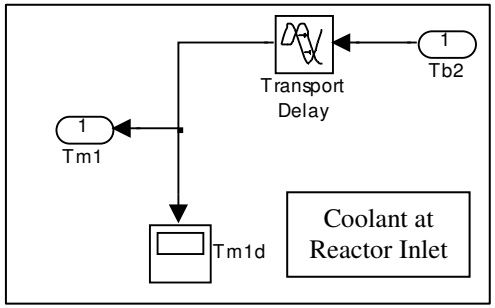

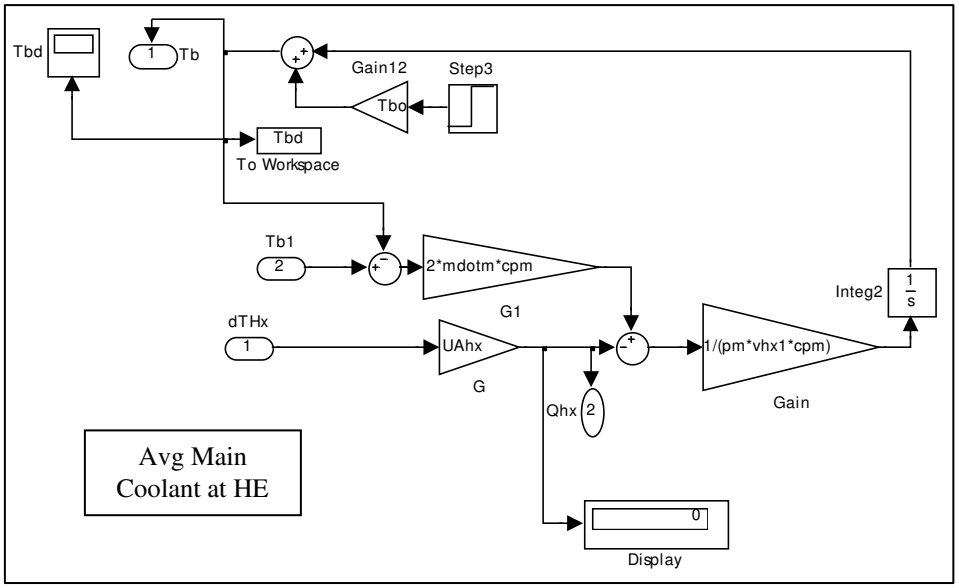

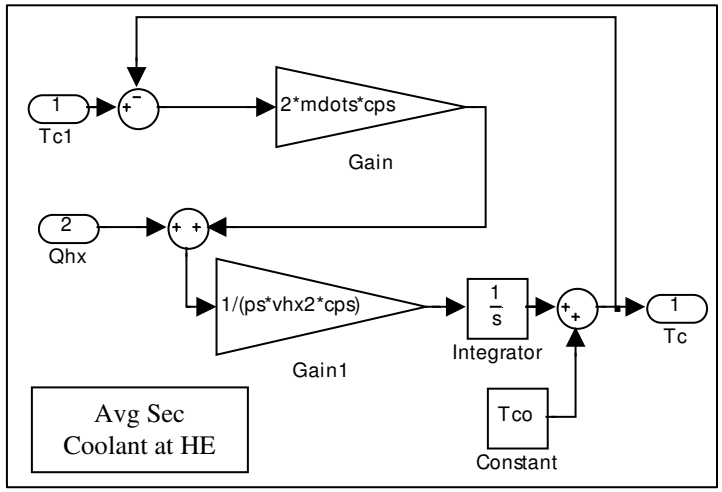

Appendix G: Simulink Model

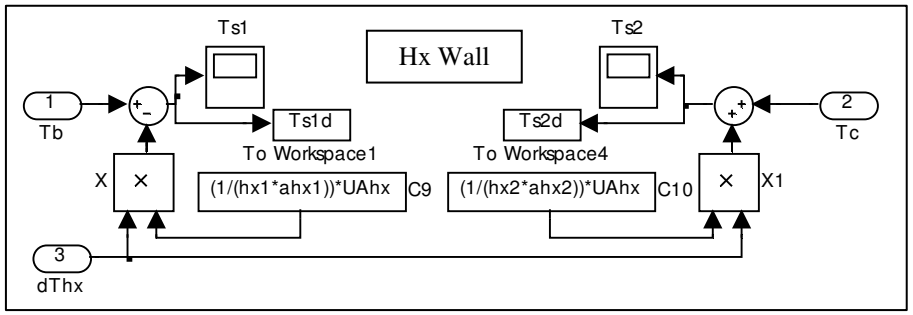


```
      Embedded MATLAB Function
function
dTHx=LMTD(Tb1,Tb2,Tc2,Tc1)
if abs((Tb1-Tc2)-(Tb2-Tc1))<=1
    dTHx=Tb1-Tc2;
else
    dTHx=(Tb1-Tc2-(Tb2-
Tc1))/log((Tb1-Tc2)/(Tb2-Tc1));
end
```

Stirling Loop

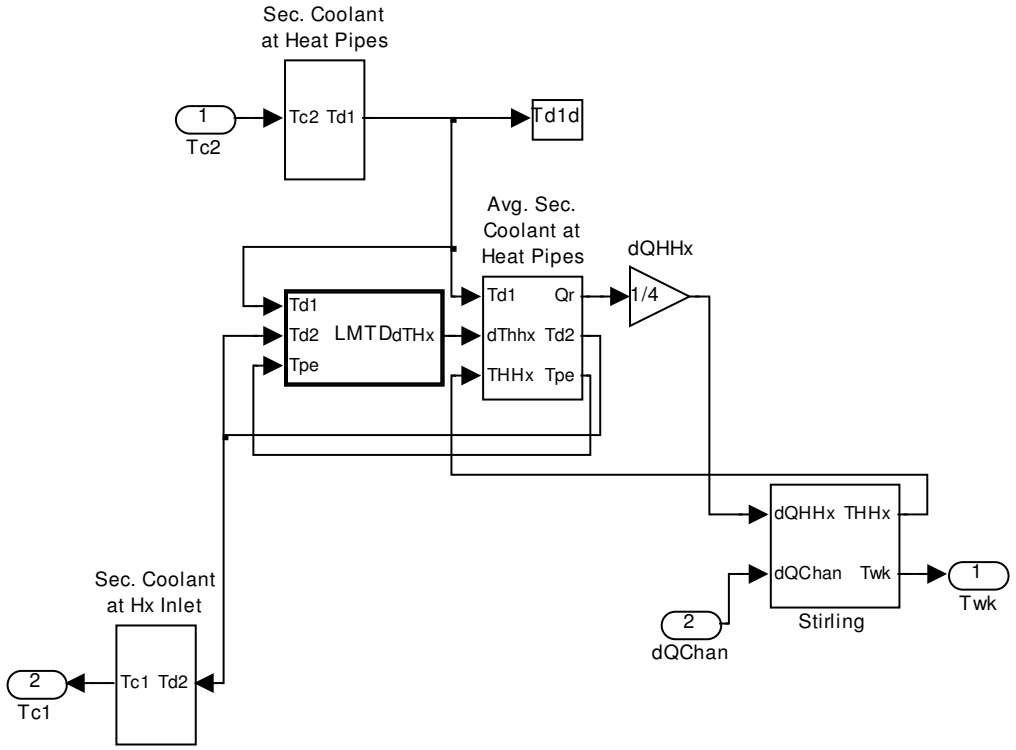

Appendix G: Simulink Model

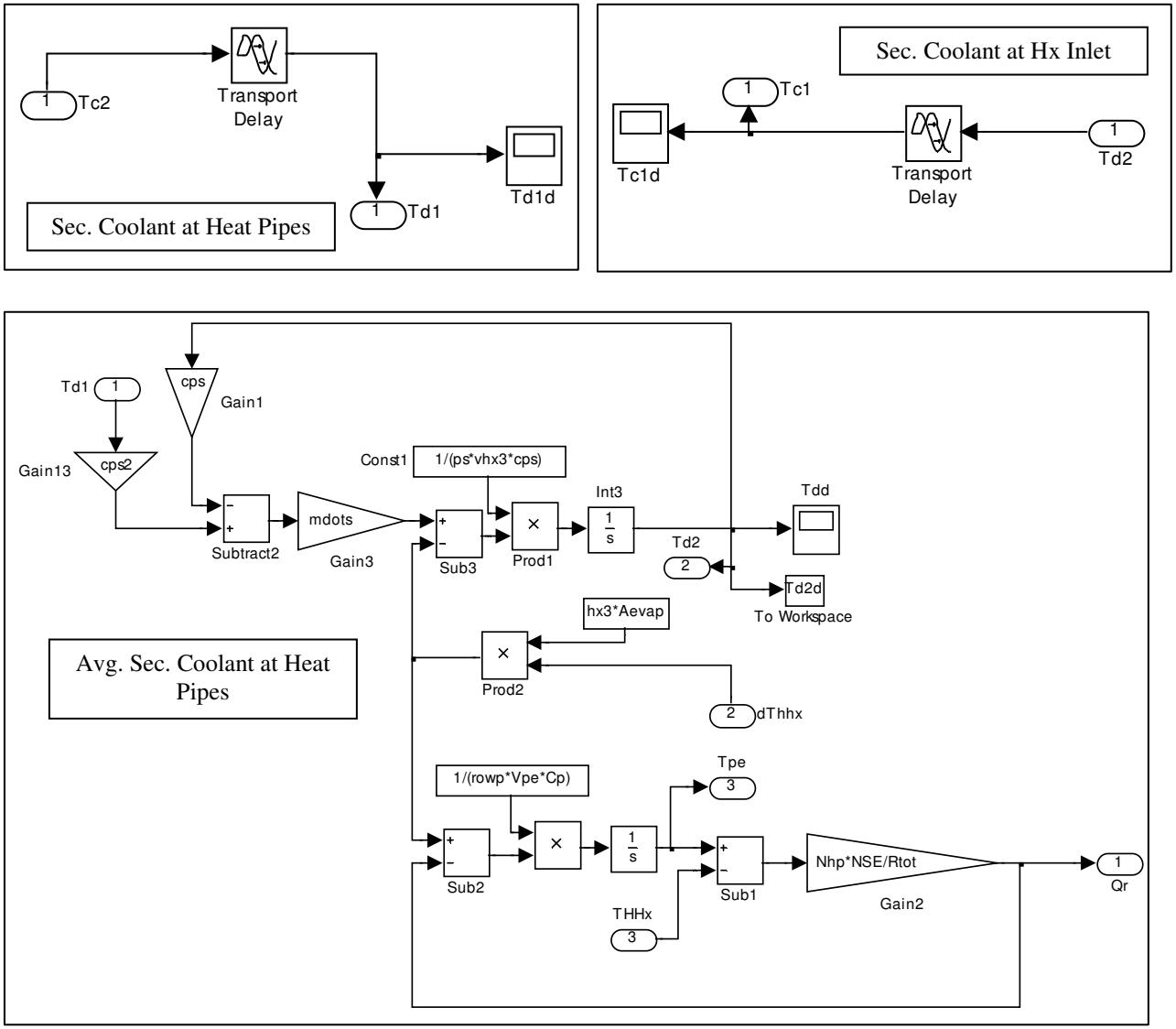

Appendix G: Simulink Model

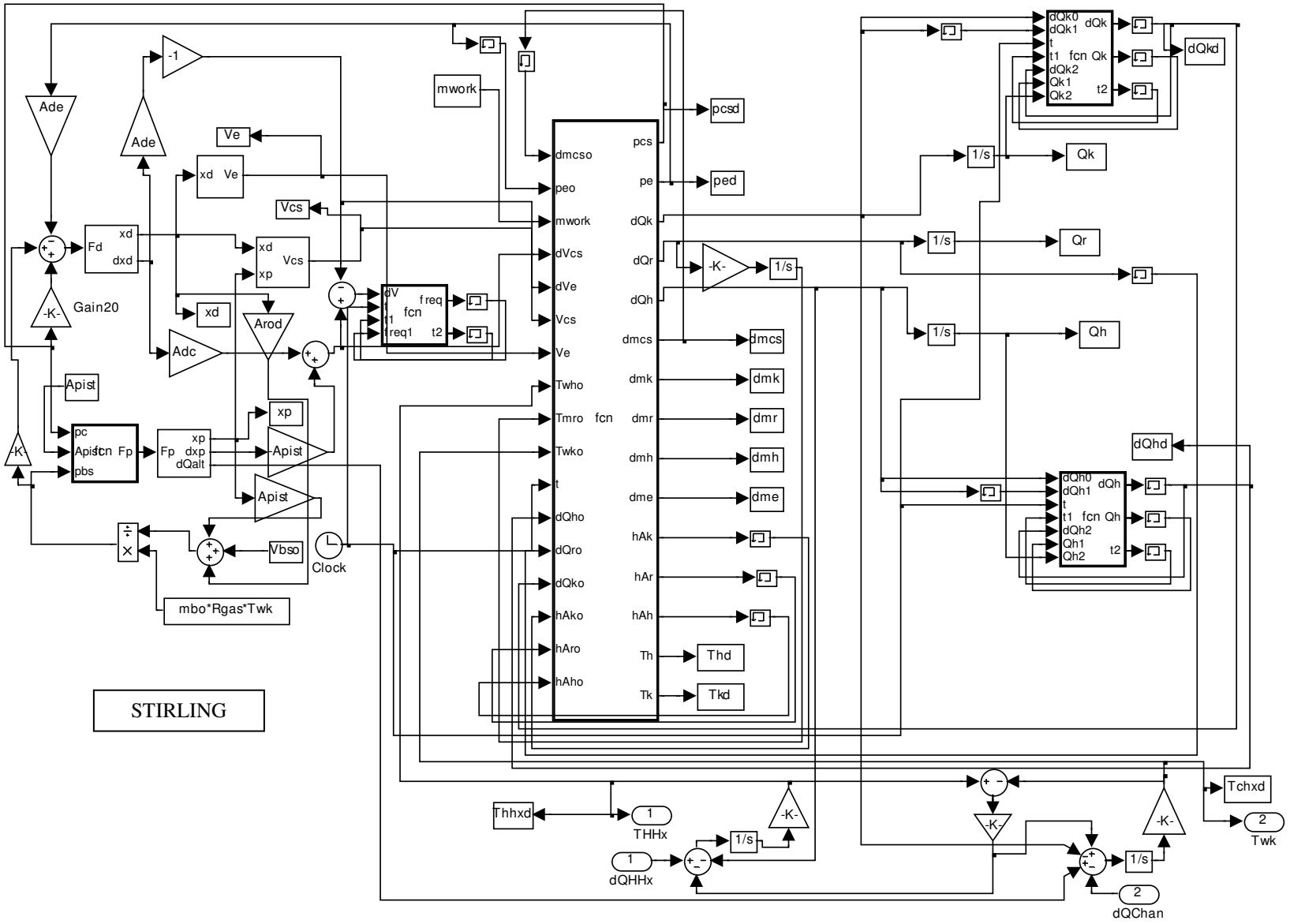

Appendix G: Simulink Model

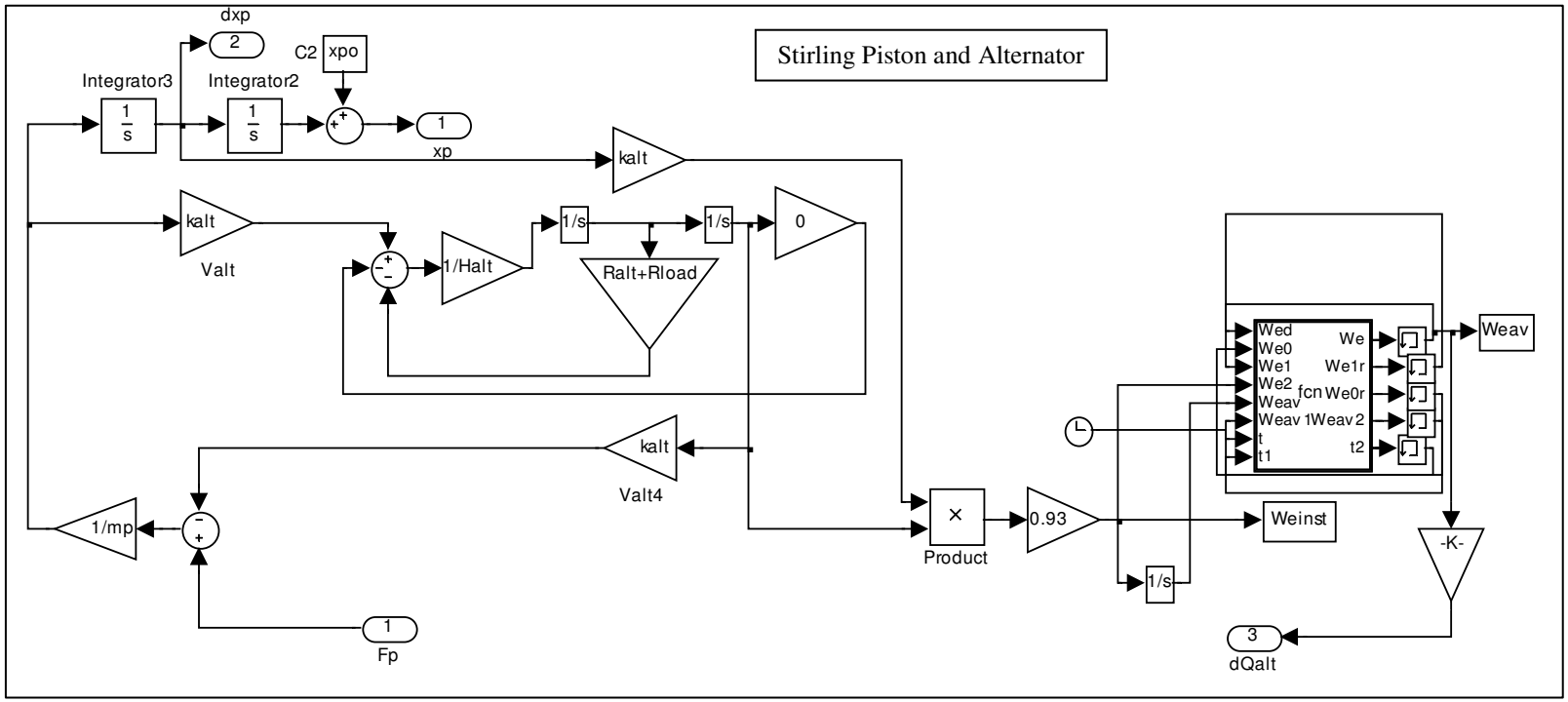

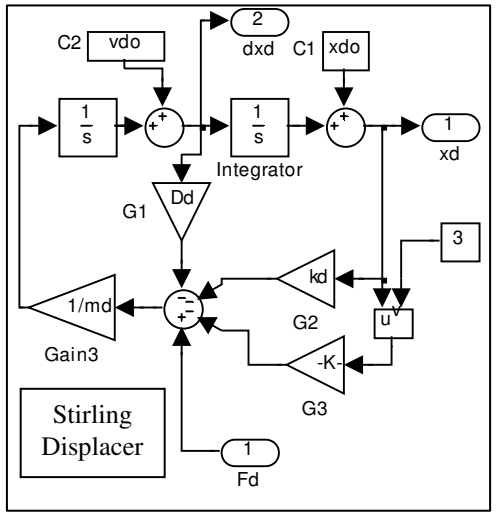

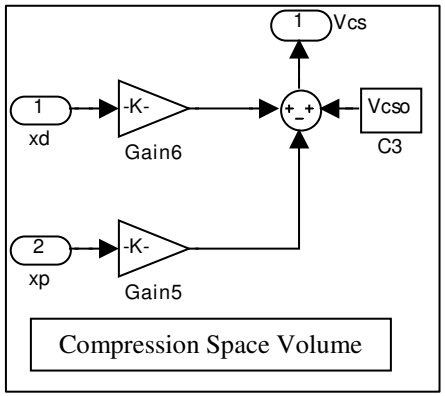

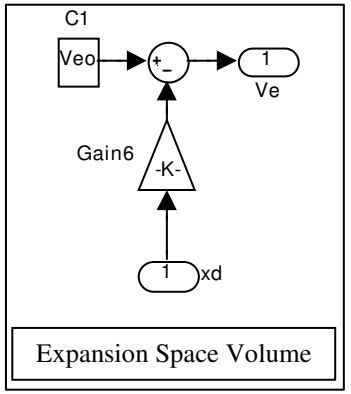

Appendix G: Simulink Model

Freq

```
function [freq,t2] =
fcn(dV,t,t1,freq1)
freq=freq1;
t2=t1;
if abs(dV)<=1*10^(-2)
    freq=1/(t-t2);
    t2=t;
end
if abs(t-t1)<=1/(2*95)
    freq=freq1;
    t2=t1;
end
if freq >= 130
    freq=freq/2;
end
```

dQk

```
function [dQk,Qk,t2] =
fcn(dQk0,dQk1,t,t1,dQk2,Qk1,Qk2)
dQk=dQk2;
Qk=Qk1;
t2=t1;
if dQk0>0 && dQk1<0
    dQk=(Qk2-Qk1)/(t-t2);
    Qk=Qk2;
    t2=t;
end
```

dQh

```
function [dQh,Qh,t2] =
fcn(dQh0,dQh1,t,t1,dQh2,Qh1,Qh2)
dQh=dQh2;
Qh=Qh1;
t2=t1;
if dQh0>0 && dQh1<0
    dQh=(Qh2-Qh1)/(t-t2);
    Qh=Qh2;
    t2=t;
end
```

Appendix G: Simulink Model

Heat Rejection System

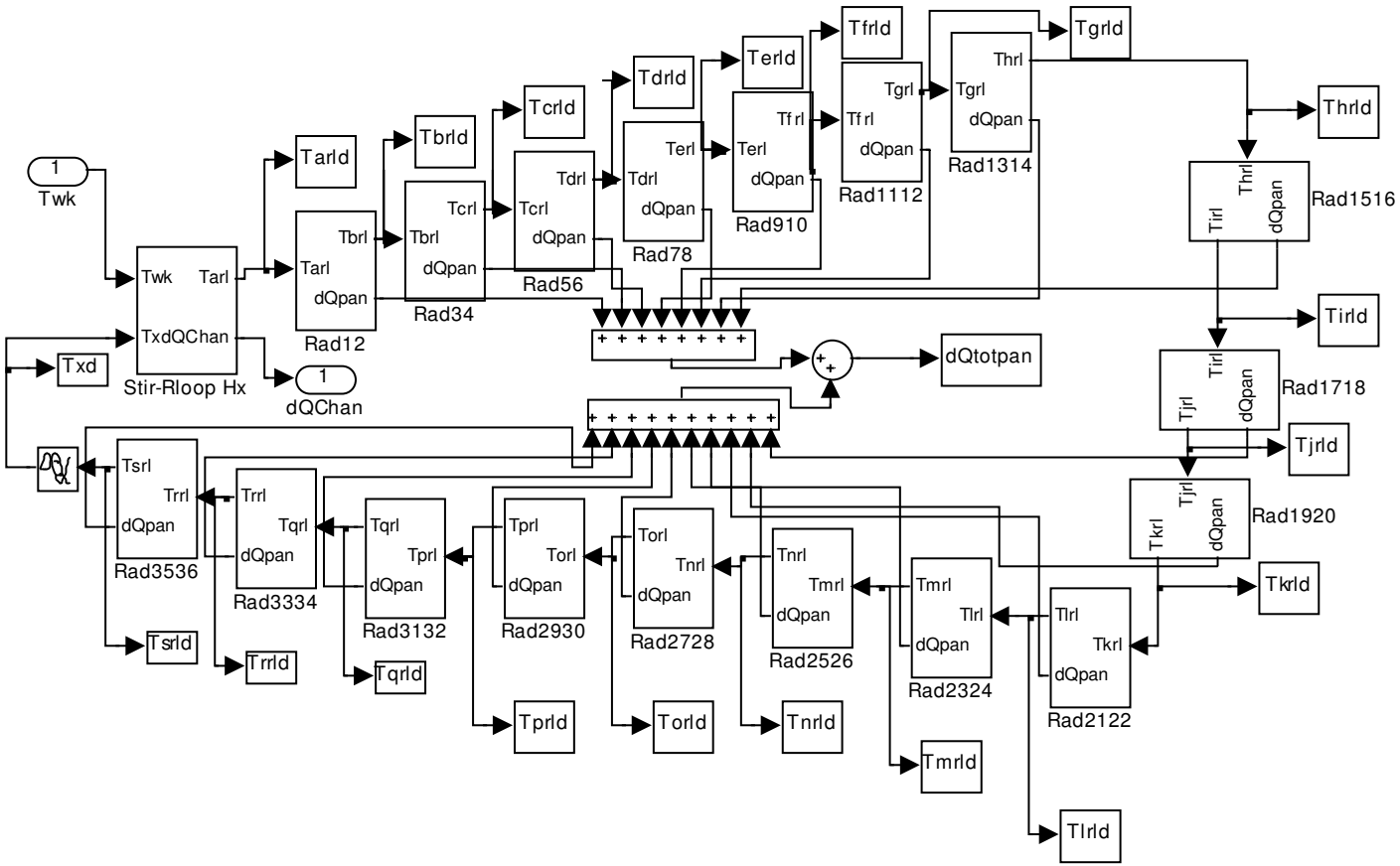

Appendix G: Simulink Model

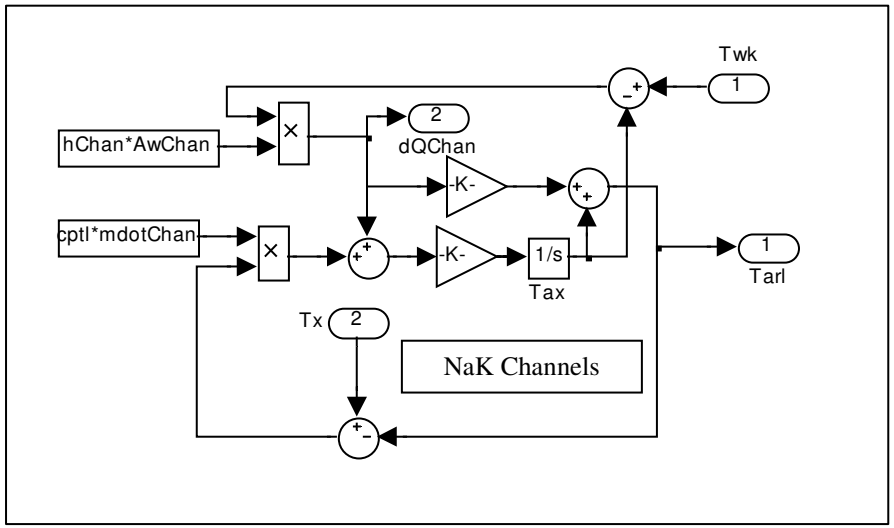

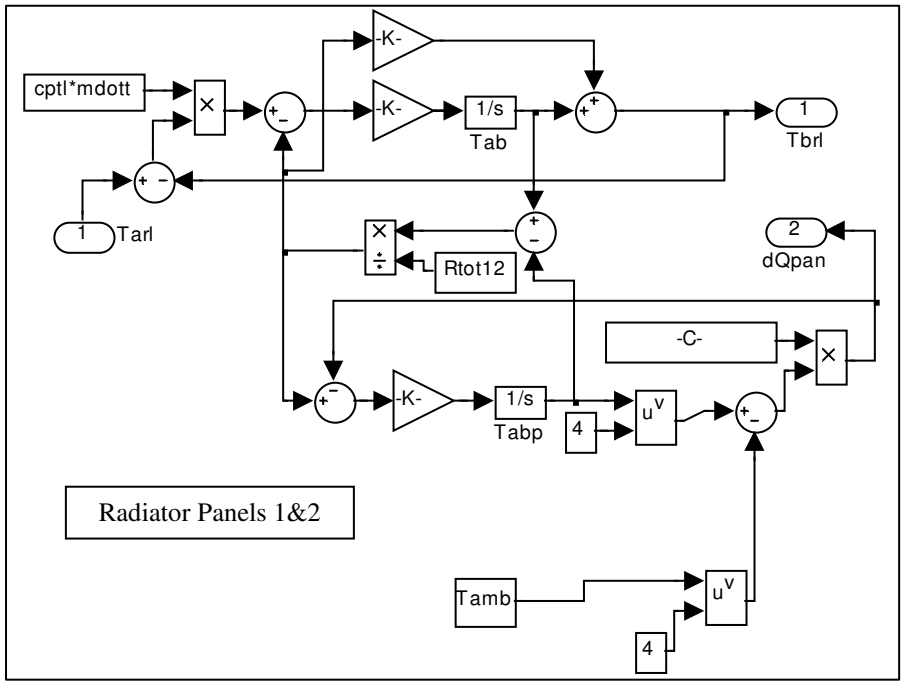

Appendix G: Simulink Model

Stirling Main Block

```
function [pcs,pe,dQk,dQr,dQh,dmcs,dmk,dmr,dmh,dme,hAk,hAr,hAh,Th,Tk] =
fcn(dmcso,peo,mwork,dVcs,dVe,Vcs,Ve,Twho,Tmro,Twko,t,dQho,dQro,dQko,hAko,hAro
,hAho)
dmcs=dmcso; %initial compression space mass flow rate (kg/s)
pe=peo; %initial expansion space mass pressure (Pa)
vc=1.3; %compression volume factor
ve=1; %expansion space volume factor
freq=90;  %stirling frequency (Hz)
Ap=0.0381; %piston area (m^2)
xpo=0;  %initial piston position (m)
vpo=0.013*2*pi*freq;
kalt=38.5; %alternator constant (Vs/m)
Ralt=0.028; %alternator resistance (ohm)
Halt=0.0002; %alternator inductance (H)
Zalt=sqrt(Ralt^2+(2*pi*freq*Halt)^2); %alternator impedance (ohms)
Ialt=kalt*vpo/Zalt; %alternator current (A)
Rload=0.6835; %alternator load resistance (ohms)
Dp=kalt^2/Zalt; %piston damping (kg/s)
mp=25; %piston mass (kg)
md=8.5; %displacer mass (kg)
drd=0.032; %displacer rod diameter (m)
Arod=pi*drd^2/4; %displacer rod area (m^2)
Ade=0.03892; %displacer area-exp. side (m^2)
Adc=Ap; %displacer area-comp. side (m^2)
phase=60; %piston-displacer phase angle (deg)
xdo=0.0084*sin(pi*phase/180);%displacer initial position (m)
vdo=0.0082*2*pi*freq*cos(pi*phase/180); %initial displacer velocity (m/s)
Dd=0; %displacer damping (kg/s)
kp1=0; %1st order piston spring constant (N/m)
kd3=0; %3rd order piston spring constant (N/m)
kd=3.1*10^6; %displacer spring constant (Pa)
pmean=13.6*10^6; %piston mean pressure (Pa)
Twk=Twko; %cooler temperature (K)
Twh=Twho; %heater temperature (K)
Twr=(Twh+Twk)/2; %regen. temperature (K)
Tmr=Tmro; %regen. matrix temp. (K)
Vcso=vc*6*10^(-4); %compression space volume (m^3)
Nkchan=3100*4; %number cold exchanger channels (dl)
CHxLg=0.075; %cold exch. length (m)
dtk=0.0014/2; %cooler channel diameter (m)
CHxpw=(pi*dtk)*Nkchan; %cooler wetted perimeter (m)
Awk=CHxpw*CHxLg; %cooler wall area (m^2)
ACHx=Nkchan*pi*dtk^2/4; %cooler cross-sectional area (m^2)
CHxDh=4*ACHx/CHxpw; %cooler hydraulic diameter (m)
Vk=ACHx*CHxLg; %cooler volume (m^3)
rLg=0.055; %regen. length (m)
por=0.88; %regen. porosity (dl)
Acr=5.017*10^(-2); %regen. area (m^2)
Ar=Acr*por; %regen. Flow area (m^2)
dr=sqrt(4*Ar/pi); %regen. diameter (m)
Awr=pi*dr*rLg; %regen. wall area (m^2)
rwd=25*10^(-6); %regen. wire diameter (m)
rpw=4*(1-por)*Acr/rwd; %reg. wetted perimeter (m)
rDh=4*Ar/rpw; %regen. hyd. diameter (m)
Amr=rpw*rLg; %regen. matrix area (m^2)
```

```
Vr=rLg*Ar; %regen. volume (m^3)
HHxLg=0.075; %heater length (m)
htd=.0013/2; %heater tube diameter (m)
Nht=2750*4; %number heater tubes (dl)
AHHx=Nht*pi/4*htd^2; %heater cross-sectional area (m^2)
Vh=AHHx*HHxLg; %heater volume (m^3)
HHxpw=Nht*pi*htd; %heater wetted perimeter (m)
HHxDh=4*AHHx/HHxpw; %heater diameter hyd. (m)
Awh=HHxpw*HHxLg; %heater wall area (m^2)
Veo=ve*4.34*10^(-4); %expansion space volume (m^3)
Vbso=14.5*10^(-3); %bounce space volume (m^3)
Vt=Vcso+Veo+Vh+Vr+Vk; %total volume (m^3)
gammaHe=1.667; %helium ratio of specific heats (dl)
Rgas=2077; %helium gas constant (J/(kg*K))
kHe=0.14; %helium conductivity (J/(kg*K))
cp=5230; %helium specific heat-const. press. (J/(kg*K))
cv=cp-Rgas; %helium specific heat-const. vol. (J/(kg*K))
cs=500; %steel specific heat (J/(kg*K))
CSutherland=1.286e-6; %Sutherland's law constant
SSutherland=8.63; %Sutherland's law constant
Diss=0; %initial total dissipation (W)
Dissk=0; %initial cooler dissipation (W)
Dissr=0; %initial regen. dissipation (W)
Dissh=0; %initial heater dissipation (W)
pcso=pmean; %initial compression space pressure (Pa)
peo=pmean; %initial expansion space pressure (Pa)
pko=pmean; %initial cooler space pressure (Pa)
pro=pmean; %initial regen. space pressure (Pa)
pho=pmean; %initial heater space pressure (Pa)
WpV=53.6*10^3; %expected cycle PV power (W)
eff=0.316; %expected cycle efficiency
dQhss=WpV/eff; %expected cycle heat addition (W)
dQkss=WpV-dQhss; %expected cycle heat rejection (W)
if t<=0.02
    Th=Twh-dQhss/hAho; %heater space temp. (K)
    Tk=Twk-dQkss/hAko; %cooler space temp. (K)
else
    Th=Twh-dQho/hAho; %heater space temp. (K)
    Tk=Twk-dQko/hAko; %cooler space temp. (K)
end
Tr=(Th-Tk)/log(Th/Tk); %regen. 1 temp. (K)
Tcs=Tk; %compression space temperature (K)
Te=Th; %expansion space temperature (K)
muk=CSutherland*Tk^1.5/(Tk+SSutherland); %cooler viscosity
muh=CSutherland*Th^1.5/(Th+SSutherland); %heater viscosity
mur=CSutherland*Tr^1.5/(Tr+SSutherland); %regen. viscosity
meo=peo*Veo/(Rgas*Th); %initial expansion space mass (kg)
mho=pho*Vh/(Rgas*Th); %initial heater space mass (kg)
mro=pro*Vr/(Rgas*Tr); %initial regen. space mass (kg)
mko=pko*Vk/(Rgas*Tk); %initial cooler space mass (kg)
mcso=pcso*Vcso/(Rgas*Tk); %initial compression space mass (kg)
mbo=pmean*Vbso/(Rgas*Tk); %initial bounce space mass (kg)
mwork=(meo+mho+mro+mko+mcso); %working space mass (kg)
kHek=(17.201+0.06764*Tk-1.25*10^(-6)*Tk^2)*418.68/10^5; %cooler gas
conductivity (W/(m*K))
```

```
kHer=(17.201+0.06764*Tr-1.25*10^(-6)*Tr^2)*418.68/10^5; %regen. gas
conductivity (W/(m*K))
kHeh=(17.201+0.06764*Th-1.25*10^(-6)*Th^2)*418.68/10^5; %heater gas
conductivity (W/(m*K))
Prk=muk*cp/kHek; %cooler gas Prandtl number
Prr=mur*cp/kHer; %regen. gas Prandtl number
Prh=muh*cp/kHeh; %heater gas Prandtl number
Kk=1.5; %cooler local loss coefficient
Kr=0; %regen. local loss coefficient
Kh=1.5; %heater local loss coefficient
pcs=mwork*Rgas/(Vcs/Tk+Vk/Tk+Vr/Tr+Vh/Th+Ve/Th); %working space pressure (Pa)
dpcs=-mwork*Rgas*(dVcs/Tk+dVe/Th)/(Vcs/Tk+Vk/Tk+Vr/Tr+Vh/Th+Ve/Th)^2;
%working space pressure time derivative (Pa/s)
dmcs=(pcs*dVcs+Vcs*dpcs)/(Rgas*Tk); %compression space mass flow (kg/s)
dmck=-dmcs; %compression-cooler boundary mass flow (kg/s)
dmk=Vk*dpcs/(Rgas*Tk); %cooler mass flow (kg/s)
dmkr=dmck-dmk; %cooler-regen. boundary mass flow (kg/s)
dme=(pe*dVe+Ve*dpcs)/(Rgas*Th); %expansion space mass flow (kg/s)
dmh=Vh*dpcs/(Rgas*Th); %heater mass flow (kg/s)
dmhe=dme; %expansion-heater boundary mass flow (kg/s)
dmrh=dme+dmh; %regen.-heater boundary mass flow (kg/s)
dmr=dmkr-dmrh; %regen. mass flow (kg/s)
mcs=pcs*Vcs/(Rgas*Tk); %compression space gas mass (kg)
mk=pcs*Vk/(Rgas*Tk); %cooler gas mass (kg)
mr=pcs*Vr/(Rgas*Tr); %regen. gas mass (kg)
mh=pcs*Vh/(Rgas*Th); %heater gas mass (kg)
me=pcs*Ve/(Rgas*Th); %expansion space gas mass (kg)
rowcs=mcs/Vcs; %compression space gas density (kg/m^3)
rowk=mk/Vk; %cooler gas density (kg/m^3)
rowr=mr/Vr; %regen. gas density (kg/m^3)
rowh=mh/Vh; %heater gas density (kg/m^3)
rowe=me/Ve; %expansion space gas density (kg/m^3)
uk=dmk/(rowk*ACHx); %cooler gas velocity (m/s)
ur=dmr/(rowr*Ar); %regen. gas velocity (m/s)
uh=dmh/(rowh*AHHx); %heater gas velocity (m/s)
Rek=rowk*abs(uk)*CHxDh/muk; %cooler gas Reynolds number
if Rek<=1.502113290507442e+003
    frk=64/Rek; %cooler gas friction factor
else
    frk=0.184/Rek^(0.2); %cooler gas friction factor
end
Fk=-Vk*(frk/CHxDh+Kk/CHxLg)*rowk*uk*abs(uk)/2; %cooler gas friction (N)
dpk=Fk/ACHx; %cooler gas pressure drop (Pa)
Dissk=abs(dpk*dmk/rowk); %cooler gas dissipation (W)
Pek=Rek*Prk; %cooler gas Peclet number
if Rek < 2300
    if Pek < 1.5
        Nuk=4.187*(1-0.0439*Pek); %cooler gas Nusselt number
    else
        Nuk=3.6568*(1+1.227/(Pek^2)); %cooler gas Nusselt number
    end
else
    Nuk=0.036*Rek^0.8*(CHxLg/CHxDh)^(-.055)*Prk^0.33; %cooler gas Nusselt
number
end
Rer=rowr*abs(ur)*rDh/mur; %regen. gas Reynolds number
```

```
frr=192/Rer+4.53*Rer^(-0.067); %regen. gas friction factor
Fr=-Vr*(frr/rDh+Kr/rLg)*rowr*ur*abs(ur)/2; %regen. gas Friction (N)
dpr=Fr/Ar; %regen. Pressure drop (Pa)
Dissr=abs(dpr*dmr/rowr); %regen. dissipation (W)
hAr=(1+1.16*(Rer*Prr)^0.66*por^2.61)*kHer*Amr/rDh; %regen. Heat transfer
coefficient (W/(m^2*K))
Reh=rowh*abs(uh)*HHxDh/muh; %heater Reynolds number
if Reh<=1.502113290507442e+003
    frh=64/Reh; %heater friction factor
else
    frh=0.184/Reh^(0.2); %heater friction factor
end
Fh=-Vh*(frh/HHxDh+Kh/HHxLg)*rowh*uh*abs(uh)/2; %heater friction (N)
dph=Fh/AHHx; %heater pressure drop (Pa)
Dissh=abs(dph*dmh/rowh); %heater dissipation (W)
Peh=Reh*Prh; %heater Peclet number
if Reh < 2300
    if Peh < 1.5
        Nuh=4.187*(1-0.0439*Peh); %heater Nusselt number
    else
        Nuh=3.6568*(1+1.227/(Peh^2)); %heater Nusselt number
    end
else
    Nuh=0.036*Reh^0.8*(HHxLg/HHxDh)^(-.055)*Prh^0.33; %heater Nusselt number
end
pe=pcs+dpk+dpr+dph; %expansion space pressure (Pa)
hAk=Nuk*kHe*Awk/CHxDh; %heater heat transfer coefficient (W/(m^2*K))
hAh=Nuh*kHe*Awh/HHxDh; %cooler heat transfer coefficient (W/(m^2*K))
dWcs=pcs*dVcs; %compression space PV power (W)
dWe=pe*dVe; %expansion space PV power (W)
dW=dWcs+dWe; %total PV power (W)
Diss=Dissh+Dissr+Dissk; %total dissipation (W)
STr=(hAr/Amr)/(rowr*abs(ur)*cp); %regen. Stanton number
NTUr=STr*(Amr/Ar)/2; %regen. Number of transfer units
reff=NTUr/(1+NTUr); %regen. effectiveness
dQr=Vr*cv*dpcs/Rgas+cp*(dpcs*(Vk+Vcs+Vh+Ve)+dW)/Rgas; %regen. Heat transfer
(W)
dQk=-Vcs*dpcs; %cooler heat transfer (W)
if dmk < 0
    dQk=dQk-abs(dQr)/dQr*abs(dQr)^(1-reff); %cooler heat transfer (W)
end
dQh=-Ve*dpcs; %heater heat transfer (W)
if dmh > 0
    dQh=dQh+abs(dQr)/dQr*abs(dQr)^(1-reff); %heater heat transfer (W)
end
```